Karlsruhe Institute of Technology

Flavour-changing neutral current processes beyond the Standard Model

zur Erlangung des akademischen Grades eines

Doktors der Naturwissenschaften

von der KIT-Fakultät für Physik
des Karlsruher Instituts für Technologie (KIT)

angenommene

Dissertation

von

M.Sc. Aliaksei Kachanovich

aus Staŭbcy (Belarus)

Tag der mündlichen Prüfung: 20. November 2020
Erster Gutachter: Prof. Dr. Ulrich Nierste
Zweiter Gutachter: Prof. Dr. Matthias Steinhauser

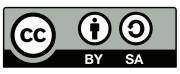

Contents

List of acronyms

2HDM - Two Higgs Doublet Model
ATLAS - A Toroidal LHC ApparatuS (an experiment at CERN)
BMHV - Breitenlohner-Maison-'t Hooft-Veltman
BSM - Beyond the SM
CDC - Central Drift Chamber
CERN - European Organization for Nuclear Research
CKM - Cabibbo-Kobayashi-Maskawa matrix
CMS - Compact Muon Solenoid (an experiment at CERN)
DM - Dark Matter
GIM - Glashow-Iliopoulos-Maiani mechanism
IBP - Integration by Parts
LHC - Large Hadron Collider (particle collider at CERN)
NDR - Naive Dimensional Regularization
PMNS - Pontecorvo–Maki–Nakagawa–Sakata matrix
QCD - Quantum Chromodynamics
QFT - Quantum Field Theory
SM - Standard Model
vev - vacuum expectation value

Acknowledgments

First of all, I would like to thank my supervisor *Ulrich Nierste*, who gave me the opportunity and introduced to me the world of particle physics, which was my dream from high school time. Also, I thank **DAAD** and **KSETA** for the support. Without this support, these ideas could not be realized. A special many thanks to my collaborator *Ivan Nišandžić*, with whom we spent many hours of discussions, without whom these projects cannot be realized in time. Also, special thanks to *Teppei Kitahara*, who inspired me all the time and helped me to learn the magic of loop calculation. Many thanks to my friend *Vlad Shtabovenko*, who helped me to join in the world of computer algebras. I also thank *Ivan Nišandžić, Joshua Davies, Christoph Fischbacher, Pavel Hájek, Martin Lang* and *Teppei Kitahara* for the proofreading of this thesis. I thank *Kirill Melnikov* for many ideas and support. I thank *Jose Zurita* for the ideas how to write texts. I thank my friend *Alexey Zhevlakov* for the ideas about future projects and moral support. Also many thanks to my colleague *Adam Smetana*, for the nice time at Czech Technical University in Prague. Many thanks to my colleagues from experimental side: *Nils Braun, Felix Metzner* and *Evgeny Andronov*, for the details about all these tricky machines. I thank my friends *Jakub Jankowski*, *Michał Kosztołowicz*, *Michał Marczenko*, *Marek Miller* and *Aneta Wojnar* for all kinds of help. I would like to thank all my present and former roommates: *Jordan Bernigaud, Marco Bonetti, Thomas Deppisch, Min He,* and *David Wellmann* and also all my colleagues with whom I ever worked at **KIT**.

Very special thanks to my wife *Irina* who refused many benefits in her life, like friends and a job, to make my dream come true. And also I thank my mom and my sister who always believed in me.

Chapter 1

Introduction

In this Thesis, I study rare decays in Higgs and B-meson physics in context of solutions to the problem of DM. I shall also discuss all aspects and techniques which have been used to perform the calculations. In this Thesis, I shall briefly highlight the mechanism of suppression of FCNC decays, like $b \to s(d)X$ by the CKM matrix. I shall also highlight the role of fundamental scalar within the SM.

At the beginning of the 20^{th} century, only two fundamental forces of nature were known, namely gravity and the electromagnetic force. In 1933 W. Pauli proposed a new fundamental force, subsequently called the weak force [1], as an explanation of the phenomenon of beta decay. Later in 1941 the electromagnetic force has been explained as invariance under $U(1)$ gauge symmetry [2]. This discovery a few years later perfectly explained shifts of the lines of the hydrogen atom spectrum [3] which have been measured by W. Lamb and R. Retherford [4]. In the 50's years there were a lot of unsuccessful attempts to explain the weak force in the same manner as have been described the electromagnetic force. In 1961 S. Glashow proposed $SU(2) \times U(1)$ symmetry to describe weak force [5], for this idea he obtained the Nobel prize in 1972. In 1963 P. Andersen who is more known from the works under the superconductivity problem proposed that symmetry which describes weak force can be broken [6]. In 1967 A. Salam and S. Weinberg presented the model [7] based on the broken $SU(2) \times U(1)$ symmetry which predicted 3 new massive bosons $W^{\pm}$ and Z and their masses (they shared the Nobel prize in 1972 together with S. Glashow). One of the most important part, namely the mechanism of the symmetry breaking, has been developed by many scientists like F. Englert and R. Brout [8], P. Higgs [9], G. S. Guralnik, C. R. Hagen, and T. W. B. Kibble [10] (F. Englert and P. Higgs obtained the Nobel prize in 2013). The Higgs mechanism has been introduced in the theory of electroweak interaction which so-called Standard Model with one single doublet. But do we have only the Higgs boson in the scalar sector?

One of the most important tasks of the *LHC* experiments *CMS* and *ATLAS* is the precise determination of the Higgs boson couplings. The SM is constructed with only one Higgs doublet, and it is a natural question whether Nature anticipates a richer Higgs sector than is provided by the SM. The disagreement between theoretical prediction [11] and experiment could be the hint for a richer Higgs sector. As of yet, *ATLAS* and *CMS* have studied the couplings of the Higgs boson to τ leptons [12–14], W [15–18] and Z [18–21] bosons, bottom [22, 23] and top [24, 25] quarks, also to photons [26, 27].

Rare Higgs decays, even for the SM Higgs sector with only one doublet, are very sensitive to BSM physics. For example, the fourth sequential fermion generation has been ruled out by a combined analysis of all Higgs signal strength [28]. Phenomenological analyses of the 2HDM usually assume simplifications of the Yukawa sector which are called type I, II, X, or Y[1]. In these

[1]This will be discussed in greater details in Chapter 3.

models different observables become correlated and heavy fermions from the third family provide the largest contribution [29–39]. Only redundant information can be obtained from processes which involve fermions from the first and second family. Nevertheless, there are well-motivated reasons to search for smoking gun signals of new physics in Higgs decays into light fermions.

In this Thesis, the SM predictions for the rare decays $h \to l\bar{l}\gamma$, where l denotes light leptons e and μ, have been studied. The amplitude $h \to l\bar{l}$ is proportional to Yukawa coupling of l and only the combination with one left- and one right-handed lepton is possible. Higher-order contributions provide only corrections to this vertex. Meanwhile, in the amplitude $h \to l\bar{l}\gamma$ in the final state, a chiral flip is possible, meaning that one can find also $l_L\bar{l}_L\gamma$ and $l_R\bar{l}_R\gamma$ final states. Additional photon emission from the vertex $h \to l\bar{l}$ cannot change the helicity. This flip is possible only at the one-loop level, this means that the leading order contribution of this effect comes from the one-loop. Because of the small Yukawa coupling, tree-level processes can be completely ignored for electrons. For muons, tree- and loop-level contributions are of the same order $\left(Br(h \to \mu\overline{\mu}\gamma) = 6.7 \times 10^{-5} \text{ vs } Br(h \to \mu\overline{\mu}) = 2 \times 10^{-4}\right)$. For τ leptons in the final state, the one loop level contributes only a tiny correction to the tree-level results. I also note that this study is important because the processes $h \to l\bar{l}$ and $h \to l\bar{l}\gamma$ probe different BSM sectors (chirality-flipping vs. chirality-conserving couplings to lepton fields) and are therefore complementary.

The study of Higgs boson decay was performed as part of a study of Higgs portals to DM [40]. The idea of the Higgs portal is not new and has already been studied for the past two decades. Viable scenarios involve an extra scalar particle which is coupled to the SM doublets. In these models, there are two physical states h_1 and h_2 where the first is the 125 GeV state observed at the *LHC* , the mass of h_2 is relatively small. These two physical states are related to each other by a mixing angle parameter θ. For a sufficiently small angle θ, the modification of the 125-GeV Higgs h_1 couplings comply with the measurements within the corresponding error bars. The second scalar h_2 mediates between the SM and the Dark Sector.

In this Thesis, the study of gauge dependence was performed in the case of one of the simplest DM models. Furthermore, the scenarios of rare B-meson decays are discussed within searches of displaced vertices in the *Belle II* experiment. This study is complementary to those of Refs. [41–45].

In Chapter 4, I also provide a brief introduction to techniques and tools used for the loop calculation in both $h \to l\bar{l}\gamma$ and $B \to K^{(\star)}+$ invisible. In Sec. 4.5 I will provide all necessary information for understanding the code, which will be revealed in Chapter 5.

Chapter 2

Electroweak theory

2.1 Introduction

The SM is a very powerful theory that describes all known particles and three out of four fundamental forces, namely: weak, electromagnetic, and strong. Within the SM, weak and electromagnetic forces are unified within electroweak theory [7, 46, 47]. The strong interaction is described by QCD.

All particles are categorised into two big groups - fermions and bosons. Fermions are half-integer spin particles which form all observed matter[1]. Bosons, which are integer spin particles, are responsible for the interactions. All known interactions, which are described by the SM, namely the strong, electromagnetic, and weak are transmitted by spin-one particles. Only one fundamental boson[2] has spin-zero - this is the Higgs boson. The Higgs boson has a very special role in the SM: it is responsible for the electroweak symmetry breaking. The Higgs boson is also responsible for the generation of the masses[3].

Fermions are divided into quarks and leptons. The difference between these particles is in which interactions these particles participate. Because of unknown reasons, only left-handed particles participate in the weak interaction. Left-handed quarks take part in all known interactions. Leptons differ from quarks in that they ignore the strong interaction. The weak interaction is mediated by massive bosons, which at first sight do not obey any symmetry. The Nobel Prize in 1979 was awarded[4] for the idea of unification of electromagnetic and weak force in one electroweak force which is described by the $SU(2)_L \times U(1)_Y$ symmetry group. According to this idea, all left-handed particles form weak isospin doublets. For the quarks, this looks like

$$Q_L^{j,1} = \begin{pmatrix} u_L^j \\ d_L'^j \end{pmatrix}, \quad Q_L^{j,2} = \begin{pmatrix} c_L^j \\ s_L'^j \end{pmatrix}, \quad Q_L^{j,3} = \begin{pmatrix} t_L^j \\ b_L'^j \end{pmatrix}, \tag{2.1}$$

where u_L^j, d_L^j, s_L^j, c_L^j, b_L^j, t_L^j are left up, down, strange, charm, bottom and top quarks respectively. Prime means that these quarks are written in the flavour base[5]. The index j runs over red, green, and blue QCD colour states.

Meanwhile, right-handed particles do not participate in weak interaction and appear as $SU(2)_L$ singlets

[1] Here, the DM phenomenon is not discussed.

[2] Fundamental scalars are very questionable. The problems of fundamental Higgs boson will be discussed in Sec. 2.4.

[3] ...but, almost all observed mass in the Universe is generated by QCD.

[4] This prize was awarded to Sheldon Glashow, Abdus Salam and Steven Weinberg.

[5] This will be discussed in greater detail in Sec. 2.3.

Field	l^i_L	l^i_R	ν^i_L	u^i_L	u^i_R	d^i_L	d^i_R	G^+	G^0
T_3	-1/2	0	1/2	1/2	0	-1/2	0	1/2	-1/2
Y_W	-1/2	-1	-1/2	1/6	2/3	1/6	-1/3	1/2	1/2
Q	-1	-1	0	2/3	2/3	-1/3	-1/3	1	0

Table 2.1: The SM weak isospin and isocharge. T_3 is the quantum number associated with the third component of weak isospin, Y_W is weak hypercharge, and Q is the electric charge

$$u_R^{j,1} = u_R^j\,, \quad u_R^{j,2} = c_R^j\,, \quad u_R^{j,3} = t_R^j\,, \tag{2.2}$$

$$d_R^{j,1} = d_R^j\,, \quad d_R^{j,2} = s_R^j\,, \quad d_R^{j,3} = b_R^j\,, \tag{2.3}$$

where as before, u_R^j, d_R^j, s_R^j, c_R^j, b_R^j, t_R^j are right up, down, strange, charm, bottom and top quarks respectively.

For leptons there is a similar situation with one difference, namely right-handed neutrinos are not observed experimentally, and because of this reason they are not included in the SM. In this case

$$L_L^1 = \begin{pmatrix} \nu_{e,\,L} \\ e_L \end{pmatrix}, \quad L_L^2 = \begin{pmatrix} \nu_{\mu,\,L} \\ \mu_L \end{pmatrix}, \quad L_L^3 = \begin{pmatrix} \nu_{\tau,\,L} \\ \tau_L \end{pmatrix}, \tag{2.4}$$

$$l_R^1 = e_R, \quad l_R^2 = \mu_R, \quad l_R^3 = \tau_R\,, \tag{2.5}$$

where e, μ, and τ are electron, muon and tau leptons, which are left- or right-handed, and ν are the corresponding neutrinos.

Here, the symmetry $U(1)_Y$ should not be confused with the very similar $U(1)_{em}$, which describes the electromagnetic interaction. Hypercharges of all particles, which correspond to the symmetry $U(1)_Y$, were determined experimentally from the relation

$$Q = I_{3L} + Y_W, \tag{2.6}$$

where Q is the electric charge, which is the same for left- and right-handed component of the Dirac spinor, I_{3L} is the quantum number associated with the third component of weak isospin, and Y_W is the hypercharge. The quantum numbers are given in Tab. 2.1.

The kinetic part of the Lagrangian for the left-handed quarks is obtained by the minimal coupling where all possible symmetries of the SM are present

$$\mathcal{L}_{q,\,L} = \overline{Q}_L^{i,\,m}\left\{ i\gamma^\mu\Big[\Big(\partial_\mu + ig'Y_W B_\mu + ig\frac{\sigma^a}{2}W_\mu^a\Big)\delta_{ij} + ig_s\frac{\lambda_{ij}^A}{2}G_\mu^A\Big]\right\}Q_L^{j,\,m}\,, \tag{2.7}$$

where $\sigma^a/2$ are the generators of the $SU(2)_L$ symmetry, where σ^a represents the three Pauli matrices, and $\lambda^A/2$ are generators of the $SU(3)$ colour symmetry, where λ^A represents the eight Gell-Mann matrices. The lowercase character index a for the Pauli matrices runs from 1 to 3, and the index denoted with capital roman letter A numbers the eight Gell-Mann matrices. The colour indices in the fundamental (complex conjugate) representation i and j span the colour

space and correspond to the QCD quantum numbers[6]. The hypercharge of left quark doublets Q_L^i is equal to 1/6.

Right-handed quarks are described by electroweak $SU(2)_L$ singlets. The corresponding gauge kinetic terms of the Lagrangians have the form

$$\mathcal{L}_{d,\,R} = \overline{d}_R^{\,i,\,m}\left\{ i\gamma^\mu\left[\left(\partial_\mu + ig'Y_W B_\mu\right)\delta_{ij} + ig_s\frac{\lambda_{ij}^A}{2}G_\mu^A\right]\right\} d_R^{j,\,m}\,, \tag{2.8}$$

$$\mathcal{L}_{u,\,R} = \overline{u}_R^{\,i,\,m}\left\{ i\gamma^\mu\left[\left(\partial_\mu + ig'Y_W B_\mu\right)\delta_{ij} + ig_s\frac{\lambda_{ij}^A}{2}G_\mu^A\right]\right\} u_R^{j,\,m}\,. \tag{2.9}$$

In the case of right-handed quarks, weak hypercharge and electric charge are the same: it is 2/3 in the case of up type quarks and $-1/3$ in the case of down type quarks.

The lepton sector looks very similar. The main difference in the lepton Lagrangian is the absence of the term, which is responsible for the strong interaction

$$\mathcal{L}_{l,\,L} = \overline{L}_L^m\left\{ i\gamma^\mu\left[\partial_\mu + ig'Y_W B_\mu + ig\frac{\sigma^a}{2}W_\mu^a\right]\right\} L_L^m\,, \tag{2.10}$$

$$\mathcal{L}_{l,\,R} = \overline{l}_R^m\left\{ i\gamma^\mu\left[\partial_\mu + ig'Y_W B_\mu\right]\right\} l_R^m\,. \tag{2.11}$$

Another difference is the lack of right-handed neutrinos. The right-handed neutrinos, if they exist, would be described by the kinetic term

$$\mathcal{L}_{\nu,\,R} = i\overline{\nu}_R^m\gamma^\mu\partial_\mu\nu_R^m\,, \tag{2.12}$$

and interact with other SM particles only through Higgs interaction. As of yet, there is no evidence for the existence of right-handed neutrinos. There might be a chance to detect one of these particles if their masses are much higher than the masses of their left-handed counterparts. Otherwise, it is very hard to imagine such an experiment where the Higgs particle is involved and the contribution of the neutrino could be observable.

The kinetic and self-interaction part of the Lagrangian for bosons is rather simple

$$\mathcal{L}_B = -\frac{1}{4}F^{\mu\nu}F_{\mu\nu} - \frac{1}{4}W^{a\,\mu\nu}W_{\mu\nu}^a - \frac{1}{4}G^{A\,\mu\nu}G_{\mu\nu}^A\,, \tag{2.13}$$

where

$$F_{\mu\nu} = \partial_\mu B_\nu - \partial_\nu B_\mu\,, \tag{2.14}$$

$$W_{\mu\nu}^a = \partial_\mu W_\nu^a - \partial_\nu W_\mu^a - g\varepsilon^{abc}W_\mu^b W_\nu^c\,, \tag{2.15}$$

$$G_{\mu\nu}^A = \partial_\mu G_\nu^A - \partial_\nu G_\mu^A - g_S f^{ABC}G_\mu^B G_\nu^C\,. \tag{2.16}$$

Here, ε^{abc} and f^{ABC} are $SU(2)_L$ and $SU(3)_c$ structure constants. The $SU(2)_L$ structure constant is represented by the totally antisymmetric Levi-Civita tensor, the $SU(3)_c$ constant are antisymmetric in index permutation and represented by

$$\begin{aligned} &f^{123} = 1\,,\\ &f^{147} = -f^{156} = f^{246} = f^{257} = f^{345} = -f^{367} = 1/2\,,\\ &f^{458} = f^{678} = \sqrt{3}/2\,. \end{aligned} \tag{2.17}$$

[6]Red, green and blue in the case of the fundamental representation and cyan, magenta, yellow (antired, antigreen, antiblue) in the case of the complex conjugate representation.

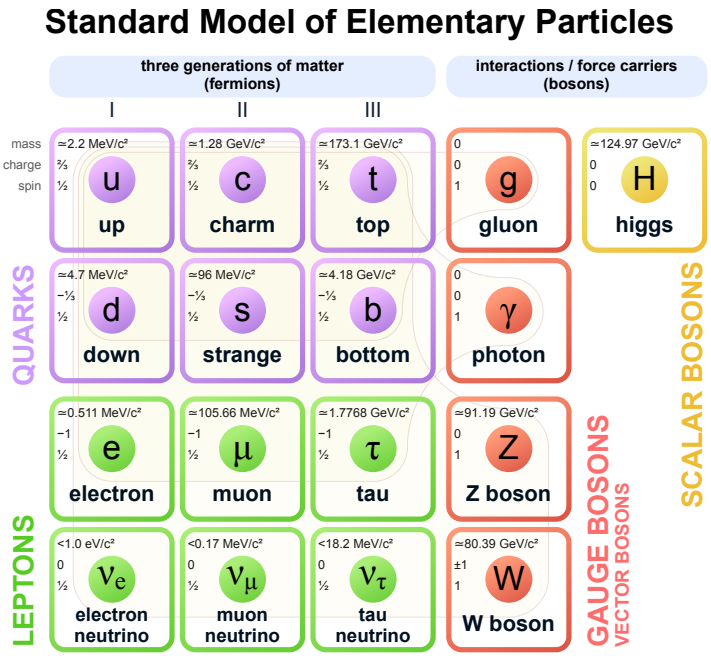

Figure 2.1: The Standard Model of elementary particles. 12 fermions are divided into quarks and leptons. Only left-handed particles participate in weak interactions. Quarks participate in all known interactions. Charged leptons participate, besides gravitational, in the electromagnetic and weak interaction, neutral neutrinos participate only in the gravitational and weak interaction. Brown loops connect fermions with corresponded bosons, which are the mediators of the interaction. The picture is taken from [48]

Until this point, all particles including the bosons B, W^a, and G^A are massless. From experiments, it is known that photons and gluons are massless, but $W^\pm$ and Z bosons are massive. This means that the symmetry $SU(2)_L \times U(1)_Y$ is broken into $U(1)_{em}$. In order to break the $SU(2)_L \times U(1)_Y$ symmetry, a few groups proposed reasonable mechanism of spontaneous breaking of the electroweak symmetry [8–10].

The idea, how to break the symmetry, was realized by introducing a complex scalar doublet

$$H = \begin{pmatrix} G^+ \\ \phi^0 \end{pmatrix} , \tag{2.18}$$

where G^+ and ϕ^0 are complex scalar fields. Neutral complex field ϕ^0 decomposes into the real scalar fields as

$$\phi^0 = (h + iG^0)/\sqrt{2} , \tag{2.19}$$

where h is represented the physical Higgs boson. These particles do not participate in the strong interaction. The Higgs boson is minimally coupled to gauge bosons as follows:

$$\mathcal{L}_H = \left((\partial_\mu + ig\frac{\sigma^a}{2} W^a_\mu + ig' Y_W B_\mu) H \right)^\dagger \left((\partial^\mu + ig\frac{\sigma^a}{2} W^{a\,\mu} + ig' Y_W B^\mu) H \right) . \tag{2.20}$$

The Higgs boson did not only solve the problem of gauge boson masses but, together with the Yukawa interaction, introduces masses for all fermions:

Notation	Description	Renormalization scheme/Scale	Value
m_e	Electron mass		511 keV
m_μ	Muon mass		105.7 MeV
m_τ	Tau lepton mass		1.78 GeV
m_u	Up quark mass	$\mu_{\overline{MS}} = 2$ GeV	1.9 MeV
m_d	Down quark mass	$\mu_{\overline{MS}} = 2$ GeV	4.4 MeV
m_s	Strange quark mass	$\mu_{\overline{MS}} = 2$ GeV	87 MeV
m_c	Charm quark mass	$\mu_{\overline{MS}} = 1.32$ GeV	1.32 GeV
m_b	Bottom quark mass	$\mu_{\overline{MS}} = 4.24$ GeV	4.24 GeV
m_t	Top quark mass	On-shell	173.5 GeV
m_h	Higgs boson mass		125.09 ± 0.24 GeV
v	Higgs vacuum expectation value		246 GeV
θ_{12}	CKM 12-mixing angle		0.229
θ_{13}	CKM 13-mixing angle		0.042
θ_{23}	CKM 23-mixing angle		0.003
δ	CKM CP violation phase		1.20
g'	$U(1)_Y$ gauge coupling	$\mu_{\overline{MS}} = 91.19$ GeV	0.357
g	$SU(2)_L$ gauge coupling	$\mu_{\overline{MS}} = 91.19$ GeV	0.652
g_S	QCD gauge coupling	$\mu_{\overline{MS}} = 91.19$ GeV	1.221
θ_c	QCD vacuum angle		$< 10^{-10}$

Table 2.2: Full list of the SM parameters [51]. Masses of neutrinos and PMNS mixing angles are not part of the SM.

$$\mathcal{L}_{Y,\,d} = Y^d_{ab}\,\overline{Q}^{j,\,a}_L H\, d^{j,\,b}_R + (Y^d_{ab})^\star\,\overline{d}^{j,\,b}_R \big(Q^{j,\,a}_L H\big)^\dagger\,, \tag{2.21}$$

$$\mathcal{L}_{Y,\,u} = Y^u_{ab}\,\overline{Q}^{j,\,a}_L \sigma_2 H^\star\, u^{j,\,b}_R + (Y^d_{ab})^\star\,\overline{d}^{j,\,b}_R \big(Q^{j,\,a}_L \sigma_2 H^\star\big)^\dagger\,, \tag{2.22}$$

$$\mathcal{L}_{Y,\,l} = Y^l_{ab}\,\overline{L}^a_L H l^b_R + (Y^l_{ab})^\star\,\overline{l}^b_R \big(L^a_L H\big)^\dagger\,, \tag{2.23}$$

where σ^2 is the second Pauli matrix, and star means complex conjugation. Masses in the SM are purely phenomenological. Within the SM there is no answer about the source of Yukawa coupling or why masses have these values.

The last important ingredient for the SM is the Higgs potential

$$V_H = -\mu^2 H^\dagger H + \frac{\lambda}{4}\left(H^\dagger H\right)^2\,, \tag{2.24}$$

with the dimensionless coupling $\lambda > 0$. The mass parameter μ^2 has "wrong" sign and is responsible for the *vev* generation, which leads to the symmetry breaking. More details about this will be discussed in the next section.

The full SM Lagrangian reads

$$\mathcal{L}_{SM} = \mathcal{L}_{q,\,L} + \mathcal{L}_{d,\,R} + \mathcal{L}_{u,\,R} + \mathcal{L}_{l,\,L} + \mathcal{L}_{l,\,R} + \mathcal{L}_B + \mathcal{L}_H + \mathcal{L}_{Y,\,u} + \mathcal{L}_{Y,\,d} + \mathcal{L}_{Y,\,l} - V_H\,. \tag{2.25}$$

One should mention that $\mathcal{L}_{\nu,\,R}$ is not part of the SM Lagrangian $\mathcal{L}_{SM}$. This means that neutrino oscillation [49,50,52] is not part of the SM. Neutrino mixing angles and neutrino masses are not included to the SM, only 19 parameters describe the SM. The values of these parameters are collected in Tab.2.2.

2.2 Higgs mechanism

The SM in the form, as it was introduced in the previous section, is completely massless. The mechanism which provides masses in the SM is called Higgs mechanism[7]. The key ingredient of this mechanism is contained in the scalar potential V_H (Eq. 2.24). The mass parameter μ of the scalar doublet is purely imaginary, implying that the mass term $\sim \mu^2$ has a negative sign.

This "wrong sign" implies two solutions for the extrema

$$\frac{\partial V_H}{\partial H} \stackrel{!}{=} 0 = H^\dagger \left(\frac{\lambda}{2} H^\dagger H - \mu^2 \right) , \tag{2.26}$$

The first solution is trivial and corresponds to a local maximum

$$H^\dagger = H = 0 . \tag{2.27}$$

The second solution corresponds to true minimum

$$H^\dagger H = \frac{2\mu^2}{\lambda} . \tag{2.28}$$

One can note few things from this analysis. First, the minima in this potential are given by the three-sphere S^3. Symmetry transformation relates points in this sphere, but any particular choice of point of this sphere breaks the symmetry spontaneously. In this case the Lagrangian of the theory is invariant under the symmetry transformation, but the ground state is not invariant. The convenient choice is

$$\langle H \rangle = \begin{pmatrix} 0 \\ v/\sqrt{2} \end{pmatrix} , \tag{2.29}$$

where $v = 2\mu/\sqrt{\lambda}$. This choice redefines Higgs field as

$$H = \begin{pmatrix} G^+ \\ (h + v + iG^0)/\sqrt{2} \end{pmatrix} . \tag{2.30}$$

In the second observation one will see that the second derivative of the potential provides the mass squared parameter for the field and shows that one of the field becomes massive while all others remain massless.

Writing down the bosonic and Higgs part of the SM Lagrangian, which are given by the Eq. 2.13 and Eq. 2.20, one obtains

$$\begin{aligned} \mathcal{L}_B + \mathcal{L}_H &= -\frac{1}{2} \left(\partial_\mu W^+_\nu - \partial_\nu W^+_\mu \right) \left(\partial^\mu W^{\nu -} - \partial^\nu W^{\mu -} \right) \\ &- \frac{1}{4} (\partial_\mu A_\nu - \partial_\nu A_\mu)(\partial^\mu A^\nu - \partial^\nu A^\mu) - \frac{1}{4} \left(\partial_\mu Z_\nu - \partial_\nu Z_\mu \right) \left(\partial^\mu Z^\nu - \partial^\nu Z^\mu \right) \\ &+ m_W^2 \left(W^+_\mu - \frac{i}{m_W} \partial_\mu G^+ \right) \left(W^{-\mu} + \frac{i}{m_W} \partial^\mu G^- \right) \\ &+ \frac{m_Z^2}{2} \left(Z_\mu - \frac{1}{m_Z} \partial_\mu G^0 \right) \left(Z^\mu - \frac{1}{m_Z} \partial^\mu G^0 \right) + \frac{1}{2} \partial_\nu h \partial^\nu h - \frac{m_H^2}{2} h^2 + \dots , \end{aligned} \tag{2.31}$$

[7] It also known as Anderson–Higgs–Kibble mechanism, Anderson–Higgs mechanism, Brout–Englert–Higgs mechanism, Englert–Brout–Higgs–Guralnik–Hagen–Kibble mechanism, Higgs–Kibble according to A. Salam and *ABEGHHK'tH* mechanism (Anderson, Brout, Englert, Guralnik, Hagen, Higgs, Kibble, and 't Hooft) according to P. Higgs.

where gluonic and interaction terms were omitted. Physical gauge bosons $W^{\pm}$ defined as

$$W^{\pm} = \frac{1}{\sqrt{2}}\left(W^1 \mp iW^2\right). \tag{2.32}$$

One needs to pay attention to the sign in the definition of the $W^{\pm}$ bosons. If one would take W^+ with positive imaginary part this would provide a problem with charge conservation in the Lagrangian. These relations one can easily read from the Lagrangian. The diagonalization of the mass matrix of the fields W^3 and B provides two new physical fields A_μ and Z_μ, which are defined as

$$\begin{aligned} A^3_\mu &= B_\mu \cos\theta_W - W^3_\mu \sin\theta_W\,, & (2.33)\\ Z_\mu &= B_\mu \sin\theta_W + W^3_\mu \cos\theta_W\,, & (2.34) \end{aligned}$$

where the Weinberg angle θ_W was introduced as a new parameter that mixes up B and W^3 bosons into physical states. Trigonometric functions $\cos\theta_W$ and $\sin\theta_W$ are expressed in terms of coupling constants as

$$\begin{aligned} \sin\theta_W &\equiv \frac{g'}{\sqrt{g^2+g'^2}}\,, & (2.35)\\ \cos\theta_W &\equiv \frac{g}{\sqrt{g^2+g'^2}}\,, & (2.36) \end{aligned}$$

where g and g' are $SU(2)_L$ and $U(1)_Y$ coupling constants, respectively. From the Lagrangian, one can also extract the SM boson masses

$$\begin{aligned} m_W &\equiv \frac{gv}{2}\,, & (2.37)\\ m_Z &\equiv m_W(\cos\theta_W)^{-1}\,, & (2.38)\\ m_H &\equiv \sqrt{\frac{\lambda v^2}{2}}\,. & (2.39) \end{aligned}$$

One should observe from these relations that the masses of the $W^{\pm}$ and Z bosons are strictly dependent on each other.

The redefinition of $W^{\pm}$ and Z fields as

$$\begin{aligned} W^{\pm}_\mu \mp \frac{i}{m_W}\partial_\mu G^{\pm} &\to W^{\pm}_\mu\,, & (2.40)\\ Z_\mu - \frac{1}{m_Z}\partial_\mu G^0 &\to Z_\mu\,, & (2.41) \end{aligned}$$

provides the Lagrangian which one expects, namely

$$\begin{aligned} \mathcal{L}_B + \mathcal{L}_H &= -\frac{1}{2}\left(\partial_\mu W^+_\nu - \partial_\nu W^+_\mu\right)\left(\partial^\mu W^{\nu-} - \partial^\nu W^{\mu-}\right)\\ &- \frac{1}{4}(\partial_\mu Z_\nu - \partial_\nu Z_\mu)(\partial^\mu Z^\nu - \partial^\nu Z^\mu)\\ &- \frac{1}{4}(\partial_\mu A_\nu - \partial_\nu A_\mu)(\partial^\mu A^\nu - \partial^\nu A^\mu) + m^2_W W^+_\mu W^{-\mu}\\ &+ \frac{m^2_Z}{2} Z_\mu Z^\mu + \frac{1}{2}\partial_\nu h \partial^\nu h - \frac{m^2_H}{2}h^2 + \dots\,. \end{aligned} \tag{2.42}$$

The Yukawa part of the SM Lagrangian is responsible for the generation of the fermion masses (Eqs. 2.21-2.23). By substituting the Higgs doublet with its *vev*, which is shown in the Eq. 2.30, one obtains

$$\mathcal{L}_{Y,\,d} + \mathcal{L}_{Y,\,u} + \mathcal{L}_{Y,\,l} = Y^{d}_{ab}\overline{d}^{\,j,\,a}_{L}\frac{v}{\sqrt{2}}d^{j,\,b}_{R} + Y^{u}_{ab}\overline{u}^{\,j,\,a}_{L}\frac{v}{\sqrt{2}}u^{j,\,b}_{R} + Y^{l}_{ab}\overline{l}^{\,a}_{L}\frac{v}{\sqrt{2}}u^{b}_{R} + h.c. + \dots\,, \tag{2.43}$$

where the interaction terms were omitted. For convenience, one can define mass matrices, which absorb Yukawa couplings, the *vev*, and constant factor $1/\sqrt{2}$ as

$$M^{d}_{ab} \equiv \frac{Y^{d}_{ab}v}{\sqrt{2}}\,, \quad M^{u}_{ab} \equiv \frac{Y^{u}_{ab}v}{\sqrt{2}}\,, \quad M^{l}_{ab} \equiv \frac{Y^{l}_{ab}v}{\sqrt{2}}\,. \tag{2.44}$$

These mass matrices have dimension 3×3. To obtain proper masses, these matrices should be diagonalized

$$\begin{aligned} M^{d}_{ab,\,\mathrm{diag}} &= \left(V^{d}_{L}\right)^{ac} M^{d}_{ce}\left(V^{d\dagger}_{R}\right)^{be}\,, \\ M^{u}_{ab,\,\mathrm{diag}} &= \left(V^{d}_{L}\right)^{ac} M^{u}_{ce}\left(V^{u\dagger}_{R}\right)^{be}\,, \\ M^{l}_{ab,\,\mathrm{diag}} &= \left(V^{l}_{L}\right)^{ac} M^{l}_{ce}\left(V^{l\dagger}_{R}\right)^{be}\,. \end{aligned} \tag{2.45}$$

This operation also redefines the fields in the mass basis

$$\begin{aligned} d^{j,\,a}_{L} &= (V^{d}_{L})^{ab} d'^{\,j,\,b}_{L}\,, & d^{j,\,a}_{R} &= (V^{d}_{R})^{ab}\, d'^{\,j,\,b}_{R}\,, \\ u^{j,\,a}_{L} &= (V^{u}_{L})^{ab} u'^{\,j,\,b}_{L}\,, & u^{j,\,a}_{R} &= (V^{u}_{R})^{ab}\, u'^{\,j,\,b}_{R}\,, \\ l^{a}_{L} &= (V^{l}_{L})^{ab}\, l'^{b}_{L}\,, & l^{a}_{R} &= (V^{d}_{R})^{ab}\, l'^{b}_{R}\,, \end{aligned} \tag{2.46}$$

where prime means that these fields are in the flavour base.

2.3 Cabibbo – Kobayashi – Maskawa matrix and Glashow – Iliopoulos – Maiani mechanism

The redefinition of the fields also implies changes in the interaction part of the SM Lagrangian. The inventors of the SM did not know about the second family of quarks [53–55], but the redefinition of fields, given by Eqs. 2.46 naturally describes weak interaction between quarks from different families. A typical vertex with quark transformation looks like

$$\mathcal{L}_{q,\mathrm{int}} = \frac{g}{\sqrt{2}}\overline{u}^{\,a}_{L,\,M}\left(V^{u}_{L}V^{d\dagger}_{L}\right)^{ab}\gamma^{\mu}W^{-}_{\mu}\,d^{b}_{L,\,M} + \frac{g}{\sqrt{2}}\overline{d}^{\,a}_{L,\,M}\left(V^{d}_{L}V^{u\dagger}_{L}\right)^{ab}\gamma^{\mu}W^{+}_{\mu}\,u^{b}_{L,\,M}\,, \tag{2.47}$$

where the colour indices are dropped for convenience. The unitary matrices, which transform left-handed up- and down-type quarks, are not the same. Because of this reason, the combination of up and down diagonalization matrices is not equal to the identity. This combination defines the Cabibbo–Kobayashi–Maskawa matrix [56], in short

$$(V_{CKM})^{ab} = \left(V^{u}_{L}V^{d\dagger}_{L}\right)^{ab}. \tag{2.48}$$

The *CKM* matrix is a 3×3 unitary matrix, with standard naming of the elements as

$$V_{CKM} = \begin{pmatrix} V_{ud} & V_{us} & V_{ub} \\ V_{cd} & V_{cs} & V_{cb} \\ V_{td} & V_{ts} & V_{tb} \end{pmatrix} . \tag{2.49}$$

This matrix connects down-type quarks in the flavour and mass basis

$$\mathbf{d} = V_{CKM}\mathbf{d}' , \tag{2.50}$$
$$\mathbf{u} = \mathbf{u}' , \tag{2.51}$$

where the vectors needs to be understood as elements of the family space. For convenience[8], up-type quarks in the mass representation are chosen the same as in the flavour one. Further, for simplicity, the index M will be dropped, and all quarks need to be understood in the mass base.

The elements of the *CKM* matrix are not completely arbitrary, it can be parametrized by 3 rotation angles and one phase (see Tab.2.2)

$$\begin{aligned} V_{CKM} &= \begin{pmatrix} c_{12} & s_{12} & 0 \\ -s_{12} & c_{12} & 0 \\ 0 & 0 & 1 \end{pmatrix} \begin{pmatrix} c_{13} & 0 & s_{13}e^{-i\delta} \\ 0 & 1 & 0 \\ -s_{13}e^{i\delta} & 0 & c_{13} \end{pmatrix} \begin{pmatrix} 1 & 0 & 0 \\ 0 & c_{23} & s_{23} \\ 0 & -s_{23} & c_{23} \end{pmatrix} \\ &= \begin{pmatrix} c_{12}c_{13} & s_{12}c_{13} & s_{13}e^{-i\delta} \\ -s_{12}c_{23} - c_{12}s_{23}s_{13}e^{i\delta} & c_{12}c_{23} - s_{12}s_{23}s_{13}e^{i\delta} & s_{23}c_{13} \\ s_{12}s_{23} - c_{12}c_{23}s_{13}e^{i\delta} & -c_{12}s_{23} - s_{12}c_{23}s_{13}e^{i\delta} & c_{23}c_{13} \end{pmatrix} , \end{aligned} \tag{2.52}$$

where $s_{ij} \equiv \cos\theta_{ij}$ and $c_{ij} \equiv \sin\theta_{ij}$. The phase δ is responsible for the CP-symmetry violation [57], and it can be chosen in many different ways. Here it was chosen to describe the relation between the first and third families.

Together with the standard, the Wolfenstein parameterization is also widely used

$$V_{CKM} = \begin{pmatrix} 1 - \lambda^2/2 & \lambda & A\lambda^3(\rho - i\eta) \\ -\lambda & 1 - \lambda^2/2 & A\lambda^2 \\ A\lambda^3(1 - \rho - i\eta) & -A\lambda^2 & 1 \end{pmatrix} + \mathcal{O}(\lambda^4) ,$$

where the four parameters θ_{12}, θ_{13}, θ_{23}, and δ were replaced by another four parameters A, ρ, η, and λ. The merit of this parameterization is simplicity[9]. Because λ is a small parameter, each element can be expanded as a power series in this parameter.

Unitarity of the *CKM* matrix also provides an interesting consequence. From the relation, which is written explicitly, namely

$$V_{CKM}V_{CKM}^{\dagger} = V_{CKM}^{\dagger}V_{CKM} = \begin{pmatrix} V_{ud} & V_{us} & V_{ub} \\ V_{cd} & V_{cs} & V_{cb} \\ V_{td} & V_{ts} & V_{tb} \end{pmatrix} \begin{pmatrix} V_{ud}^{\star} & V_{cd}^{\star} & V_{td}^{\star} \\ V_{us}^{\star} & V_{cs}^{\star} & V_{ts}^{\star} \\ V_{ub}^{\star} & V_{cb}^{\star} & V_{tb}^{\star} \end{pmatrix} = \begin{pmatrix} 1 & 0 & 0 \\ 0 & 1 & 0 \\ 0 & 0 & 1 \end{pmatrix} , \tag{2.53}$$

a few unitarity relations follows:

$$\begin{aligned} &V_{ud}V_{ud}^{\star} + V_{us}V_{us}^{\star} + V_{ub}V_{ub}^{\star} = 1 , \\ &V_{cd}V_{cd}^{\star} + V_{cs}V_{cs}^{\star} + V_{cb}V_{cb}^{\star} = 1 , \\ &V_{td}V_{td}^{\star} + V_{ts}V_{ts}^{\star} + V_{tb}V_{tb}^{\star} = 1 , \end{aligned} \tag{2.54}$$

[8] This is only one possible choice of the flavour basis.

[9] nice discusion of the Wolfenstein parametrization can be found in e.g. Ref. [58].

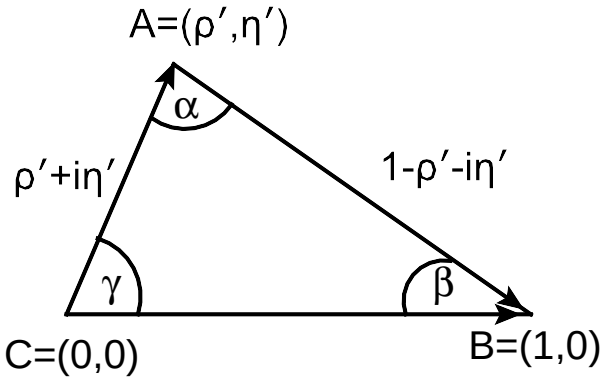

Figure 2.2: Unitary triangle.

---

which is the so-called *weak universality*, because the sum of the coupling strengths of the up-type quarks from each family to each down-type quarks is equal. Besides, the sum which is very close to 1 suppresses the possibility of a fourth family of quarks[10]. Another 12 relations are provided by *orthogonality conditions*, 6 relations from the $V_{CKM}V_{CKM}^{\dagger} = 1$ condition

$$\begin{aligned}
&V_{ud}V_{cd}^{\star} + V_{us}V_{cs}^{\star} + V_{ub}V_{cb}^{\star} = 0\,,\\
&V_{ud}V_{td}^{\star} + V_{us}V_{ts}^{\star} + V_{ub}V_{tb}^{\star} = 0\,,\\
&V_{cd}V_{ud}^{\star} + V_{cs}V_{us}^{\star} + V_{cb}V_{ub}^{\star} = 0\,,\\
&V_{cd}V_{td}^{\star} + V_{cs}V_{ts}^{\star} + V_{cb}V_{tb}^{\star} = 0\,,\\
&V_{td}V_{ud}^{\star} + V_{ts}V_{us}^{\star} + V_{tb}V_{ub}^{\star} = 0\,,\\
&V_{td}V_{cd}^{\star} + V_{ts}V_{cs}^{\star} + V_{tb}V_{cb}^{\star} = 0\,,
\end{aligned} \tag{2.55}$$

and also 6 relations from the $V_{CKM}^{\dagger}V_{CKM} = 1$ condition

$$\begin{aligned}
&V_{ud}^{\star}V_{us} + V_{cd}^{\star}V_{cs} + V_{td}^{\star}V_{ts} = 0\,,\\
&V_{ud}^{\star}V_{ub} + V_{cd}^{\star}V_{cb} + V_{td}^{\star}V_{tb} = 0\,,\\
&V_{us}^{\star}V_{ud} + V_{cs}^{\star}V_{cd} + V_{ts}^{\star}V_{td} = 0\,,\\
&V_{us}^{\star}V_{ub} + V_{cs}^{\star}V_{cb} + V_{ts}^{\star}V_{tb} = 0\,,\\
&V_{ub}^{\star}V_{ud} + V_{cb}^{\star}V_{cd} + V_{tb}^{\star}V_{td} = 0\,,\\
&V_{ub}^{\star}V_{us} + V_{cb}^{\star}V_{cs} + V_{tb}^{\star}V_{ts} = 0\,.
\end{aligned} \tag{2.56}$$

Each of these relations contains a complex phase. Because of this, they can be represented by a unitary triangle Fig 2.2. The quantities η' and ρ' are defined as

$$\eta' = \eta\left(1 - \frac{\lambda}{2}\right)\,, \quad \rho' = \rho\left(1 - \frac{\lambda}{2}\right)\,. \tag{2.57}$$

[10]The actual experimental status of the parameters [51] is

$$|V_{CKM}| = \begin{pmatrix} 0.97446 \pm 0.00010 & 0.22452 \pm 0.00044 & 0.00365 \pm 0.00012 \\ 0.22438 \pm 0.00044 & 0.97359^{+0.00010}_{-0.00011} & 0.04214 \pm 0.00076 \\ 0.00896^{+0.00024}_{-0.00023} & 0.04133 \pm 0.00074 & 0.999105 \pm 0.000032 \end{pmatrix}\,,$$

e.g. $|V_{ud}|^2 + |V_{us}|^2 + |V_{ub}|^2 = 0,999 \pm 0,0011$.

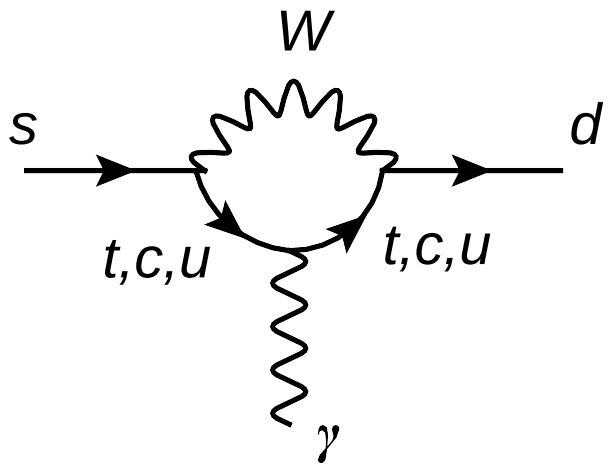

Figure 2.3: Typical flavour changing process with conserved charge

2.3.1 FCNC and GIM

The relations shown in Eqs. 2.55 and 2.56 suppress all electroweak processes for which electric charge is conserved during changes of flavour. First of all, in the SM, at tree-level, there is no such vertex, which connects two quarks with the same charge from different families. Processes, which provide flavour changing, necessarily involve $W^{\pm}$ bosons. To obtain a flavour changing process with conserved electric charge, the W-vertex needs to appear in the process an even number of times. This is only possible within a loop process, but the contribution of such loops is highly suppressed.

As an example why flavour changing neutral current processes are suppressed in the SM, one can consider the process $s \to d\gamma$, one of the diagrams of this process is shown on Fig. 2.3. The contribution from this process $\mathcal{A}$ can be divided into two parts $\mathcal{A}_x + \mathcal{A}_y = \mathcal{A}$. One of these parts is proportional to the direct sum of the elements of the *CKM* pairs

$$\mathcal{A}_x \propto (V_{ts}V_{td}^{\star} + V_{cs}V_{cd}^{\star} + V_{us}V_{ud}^{\star}) \,, \tag{2.58}$$

another contribution is proportional to the sum of pairs of *CKM* elements, where each of the pairs is also multiplied by corresponding propagators

$$\mathcal{A}_y \propto (V_{ts}V_{td}^{\star}G(m_t) + V_{cs}V_{cd}^{\star}G(m_c) + V_{us}V_{ud}^{\star}G(m_u)) \,, \tag{2.59}$$

where $G(m_x)$ is an arbitrary function that is proportional to the mass of corresponding quark m_x. In the first case, this contribution simply equals zero because of the orthogonality condition given in Eq.2.56. In the second case, using the same orthogonality condition, one can rewrite Eq. 2.59 as

$$\mathcal{A}_y \propto (V_{ts}V_{td}^{\star}G(m_t) + V_{cs}V_{cd}^{\star}G(m_c) - (V_{ts}V_{td}^{\star} + V_{cs}V_{cd}^{\star})G(m_u)) \,. \tag{2.60}$$

In a comparison with top quark mass m_t, with good approximation, the masses of the charm quark m_c and up quark m_u can be set as equal. In this case $\mathcal{A}_y$ reduces to

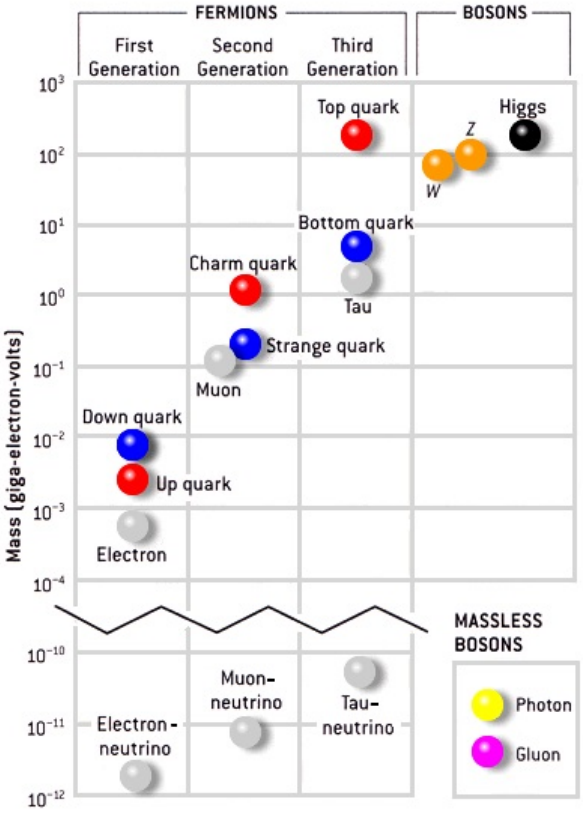

Figure 2.4: Masses of the SM particles on corresponding mass scale. The picture is taken from [85]

$$\mathcal{A}_y \sim V_{ts}V_{td}^{\star}G(m_t) \sim V_{ts}V_{td}^{\star}F\left(\frac{m_t^2}{m_W^2}\right). \tag{2.61}$$

The contribution is not only suppressed by the loop factor $1/(4\pi)^2$, but it is also suppressed by the very small element V_{td} which is proportional to the third power of the Wolfenstein parameter λ. This effect is the so-called *GIM* mechanism [60].

2.4 Problems of the Standard Model

The SM, which includes the Weinberg-Salam electroweak theory and QCD [61], together with General Relativity and quantum mechanics was one of the biggest scientific successes of the 20^{th} century. The SM predicted the mediators of the weak interaction - W and Z and the relation between their masses [62–64]. As well, by the SM, the charm [54,55] and top [65,66] quarks were predicted. The Higgs boson [67,68] is also a SM prediction.

Nevertheless, the SM cannot be a final theory. First of all, in the SM there is no place for the fourth fundamental force. Gravity, which is the longest known of all discovered forces, is completely ignored by the SM. Moreover, there is no space to incorparate gravity in the SM. The SM is a quantum theory, but it is unknown if it is possible to quantize gravity. Attempts to quantize gravity classically end up with theories which are non-renormalizable or non-unitary [69].

Another big problem is Dark Matter and Dark Energy. Only particle-like DM satisfies all

observational evidence [70–77]. And this particle or these particles are not a part of the SM [78]. With dark energy even more questions arise and this phenomenon, as well, is not included in the SM.

As it was mentioned in Sec.2.1, neutrino masses are not part of the SM. One of the solutions to the mass problem is the introduction of the term given by Eq. 2.12, but neutrinos can be their own anti-particles and can be described by a Majorana Lagrangian without right-handed counterparts. A modification to the lepton Lagrangian (Eq.2.10) would look like

$$\mathcal{L}_{\nu,mass} = -\frac{m}{2}\left(\overline{\nu}_L \nu_L^c + h.c.\right), \tag{2.62}$$

where $\nu^c = C\overline{\nu}_L^T$, and C is the charge conjugation operator represented as $C = i\gamma^0\gamma^2$. In this case, the source of the neutrino mass is not a Yukawa term. Confirmation of the Majorana nature of neutrinos could be the observation of neutrinoless double beta decay, but actual searches have found no evidence for this type of decay, or any evidence of the existence of right-handed neutrinos.

Another problem of the SM is baryon and lepton asymmetry. The observed universe consists of matter and not of anti-matter. To describe the baryon asymmetry, the model needs to satisfy with a few conditions which are formulated by Sakharov [80]. The SM does not satisfy these conditions. CP-violation which is provided by the SM is restricted very much by B-meson [81] and kaon [59,82,83] physics and not large enough to describe the observed Universe. Also the SM does not provide a good source for the first-order phase transition [84]. A similar story concerns leptogenesis.

In the QCD sector, the SM cannot explain the strong CP-problem. The QCD Lagrangian can be extended without breaking any, including gauge $SU(3)$, symmetries by the term

$$\mathcal{L}_{\theta_s} = \frac{\theta_s}{16\pi^2} F^A_{\mu\nu} \tilde{F}^{A\mu\nu}, \tag{2.63}$$

where

$$\tilde{F}^{A\mu\nu} = \epsilon^{\mu\nu\lambda\rho} F^A_{\lambda\rho}, \tag{2.64}$$

and where $\epsilon^{\mu\nu\lambda\rho}$ is the totally antisymmetric tensor. This term is a source of CP-violation, but experiment has shown that $\theta < 10^{-10}$. There are a few explanations of this curious fact [86]: 1) unconventional dynamics[11], 2) spontaneously broken CP-symmetry, 3) extra chiral symmetry. And none of these explanations is originated from the SM.

Another reason, why the SM cannot be the final theory, are 19 ad-hoc parameters, which must be determined from experiment. The SM cannot explain the difference between masses of particles, e.g. does not provide an explanation why the up quark is lighter than the down quark, but in 2$^{\text{nd}}$ and 3$^{\text{rd}}$ families up-type quarks are heavier than the corresponding down-type[12]. The SM does not shed the light on the structure of the CKM matrix. The SM cannot explain the difference in scales, why there is a difference between the weak force and gravity of 24 orders of magnitude.

The SM has also problems with the Higgs boson [87,88]: The Higgs boson mass, $m_H^2 = \lambda v^2/2$, is quadratically unstable against radiative corrections. For the Higgs boson there is no symmetry in the SM that protects its mass from radiative corrections.

[11] This problem is resolved e.g. by axions.

[12] Masses of particles with corresponding scales are shown in Fig.2.4.

Chapter 3

New physics

3.1 Baryogenesis problem

The problems that were discussed in Sec. 2.4 are hard to solve. This thesis does not pretend to solve all problems of the SM, but here ideas will be proposed on how to solve some of them. In this chapter, an extended scalar sector will be discussed, which can be the solution for a few problems at once.

One of the SM's problems, which was discussed in the previous chapter, is the impossibility to provide the baryonic and leptonic asymmetry observed in the Universe. In the SM, there is a source of CP-symmetry breaking, but this source cannot provide the result which is observed. To measure this, one can introduce the Jarlskog invariant [89]

$$J = (m_t^2 - m_c^2)(m_t^2 - m_u^2)(m_c^2 - m_u^2)(m_b^2 - m_s^2)(m_b^2 - m_d^2)(m_s^2 - m_d^2) \cdot K \,, \tag{3.1}$$

where

$$K = s_1^2 s_2 s_3 c_1 c_2 c_3 \sin\delta = \operatorname{Im} V_{ii} V_{jj} V_{ij}^\star V_{ji}^\star \,, \tag{3.2}$$

for $i \neq j$. This function is invariant under the quark redefinition and can be obtained from the determinant of the up- and down-types quarks square mass matrices commutator

$$J = \det\left[M^u M^{u\dagger},\, M^d M^{d\dagger}\right] . \tag{3.3}$$

The relevant dimensionless proportionality factor that enters the prediction of baryon asymmetry is denoted by δ_{CP}. To obtain this suppression factor, one must divide the Jarlskog invariant by the temperature of the electroweak phase transition, which for the minimal temperature ~ 100 GeV (which is enough to produce sufficiently large non-perturbative sphalerons effects[1]) produces the result

$$\delta_{CP} \simeq \frac{J}{(T_c^{BG})^{12}} \simeq 10^{-20} \,, \tag{3.4}$$

which is much smaller than $\delta_{CP} \sim 10^{-10}$ needed for electroweak baryogenesis [90, 91].

To explain baryogenesis one needs to find additional sources of CP-violation. One such source can be obtained from models with a second Higgs doublet [92–96]. 2HDMs are not the only possible solution of this problem, moreover, 2HDMs do not help to solve other problems

[1] Sphalerons effects need for baryon number violation, which is important for the generation of the baryon and lepton asymmetry.

of the electroweak baryogenesis, but 2HDMs have other merits why these models deserve the attention.

Another motivation for 2HDM comes from the strong CP-problem. The problematic term can be rotated away in models with an additional global $U(1)$ symmetry, and the 2HDM is one of the simplest models in which this can be realised [97]. The original model, which was proposed by Peccei and Quinn, is already excluded by experiments, but the variations of this model with singlets at high scales are still viable (e.g. [98]).

3.2 2HDM

2HDMs provide a much richer vacuum structure than the SM Higgs doublet. The most general scalar potential can have CP-conserving or CP-violating minima, as well as a minimum which can violate charge. Some of these terms violate CP-symmetry in the sector which corresponds to the SM Higgs sector. The most general potential which is absent of these undesirable features is written as [99]

$$\begin{aligned} V_{2HD} &= m_{11}^2\, H_1^\dagger H_1 + m_{22}^2\, H_2^\dagger H_2 - m_{12}^2 \left(H_1^\dagger H_2 + H_2^\dagger H_1\right) + \frac{\lambda_1}{2}\left(H_1^\dagger H_1\right)^2 + \frac{\lambda_2}{2}\left(H_2^\dagger H_2\right)^2 \\ &+ \lambda_3\, H_1^\dagger H_1\, H_2^\dagger H_2 + \lambda_4\, H_1^\dagger H_2\, H_2^\dagger H_1 + \frac{\lambda_5}{2}\Big[\left(H_1^\dagger H_2\right)^2 + \left(H_2^\dagger H_1\right)^2\Big], \end{aligned} \tag{3.5}$$

where the second Higgs doublet H_2 has hypercharge -1/2, and is written explicitly as

$$H_a = \begin{pmatrix} G_a^+ \\ (h_a + v_a + iG_a^0)/\sqrt{2} \end{pmatrix}, \tag{3.6}$$

where $a = 1, 2$ denotes the affiliation to the first or second Higgs doublet. Three of these Goldstone bosons $G_1^\pm$ and G_1^0 are eaten to produce the masses of the $W^\pm$ and Z^0 gauge bosons, another scalar boson h_1 corresponds to the SM Higgs particle, and additionally two charged scalars $G_2^\pm$, one real scalar h_2 and one pseudoscalar G_2^0 are produced. The charged scalars obtain their masses from the relation [99]

$$\mathcal{L}_{G^\pm,\,m} = \big(m_{12}^2 - (\lambda_4+\lambda_5)v_1v_2\big)\begin{pmatrix} G_1^- & G_2^- \end{pmatrix}\begin{pmatrix} v_2/v_1 & -1 \\ -1 & v_1/v_2 \end{pmatrix}\begin{pmatrix} G_1^+ \\ G_2^+ \end{pmatrix}, \tag{3.7}$$

where one extracts the mass of charged scalar as $m_{G_2^\pm}^2 = [m_{12}^2/(v_1v_2) - \lambda_4 - \lambda_5]\big(v_1^2 + v_2^2\big)$.
The mass for the pseudoscalar is extracted from

$$\mathcal{L}_{G^0} = \big[m_{12}^2/(v_1v_2) - 2\lambda_5\big]\begin{pmatrix} G_1^0 & G_2^0 \end{pmatrix}\begin{pmatrix} v_2^2 & -v_1v_2 \\ -v_1v_2 & v_1^2 \end{pmatrix}\begin{pmatrix} G_1^0 \\ G_2^0 \end{pmatrix}, \tag{3.8}$$

providing a mass for the physical pseudoscalar $m_{G_2^0}^2 = \big[m_{12}^2/(v_1v_2) - 2\lambda_5\big]\big(v_1^2 + v_2^2\big)$.
The scalar mass terms are given by

$$\mathcal{L}_{h^0} = \begin{pmatrix} h_1 & h_2 \end{pmatrix}\begin{pmatrix} m_{12}^2 v_2/v_1 + \lambda_1 v_1^2 & -m_{12}^2 + (\lambda_3+\lambda_4+\lambda_5)v_1v_2 \\ -m_{12}^2 + (\lambda_3+\lambda_4+\lambda_5)v_1v_2 & m_{12}^2 v_1/v_2 + \lambda_2 v_2^2 \end{pmatrix}\begin{pmatrix} h_1 \\ h_2 \end{pmatrix}. \tag{3.9}$$

The scalar boson mass matrix can be diagonalized. The standard naming of the angle parameter, which corresponds to the scalar mass matrix rotation, is α.

Another parameter, which rotates the mass matrices of the pseudo- and charged scalars, is β. This angle can be defined as

$$\tan\beta \equiv \frac{v_2}{v_1}\,. \tag{3.10}$$

One can redefine the doublets such that the *vev*s remain only in the first one, namely

$$\begin{aligned} H_1' &= \cos\beta H_1 + \sin\beta H_2\,, \\ H_2' &= -\sin\beta H_1 + \cos\beta H_2\,. \end{aligned} \tag{3.11}$$

This provides explicitly

$$H_1' = \begin{pmatrix} G_1'^{+} \\ (h_1' + v + iG_2'^{0})/\sqrt{2} \end{pmatrix}\,, \quad H_2' = \begin{pmatrix} G_2'^{+} \\ (h_2' + iG_2'^{0})/\sqrt{2} \end{pmatrix}\,, \tag{3.12}$$

where $v \equiv \left(v_1^2 + v_2^2\right)^{1/2}$. The two parameters α and β determine the interactions between all these new particles produced by 2HDMs, and the SM bosons and fermions.

For a general 2HDM, the largest problem is the appearance of FCNCs at the tree level. To avoid this, all fermions with the same quantum numbers need to be coupled to only one Higgs multiplet. Absence of FCNC, in this case, is ensured by the Paschos - Glashow - Weinberg theorem [100, 101]. This theorem says that in multi-Higgs models, it is sufficient that all right-handed fermions of the same charge couple to the same scalar multiplet. In 2HDM this can be realized if an extra discrete or continuous symmetry exists. It can be realized only in two ways: first, all quarks are coupled to the same multiplet, conventionally, it is usually H_2, and these types of models are called 2HDM type I. The second possibility is that up-type quarks couple to the one doublet, the standard choice is usually H_2, and down-type quarks couple to the other doublet H_1. The presence of the symmetry $H_1 \to -H_1$ automatically provides the 2HDM type I. While, the theory automatically satisfies type II if it preserves the same symmetry $H_1 \to -H_1$ together with the symmetry $d_R^m \to -d_R^m$, where m is a family index and the colour index is dropped for convenience. Concerning the coupling of leptons, there are also two models - Lepton-specific and Flipped. In Lepton-specific models, both right-handed down- and up-type quarks are coupled to H_2 doublets, while right-handed leptons are coupled to H_1. In Flipped models, up-type quarks and charged leptons are coupled to the same doublet H_2, while right-handed down-type quarks are coupled to the H_1 doublet [99].

3.3 Extra scalar and Higgs portal

A simpler solution of the CP-violation problem in baryogenesis, which is explained in Sec. 3.1, is a real scalar singlet [102]. These models also provide a solution to the DM problems.

The most general renormalizable Lagrangian for such models is

$$\begin{aligned} V_S &= -\frac{\mu^2}{2}H^\dagger H + \frac{\lambda}{4}\left(H^\dagger H\right)^2 + \frac{\alpha_1}{2}H^\dagger H\phi + \frac{\alpha_2}{2}H^\dagger H\phi^2 \\ &- \frac{\alpha_1\mu^2}{2\lambda}\phi + \frac{m^2}{2}\phi^2 + \frac{\kappa_3}{3}\phi^3 + \frac{\kappa_4}{4}\phi^4\,, \end{aligned} \tag{3.13}$$

where H is the standard Higgs doublet defined in Eq. 2.30, λ and μ are the same parameters as were defined in Eq. 2.24. The linear term $\alpha_1\mu^2\phi/2\lambda$ is needed to not acquire *vev* for the scalar ϕ. The parameter α_1 controls the degree of mixing between the scalar ϕ and the SM Higgs h. For the models where this term is absent, the mass of the scalar ϕ is determined by the parameters α_2 and m^2. The unification of the SM and Dark sector described by the potential V_S (Eq. 3.13) so-called Higgs portal.

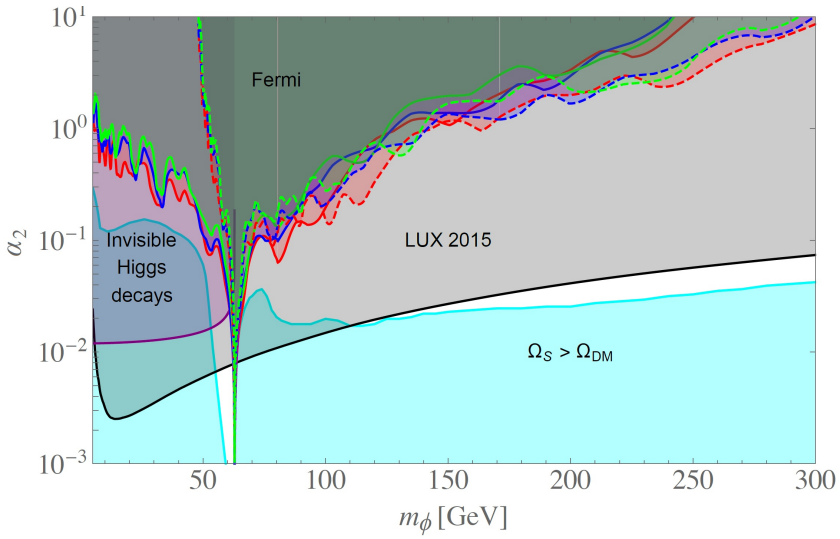

Figure 3.1: For DM that is represented by an extra scalar the correct relic abundance is given by the cyan line. The region below the solid cyan line corresponds to the overabundance and the region above the solid black line is excluded by collider experiments. The plot is taken from Ref. [106].

The light scalar particle ϕ couples to the same vertices as the SM Higgs h because of its mixing with SM Higgs. The decay rates of the lightest mixed scalar state h_2 are equal to the decay rates of the SM Higgs boson reduced by $\sin^2\theta$, where θ is the mixing parameter. The decay rates of the heaviest state h_1 are not only reduced by $\cos^2\theta$ but also, in the case $m_{h_1} > 2m_{h_2}$, further modified due to the opening of the decay channel $h_1 \to 2h_2$. The observed excess of $h \to b\bar{b}b\bar{b}$ or $b\bar{b}\tau\bar{\tau}$ could be the evidence of the presence of the $h_1 \to 2h_2$ process [102]. This process can provide an electroweak phase transition of the first order and explain the baryon asymmetry of the universe [103].

An extra scalar cannot be a candidate for DM in a model with all non-zero parameters because of its instability. However, in the case of the invariance of the potential with an extra scalar (Eq. 3.13) under a Z_2 symmetry, which is equivalent to the choice $\alpha_1 = 0$ and $\kappa_3 = 0$, the scalar can be a candidate to the DM particle [104, 105]. After electroweak symmetry breaking in such models, the potential is

$$V_S = \frac{\mu^4}{4\lambda} + \mu^2 h^2 + \lambda v h + \frac{\lambda}{4}h^4 + \frac{1}{2}(m^2 + \kappa_2 v^2)\phi^2 + \frac{\kappa_4}{4}\phi^4 + \alpha_2 v \phi^2 h + \frac{\alpha_2}{2}\phi^2 h^2 . \quad (3.14)$$

Necessary conditions for the DM, which is represented by an extra scalar particle ϕ, are $\lambda \geq 0$, $\kappa_4 \geq 0$, and $\lambda\kappa_4 \geq \alpha_2^2$ for negative α_2 [106]. All phenomenological properties of such models are completely determined by the parameters α_2 and m or α_2 and $m_\phi = m^2 + \kappa_2 v^2$. Phenomenological restrictions are shown in Fig. 3.1.

3.3.1 Second Higgs boson represented by an extra scalar

An extra scalar can represent a CP-odd Higgs boson, which can be a source of CP-symmetry violation [107–111]. It is convenient to mix two scalars h and ϕ into two physical states in the mass eigenbasis

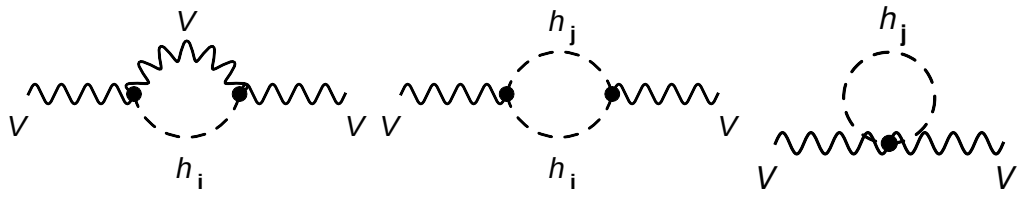

Figure 3.2: Z and W propagators with polarization loops, where h_i denotes both heavy and light scalar bosons

$$\begin{pmatrix} h_1 \\ h_2 \end{pmatrix} = \begin{pmatrix} \cos\theta & -\sin\theta \\ \sin\theta & \cos\theta \end{pmatrix} \begin{pmatrix} h \\ \phi \end{pmatrix} . \tag{3.15}$$

The branching fraction for the heaviest boson decaying into SM particles in the case that the decay into the two lightest bosons is kinematically allowed, according to Ref. [102] is given by

$$Br(h_1 \to X_{\rm SM}) = \frac{\sin^2\theta\, Br(h \to X_{\rm SM})\Gamma_h}{\sin^2\theta\,\Gamma_h + \Gamma(h_1 \to h_2 h_2)} , \tag{3.16}$$

where Γ_h is the total decay rate of the SM Higgs boson, and where the decay rate of the heaviest scalar into two lightest is given by

$$\Gamma(h_1 \to h_2 h_2) = \frac{|g_{122}|^2}{32\pi m_{h_1}} \sqrt{1 - \frac{4m_{h_2^2}}{m_{h_1^2}}} , \tag{3.17}$$

where the coupling g_{122} is given by

$$\begin{aligned} g_{122} &= \frac{1}{2}\alpha_1 \cos^3\theta + (2\kappa_3 - \alpha_1)\sin^2\theta\cos\theta \\ &- \frac{v}{2}\sin\theta(3\lambda\cos^2\theta + 2\alpha_2(1 - 3\cos^2\theta)) . \end{aligned} \tag{3.18}$$

The decay is kinematically allowed only for

$$(\lambda - 4\lambda_\phi)(4\lambda - \lambda_\phi) + 25\frac{\alpha_1^2}{v^2} > 0 , \tag{3.19}$$

where $\lambda_\phi = \alpha_2 + 2m^2/v^2$.

The main restriction on such models comes from the electroweak precision observables. An extra scalar affects the W and Z gauge boson propagators which are generated by the one-loop diagrams shown in Fig. 3.2 [102].

Chapter 4

Loop Calculations

4.1 Introduction

The main goal of QFT is a description of physics at the particle level. It is not a deterministic theory, QFT can only describe the probability of the evolution from one quantum state to another. The normalised differential probability is given by the formula

$$dP_{fi} = \frac{|\langle f|S|i\rangle|^2}{\langle i|i\rangle\langle f|f\rangle} d\Pi\,, \tag{4.1}$$

where $\langle f|$ is a final state, $|i\rangle$ is an initial state, and S is the S-matrix which contains all information about the evolution of states in time, $d\Pi$ is the normalised infinitesimal final state momenta

$$d\Pi = \prod_i \frac{V}{(2\pi)^3} d^3p_i\,. \tag{4.2}$$

Squared modulus of S-matrix $S_{fi} = \langle f|S|i\rangle$ is given as

$$|\langle f|S|i\rangle|^2 = TV(2\pi)^4\delta\big(\sum_i p_i\big)|\langle f|\mathcal{A}|i\rangle|^2\,, \tag{4.3}$$

where $\mathcal{A}$ is a scattering amplitude, p_i are all external four-momenta, T is the time interval and V the volume. In general, both of these values are infinitely large, but in the case of normilised differential probability T and V are canceled out in the final expression.

The time ordered S-matrix according to unitary transformation analysis has the form

$$S = U(\infty, -\infty) = \lim_{\kappa\to 0} T\left(\exp\Big(-\int_{-\infty}^{\infty} dt H_I^{(\kappa)}(t)\Big)\right), \tag{4.4}$$

where

$$\lim_{\kappa\to 0} H_I^{(\kappa)}(t) = \lim_{\kappa\to 0} e^{-\kappa|t|} H_I(t), \tag{4.5}$$

where T is a time ordering operator, and H_I is the interaction part of the Hamiltonian in the interaction picture, κ is a regulative parameter. The only known way to obtain the probability is to expand the exponent in the series

$$\begin{aligned} S &= 1 - \lim_{\kappa\to 0} i\int_{-\infty}^{\infty} dt\, H_I^{(\kappa)}(t) \\ &+ \lim_{\kappa\to 0} \frac{(-i)^2}{2!}\iint_{-\infty}^{\infty} dt' dt\, T\big(H_I^{(\kappa)}(t') H_I^{(\kappa)}(t)\big) + \dots\,. \end{aligned} \tag{4.6}$$

For the evaluation one needs to substitute the Hamiltonian in its explicit form, then one needs to apply the Wick theorem and to evaluate every term one by one. For convenience, Feynman diagrams have been introduced. In the Feynman diagrams method, every term, which was obtained from Wick's theorem, corresponds to a diagram. For every diagram, one obtains expressions for further evaluation according to the initially determined rules. At least one Feynman diagram corresponds to every order of perturbation theory. Trivial diagrams correspond to the first order of the expansion, without any interactions. The second order of the expansion is called the tree level. Any evaluation of initial states is possible only starting from the tree level.

The series needs to be convergent in order to obtain the probability. This means that every next element of the series expansion provides smaller contributions to the S-matrix. In many cases, the probability, which is obtained for the tree level, agrees very well with experimental results, and it seems that higher-order terms in the expansion are not important and can be neglected. Besides precision calculations, there are many processes, which appear only at the third order of the S-matrix expansion or at the one-loop level. The next two sections will be dedicated to such processes. In this section, I briefly try to explain ideas and techniques which are necessary to perform one loop calculations.

4.2 Simple example

Dimensional regularization is very convenient to evaluate Feynman integrals. This type of regularization preserves Lorentz and gauge invariance, which is not true for many other popular methods of regularization like cut-off or Pauli–Villars.

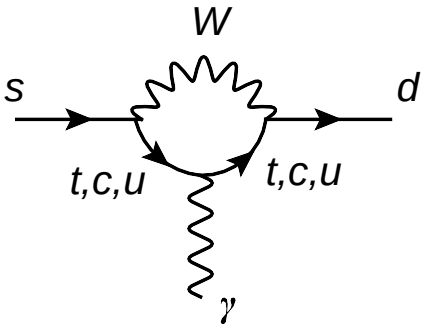

Figure 4.1: One of the loop diagrams for the process $s \to d\gamma$

In this subsection, the evaluation of a diagram from the process $s \to d\gamma$ (Fig.4.1) will be presented as an example of the standard method of integration over internal loop momentum. The example is not the simplest but it contains all necessary features which need to be considered in Sec.4.5 about semiautomatic tools for the loop-amplitudes evaluation. The diagram with virtual W-boson exchange reads

$$\begin{aligned} i\mathcal{A} &= -\int \frac{d^D k}{(2\pi)^D}\Big[\Big(ig^{\nu\rho}\epsilon^{\mu}(p_\gamma)\overline{d}(p_1)\frac{i\bar{e}V_{Ud}^{*}\gamma_\nu P_L}{\sqrt{2}\sin\theta_W}(\gamma_\beta k^\beta + m_U)\left(-\frac{2i\bar{e}}{3}\gamma_\mu\right) \\ &\times \big(\gamma_\alpha(k-p_1-p_2)^\alpha + m_U\big)\frac{i\bar{e}V_{Us}\gamma_\rho P_L}{\sqrt{2}\sin\theta_W}s(p_2)\Big)/\Big((k^2-m_U^2) \\ &\times \big((k-p_1)^2-m_W^2\big)\big((k-p_1-p_2)^2-m_U^2\big)\Big)\Big], \end{aligned} \tag{4.7}$$

where m_U denotes the masses of all up-type quarks in the loop, k is a loop momentum, p_1 and p_2 are external momenta of d- and s-quarks, respectively, and $\bar{e}$ is the coupling constant

in D dimensions, $P_L = (1-\gamma_5)/2$ denotes the projection operator on the left-handed chiral states. Here, the Feynman rules are applied to all vertices and propagators without further simplification. The expression becomes more compact after the simplification

$$\begin{aligned} i\mathcal{A} &= \int \frac{d^D k}{(2\pi)^D} \Big[\bar{e}^3 \sin\theta_W V_{Ud}^* V_{Us} \overline{d}(p_1)\gamma^\rho P_L (\gamma\cdot k + m_U)(\epsilon(p_\gamma)\cdot\gamma) \\ &\times \big(\gamma\cdot(k-p_1-p_2)+m_U\big)\gamma_\rho P_L s(p_2)\Big] \Big/ \Big[3(k^2-m_U^2) \\ &\times \big((k-p_1)^2-m_W^2\big)\big((k-p_1-p_2)^2-m_U^2\big)\Big]. \end{aligned} \tag{4.8}$$

All tasks for this amplitude evaluation can be divided into two steps: 1) evaluation of the Dirac algebra 2) evaluation of scalar integrals. From the numerator, one can extract three Dirac structures

$$N_{1,\mathrm{Dirac}} = \overline{d}(p_1)\gamma^\rho P_L \gamma^\alpha \gamma^\beta \gamma^\mu \gamma_\rho P_L s(p_2)\,, \tag{4.9}$$
$$N_{2,\mathrm{Dirac}} = \overline{d}(p_1)\gamma^\rho P_L \gamma^\alpha \gamma^\beta \gamma_\rho P_L s(p_2)\,, \tag{4.10}$$
$$N_{3,\mathrm{Dirac}} = \overline{d}(p_1)\gamma^\rho P_L \gamma^\alpha \gamma_\rho P_L s(p_2)\,. \tag{4.11}$$

Also, there are one scalar and two tensor integrals for the evaluation

$$L_1 = \bar{e}^3 \int \frac{d^D k}{(2\pi)^D} \frac{1}{(k^2-m_U^2)\big((k-p_1)^2-m_W^2\big)\big((k-p_1-p_2)^2-m_U^2\big)}\,, \tag{4.12}$$
$$L_2 = \bar{e}^3 \int \frac{d^D k}{(2\pi)^D} \frac{k^\mu}{(k^2-m_U^2)\big((k-p_1)^2-m_W^2\big)\big((k-p_1-p_2)^2-m_U^2\big)}\,, \tag{4.13}$$
$$L_3 = \bar{e}^3 \int \frac{d^D k}{(2\pi)^D} \frac{k^\mu k^\nu}{(k^2-m_U^2)\big((k-p_1)^2-m_W^2\big)\big((k-p_1-p_2)^2-m_U^2\big)}\,. \tag{4.14}$$

One of the main disadvantages of the dimensional regularization is a complication with the Dirac algebra. The problem arises from the impossibility to define the γ_5 matrix explicitly. For one-loop integrals, when the number of gamma matrices is not large, it is possible to use the NDR scheme, in which the γ_5 matrix is defined by the anticommutation relation $\{\gamma^\mu, \gamma_5\} = 0$. More details about the evaluation of the Dirac algebra will be provided in the Sect.4.4. Applying the anticommutation relation $\{\gamma^\mu,\, \gamma^\nu\} = 2\, g^{\mu\nu}$, the result of the Dirac algebra evaluation is

$$N_{1,\mathrm{Dirac}} = \overline{d}(p_1)\big((4-D)\gamma^\alpha\gamma^\beta\gamma^\mu P_L - 2\gamma^\mu\gamma^\beta\gamma^\alpha P_L\big)s(p_2)\,, \tag{4.15}$$
$$N_{2,\mathrm{Dirac}} = 0\,, \tag{4.16}$$
$$N_{3,\mathrm{Dirac}} = \overline{d}(p_1)(2-D)\gamma^\alpha P_L s(p_2)\,. \tag{4.17}$$

The standard method to evaluate loop integrals with dimensional regularization is the Feynman parameterization. The idea of the Feynman parametrization is to reduce the integral to the form of the Euler integral of the first kind, which can be decomposed to the Euler B-function. This can be realized with rewriting the propagator's denominator from product to the sum, using the Feynman trick

$$\frac{1}{A_1\ldots A_n} = \int_0^1 dx_1 \ldots \int_0^1 dx_n \frac{\delta(1-x_1-\ldots-x_n)}{(x_1A_1+\ldots+x_nA_n)^n}. \tag{4.18}$$

It is not necessary to show how to evaluate all of the tensor integrals L_1, L_2, and L_3, because all of them can be evaluated with the same techniques. It is enough to show how to calculate one of them, for example L_2. Applying the Feynman trick to this integral, one obtains:

$$\begin{aligned} L_2 &= \bar{e}^3 \int \frac{d^D k}{(2\pi)^D} \int_0^1 dx \int_0^{1-x} dy \; \frac{k^\mu}{D_2} = \bar{e}^3 \int_\infty^{-\infty} \frac{d^D k}{(2\pi)^D} \int_0^1 dx \int_0^{1-x} dy \\ &\times \frac{k^\mu}{\big[(1-x-y)(k^2-m_U^2) + x\big((k-p_1)^2 - m_W^2\big) + y\big((k-p_1-p_2)^2 - m_U^2\big)\big]^3}. \end{aligned} \tag{4.19}$$

One of the ideas of this trick is to rewrite the denominator with only one loop momentum k

$$\begin{aligned} D_2 &= \big(k - (x+y)p_1 - yp_2\big)^2 - \big((x+y)p_1 + yp_2\big)^2 \\ &+ y(p_1+p_2)^2 - xm_W^2 + xp_1^2 + (x-1)m_U^2 \,, \end{aligned} \tag{4.20}$$

and to redefine the loop as k' with adding constant terms

$$k' = k - (x+y)p_1 - yp_2 \,. \tag{4.21}$$

The measure is invariant under this translation $d^D k' = d^D k$. It is also convenient to put all terms in the denominator which are not dependent on loop momentum to the function L

$$\begin{aligned} L &= \big((x+y)p_1 + yp_2\big)^2 - y(p_1+p_2)^2 + xm_W^2 - xp_1^2 - (x-1)m_U^2 \\ &= \big((x+y)p_1 + yp_2\big)^2 + xm_W^2 - (x-1)m_U^2 \,, \end{aligned} \tag{4.22}$$

where the on-shell relations $(p_1+p_2)^2 = p_\gamma^2 = 0$ and $p_1^2 = m_d^2 \approx 0$ have been applied. After all these manipulations, the integral obtains the form

$$L_2 = \bar{e}^3 \int \frac{d^D k}{(2\pi)^D} \int_0^1 dx \int_0^{1-x} dy \; \frac{k'^\mu + (x+y)p_1^\mu + yp_2^\mu}{\big[(k')^2 - L\big]^3} \,, \tag{4.23}$$

where, without any further evaluation, one can recognize

$$\int \frac{d^D k}{(2\pi)^D} \int_0^1 dx \int_0^{1-x} dy \; \frac{k'^\mu}{\big[(k')^2 - L\big]^3} = 0 \,. \tag{4.24}$$

The next trick which one can apply to this integral before it will obtain the form in which one can recognize the Euler B-function, is Wick rotation in the complex k_0' plane. This procedure looks the same in D-dimensional space exactly as in four dimensions. The measure and the four-momentum transform as

$$d^D k' = i d^D k_E, \quad k'^2 = -k_E^2, \quad k_E^\mu = \{k_0, \mathbf{k}\} \,. \tag{4.25}$$

It is possible to evaluate this integral in spherical coordinates where $d^D k_E = k_E^{D-1} dk_E d\Omega_D$, and where Ω_D is a solid angle in D-dim,

$$\int d\Omega_D = \frac{2\pi^{D/2}}{\Gamma(D/2)} \,, \tag{4.26}$$

and according to the definition of Euler integral of the first kind

$$\int_0^\infty dx \frac{x^{p-1}}{(1+x)^{p+q}} \equiv B(p,q) \,, \tag{4.27}$$

the integral L_2 turns into

$$L_2 = i\bar{e}^3 \int_0^1 dx \int_0^{1-x} dy \; \frac{\left[(x+y)p_1^\mu + yp_2^\mu\right] B(D/2, 3-D/2)}{(4\pi)^{D/2}\Gamma(D/2)} L^{D/2-4}, \tag{4.28}$$

which can be further simplified according to the relation between Euler B- and Γ- functions

$$B(D/2, 3-D/2) = \frac{\Gamma(D/2)\Gamma(3-D/2)}{\Gamma(3)}\,. \tag{4.29}$$

This brings the integral L_2 to the form

$$L_2 = i\bar{e}^3 \int_0^1 dx \int_0^{1-x} dy \; \frac{\left[(x+y)p_1^\mu + yp_2^\mu\right] \Gamma(3-D/2)}{2(4\pi)^{D/2}} L^{D/2-3}\,. \tag{4.30}$$

It is important to substitute the dimension $D = 4 - 2\varepsilon$ explicitly for further evaluation. It is also important to remember that in the dimensional regularization method, the coupling constant $\overline{g}$ is not dimensionless. To obtain a dimensionless coupling constant one introduces the mass scale parameter μ with dimension ε

$$\bar{e} = e\mu^{2-D/2}, \tag{4.31}$$

where g is a dimensionless coupling constant. The integral L_2 turns into

$$L_2 = ie^3\mu^{3\varepsilon} \int_0^1 dx \int_0^{1-x} dy \; \frac{\left[(x+y)p_1^\mu + yp_2^\mu\right] \Gamma(1-\varepsilon)}{2(4\pi)^{2-\varepsilon}} L^{-1-\varepsilon}\,. \tag{4.32}$$

For the terms with powers of ε, it is convenient to rewrite as logarithms, and the Euler gamma function is expanded in a Taylor series

$$\begin{aligned} L_2 &= ie^3 \int_0^1 dx \int_0^{1-x} dy \; \frac{\left[(x+y)p_1^\mu + yp_2^\mu\right](1 - \gamma\varepsilon + O(\varepsilon^2))}{2(4\pi)^2} \\ &\quad \times \left(1 + \varepsilon \log\left(\frac{1}{4\pi\mu^3 L}\right)\right) L^{-1}\,. \end{aligned} \tag{4.33}$$

The integral L_2, after removing all terms which are proportional to ε, turns to

$$L_2 = ie^3 \int_0^1 dx \int_0^{1-x} dy \; \frac{\left[(x+y)p_1^\mu + yp_2^\mu\right]}{2(4\pi)^2} L^{-1}\,. \tag{4.34}$$

Substituting the constant L back and integrating over dx and dy yields

$$\begin{aligned} L_2 &= \frac{-i}{64\pi^2(m_t - m_W)^3(m_t + m_W)^3} \\ &\quad \times \left[p_1^\mu(-4m_t^2 m_W^2\left(1 + \log\left(\frac{m_t^2}{m_W^2}\right)\right) + m_W^4\left(2 + \log\left(\frac{m_t^2}{m_W^2}\right)\right)\right. \\ &\quad + \left. p_2^\mu\left(-4m_t^2 m_W^2 + 2m_W^4 \log\left(\frac{m_t^2}{m_W^2}\right) + m_t^4 + 3m_W^4\right)\right]. \end{aligned} \tag{4.35}$$

The integrals L_1 and L_3 can be evaluated analogously.

4.3 Passarino-Veltman reduction

There are processes which contain a lot of amplitudes involving hundreds of loop integrals. The goal of this Section is to introduce a method which reduces the number of integrals that need to be explicitly integrated during the one-loop processes calculation. This method shows how to reduce hundreds of different integrals to four basic[1] ones in a systematic way.

4.3.1 Definition

All one-loop integrals are represented by the diagram in Fig.4.2. For further purposes, it is enough to consider integrals with up to four propagators with loop momentum. The standard notation for these integrals is A, B, C, D, which denotes one-, two-, three- and four-point functions correspondingly.

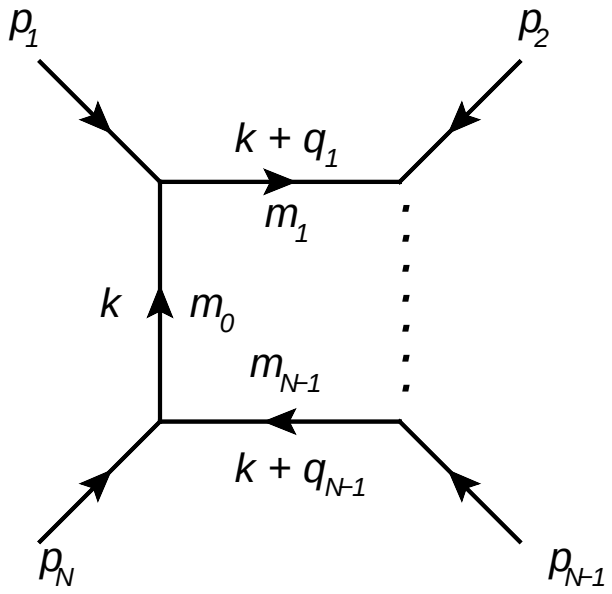

Figure 4.2: One loop diagram with N-legs. p_i denotes external momenta, q_i are momenta in the loop

It is convenient to introduce the following notation[2]: basic scalar integrals are denoted with sub-index "0"

$$i\pi^2 A_0(m_0^2) = \int \frac{d^D k}{k^2 - m_0^2} \tag{4.36}$$

$$i\pi^2 B_0(p_1^2, m_0^2, m_1^2) = \int \frac{d^D k}{(k^2 - m_0^2)((k+p_1)^2 - m_1^2)}\,, \tag{4.37}$$

$$i\pi^2 C_0(p_1^2, p_2^2, (p_1+p_2)^2, m_0^2, m_1^2, m_2^2) = \int \frac{d^D k}{(k^2 - m_0^2)((k+p_1)^2 - m_1^2)((k+p_1+p_2)^2 - m_2^2)}\,, \tag{4.38}$$

[1] In general, for different combination of non-zero arguments separate solution exists.

[2] This is one of the standard notations which is used by A. Denner in all his programs for loop calculations.

$$i\pi^2 D_0(p_1^2,p_2^2,p_3^2,p_4^2,(p_1+p_2)^2,(p_2+p_3)^2,m_0^2,m_1^2,m_2^2,m_3^2) \tag{4.39}$$
$$= \int \frac{d^Dk}{\left(k^2-m_0^2\right)\left((k+p_1)^2-m_1^2\right)\left((k+p_1+p_2)^2-m_2^2\right)\left((k+p_1+p_2+p_3)^2-m_3^2\right)}\,.$$

The general definition of a tensor integral is

$$X^{\mu_1\dots\mu_n} = \int \frac{d^Dk}{i\pi^2}\frac{k^{\mu_1\dots\mu_n}}{\left(k^2-m_0^2\right)\dots\left((k+q_x)^2-m_x^2\right)}\,, \tag{4.40}$$

where $X = B, C, D$ and lower case $x = 1, 2, 3$, correspondingly.
For example, the tensor integrals[3] D contain a corresponding number of loop-momenta k in the numerator

$$D^{\mu} = \int \frac{d^Dk}{i\pi^2}\frac{k^{\mu}}{\left(k^2-m_0^2\right)\left((k+q_1)^2-m_1^2\right)\left((k+q_2)^2-m_2^2\right)((k+q_3)^2-m_3^2)}\,, \tag{4.41}$$

$$D^{\mu_1\dots\mu_n} = \int \frac{d^Dk}{i\pi^2}\frac{k^{\mu}\dots k^{\mu_n}}{(k^2-m_0^2)((k+q_1)^2-m_1^2)((k+q_2)^2-m_2^2)((k+q_3)^2-m_3^2)}\,, \tag{4.42}$$

where the momenta q_i are defined in terms of external momenta as

$$q_i = \sum_{l=1}^{i} p_l\,. \tag{4.43}$$

In the next subsections, the decomposition of these integrals will be shown.

4.3.2 Two-point function B

The most general decomposition of the tensor integral B^{μ} reads

$$B^{\mu}(p_1,m_0,m_1) = i\pi^2 p_1^{\mu} B_1(p_1,m_0,m_1)\,. \tag{4.44}$$

Contracting both sides with p_1^{μ} provides the following relation for $B_1(p_1,m_0,m_1)$

$$B_1(p_1,m_0,m_1) = -\frac{1}{2p_1^2}\left((m_0^2-m_1^2+p_1^2)B_0(p_1,m_0,m_1) - A_0(m_0^2) - A_0(m_1^2)\right)\,. \tag{4.45}$$

The most general decomposition for the tensor integral of rank two is

$$B^{\mu\nu}(p_1^2,m_0^2,m_1^2) = i\pi^2\left(g^{\mu\nu}B_{00}(p_1,m_0,m_1) + p_1^{\mu}p_1^{\nu}B_{11}(p_1,m_0,m_1)\right)\,. \tag{4.46}$$

Contracting both sides with the external momentum p_1 and metric tensor $g^{\mu\nu}$ provides expressions for B_{00} and B_{11}

[3]The kinematics arguments are the same as in Eq.4.39 and they are and are not explicitly shown here, for simplicity.

$$\begin{aligned} B_{00}(p_1^2, m_0^2, m_1^2) &= \frac{1}{4(1-D)p_1^2}\Big(\big(2p_1^2(m_0^2+m_1^2)^2 - (m_0^2-m_1^2)^2 - (p_1^2)^2\big) \\ &\times \quad B_0(p_1^2, m_0^2, m_1^2) + (m_0^2 - m_1^2 + p_1^2)A_0(m_0^2) \\ &\qquad + (m_1^2 - m_0^2 + p_1^2)A_0(m_1^2)\Big)\,, \end{aligned} \tag{4.47}$$

$$\begin{aligned} B_{11}(p_1^2, m_0^2, m_1^2) &= \frac{1}{4(1-D)(p_1^2)^2}\Big[\big(2p_1^2\big((D-2)m_0^2 - Dm_1^2\big)^2 \\ &+ \quad D(m_0^2 - m_1^2)^2 + D(p_1^2)^2\big)B_0(p_1^2, m_0^2, m_1^2) \\ &+ \quad (m_0^2 - m_1^2 + p_1^2)A_0(m_0^2) + (m_1^2 - m_0^2 + p_1^2)A_0(m_1^2)\Big]\,. \end{aligned} \tag{4.48}$$

4.3.3 Three-point function C

The most general decomposition of tensors of rank 1,2 and 3 is represented as

$$C^\mu = q_1^\mu C_1 + q_2^\mu C_2 = \sum_{i=1}^{2} q_i^\mu C_i\,, \tag{4.49}$$

$$C^{\mu\nu} = g^{\mu\nu}C_{00} + q_1^\mu q_1^\nu C_{11} + q_1^\mu q_2^\nu C_{12} + q_2^\mu q_1^\nu C_{21} + q_2^\mu q_2^\nu C_{22} = g^{\mu\nu}C_{00} + \sum_{i,j=1}^{2} q_i^\mu q_j^\nu C_{ij}\,, \tag{4.50}$$

$$C^{\mu\nu\rho} = \sum_{i=1}^{2}\left(g^{\mu\nu}q_i^\rho + g^{\mu\rho}q_i^\nu + g^{\mu\rho}q_i^\mu\right)C_{00i} + \sum_{l,m,n=1}^{2} q_l^\mu q_m^\nu q_n^\rho C_{lmn}\,, \tag{4.51}$$

where

$$q_1 = p_1, \quad q_2 = p_1 + p_2\,. \tag{4.52}$$

Performing all possible contractions with the metric tensor $g^{\mu\nu}$ and external momenta p_i provides relations for elements C_{00}, C_{000}, C_{00i}, C_{ij} and C_{lmn}. The procedure of obtaining a specific coefficient can be generalized with the Gram matrix G, which contains all possible pairs of all external momenta p_i

$$G_i = \begin{pmatrix} p_1\cdot p_1 & p_1\cdot p_2 & \dots & p_1\cdot p_i \\ p_2\cdot p_1 & p_2\cdot p_2 & \dots & p_2\cdot p_i \\ \vdots & \vdots & \ddots & \vdots \\ p_i\cdot p_1 & p_i\cdot p_2 & \dots & p_i\cdot p_i \end{pmatrix}\,. \tag{4.53}$$

To determine the coefficients C_{ij} one needs to consider the matrix G_2

$$G_2\begin{pmatrix} C_{11} \\ C_{12}\end{pmatrix} = \begin{pmatrix} R_1^{C_1} \\ R_2^{C_1}\end{pmatrix}\,, \qquad G_2\begin{pmatrix} C_{12} \\ C_{22}\end{pmatrix} = \begin{pmatrix} R_1^{C_2} \\ R_2^{C_2}\end{pmatrix}\,, \tag{4.54}$$

where R_1^1, R_2^1, R_1^2 and R_2^2 can be determined from contraction of the lower rank tensors with external momenta.

$$
\begin{aligned}
R_1^{C_1} &= \frac{1}{2}\Big[(m_1^2 - m_0^2 - p_1^2)\; C_1\big(p_1^2, p_2^2, (p_1+p_2)^2, m_0^2, m_1^2, m_2^2\big) \\
&\quad + B_1\big(p_1^2, m_0^2, m_2^2\big) + B_0\big(p_2^2, m_1^2, m_2^2\big) \\
&\qquad -2C_{00}\big(p_1^2, p_2^2, (p_1+p_2)^2, m_0^2, m_1^2, m_2^2\big)\Big]\,, \qquad (4.55)\\
R_2^{C_1} &= \frac{1}{2}\Big[(m_2^2 - m_1^2 - p_2^2 - 2p_1\cdot p_2)\; C_1\big(p_1^2, p_2^2, (p_1+p_2)^2, m_0^2, m_1^2, m_2^2\big) \\
&\quad + B_1\big(p_1^2, m_0^2, m_1^2\big) - B_1\big(p_2^2, m_1^2, m_2^2\big)\Big]\,, \qquad (4.56)\\
R_1^{C_2} &= \frac{1}{2}\Big[(m_1^2 - m_0^2 - p_1^2)\; C_2\big(p_1^2, p_2^2, (p_1+p_2)^2, m_0^2, m_1^2, m_2^2\big) \\
&\quad + B_1\big(p_1^2, m_0^2, m_2^2\big) - B_1\big(p_2^2, m_1^2, m_2^2\big)\Big]\,, \qquad (4.57)\\
R_2^{C_2} &= \frac{1}{2}\Big[(m_2^2 - m_1^2 - p_2^2 - 2p_1\cdot p_2)\; C_2\big(p_1^2, p_2^2, (p_1+p_2)^2, m_0^2, m_1^2, m_2^2\big) \\
&\quad + B_1\big(p_1^2, m_0^2, m_2^2\big) - 2C_{00}\big(p_1^2, p_2^2, (p_1+p_2)^2, m_0^2, m_1^2, m_2^2\big)\Big]\,. \qquad (4.58)
\end{aligned}
$$

The rest of the coefficients is determined from the system of four equations

$$
\begin{aligned}
G_2\begin{pmatrix} C_{001} \\ C_{002}\end{pmatrix} &= \begin{pmatrix} R_1^{C_{00}} \\ R_2^{C_{00}}\end{pmatrix}\,, \qquad G_2\begin{pmatrix} C_{111} \\ C_{122}\end{pmatrix} = \begin{pmatrix} R_1^{C_{11}} \\ R_2^{C_{11}}\end{pmatrix}\,, \\
G_2\begin{pmatrix} C_{112} \\ C_{122}\end{pmatrix} &= \begin{pmatrix} R_1^{C_{12}} \\ R_2^{C_{12}}\end{pmatrix}\,, \qquad G_2\begin{pmatrix} C_{122} \\ C_{222}\end{pmatrix} = \begin{pmatrix} R_1^{C_{22}} \\ R_2^{C_{22}}\end{pmatrix}\,,
\end{aligned} \qquad (4.59)
$$

where the coefficients R read

$$
\begin{aligned}
R_1^{C_{11}} &= \frac{1}{2}\Big[(m_1^2 - m_0^2 - p_1^2)\; C_{11}\big(p_1^2, p_2^2, (p_1+p_2)^2, m_0^2, m_1^2, m_2^2\big) \\
&\quad + B_{11}\big(p_1^2, m_0^2, m_2^2\big) + B_0\big(p_2^2, m_1^2, m_2^2\big) \\
&\qquad - 4C_{001}\big(p_1^2, p_2^2, (p_1+p_2)^2, m_0^2, m_1^2, m_2^2\big)\Big]\,, \qquad (4.60)\\
R_2^{C_{11}} &= \frac{1}{2}\Big[(m_2^2 - m_1^2 - p_2^2 - 2p_1\cdot p_2)\; C_{11}\big(p_1^2, p_2^2, (p_1+p_2)^2, m_0^2, m_1^2, m_2^2\big) \\
&\quad + B_{11}\big(p_1^2, m_0^2, m_1^2\big) - B_{11}\big(p_2^2, m_1^2, m_2^2\big)\Big]\,, \qquad (4.61)\\
R_1^{C_{22}} &= \frac{1}{2}\Big[(m_1^2 - m_0^2 - p_1^2)\; C_{22}\big(p_1^2, p_2^2, (p_1+p_2)^2, m_0^2, m_1^2, m_2^2\big) \\
&\quad + B_{11}\big(p_1^2, m_0^2, m_2^2\big) - B_{11}\big(p_2^2, m_1^2, m_2^2\big)\Big]\,, \qquad (4.62)\\
R_2^{C_{22}} &= \frac{1}{2}\Big[(m_2^2 - m_1^2 - p_2^2 - 2p_1\cdot p_2)\; C_{22}\big(p_1^2, p_2^2, (p_1+p_2)^2, m_0^2, m_1^2, m_2^2\big) \\
&\quad + B_{11}\big(p_1^2, m_0^2, m_2^2\big) - 4C_{002}\big(p_1^2, p_2^2, (p_1+p_2)^2, m_0^2, m_1^2, m_2^2\big)\Big]\,, \qquad (4.63)
\end{aligned}
$$

$$
\begin{aligned}
R_1^{C_{12}} &= \frac{1}{2}\Big[(m_1^2 - m_0^2 - p_1^2)\; C_{12}\big(p_1^2, p_2^2, (p_1+p_2)^2, m_0^2, m_1^2, m_2^2\big) \\
&+ B_{11}\big(p_1^2, m_0^2, m_2^2\big) - B_1\big(p_2^2, m_1^2, m_2^2\big) \\
&\qquad - 2C_{002}\big(p_1^2, p_2^2, (p_1+p_2)^2, m_0^2, m_1^2, m_2^2\big)\Big]\,, \qquad (4.64)
\end{aligned}
$$

$$
\begin{aligned}
R_2^{C_{12}} &= \frac{1}{2}\Big[(m_2^2 - m_1^2 - p_2^2 - 2p_1\cdot p_2)\; C_{11}\big(p_1^2, p_2^2, (p_1+p_2)^2, m_0^2, m_1^2, m_2^2\big) \\
&- B_{11}\big(p_1^2, m_0^2, m_1^2\big) - 2C_{001}\big(p_1^2, p_2^2, (p_1+p_2)^2, m_0^2, m_1^2, m_2^2\big)\Big]\,, \qquad (4.65)
\end{aligned}
$$

$$
\begin{aligned}
R_1^{C_{00}} &= \frac{1}{2}\Big[(m_1^2 - m_0^2 - p_1^2)\; C_{00}\big(p_1^2, p_2^2, (p_1+p_2)^2, m_0^2, m_1^2, m_2^2\big) \\
&+ B_{00}\big(p_1^2, m_0^2, m_2^2\big) + B_{00}\big(p_2^2, m_1^2, m_2^2\big) \qquad (4.66) \\
R_2^{C_{00}} &= \frac{1}{2}\Big[(m_2^2 - m_1^2 - p_2^2 - 2p_1\cdot p_2)\; C_{00}\big(p_1^2, p_2^2, (p_1+p_2)^2, m_0^2, m_1^2, m_2^2\big) \\
&+ B_{00}\big(p_1^2, m_0^2, m_1^2\big) - B_{00}\big(p_2^2, m_1^2, m_2^2\big)\Big]\,, \qquad (4.67)
\end{aligned}
$$

4.3.4 Four-point function D

For the D function, the maximal tensor integral has rank 4. For the tensor of rank one, two and three, the decomposition looks very similar to these, which have been presented for the functions B and C.

$$D^\mu = \sum_{i=1}^{3} q_i^\mu C_i\,, \qquad (4.68)$$

where

$$q_3 = p_1 + p_2 + p_3\,, \qquad (4.69)$$

$$D^{\mu\nu} = g^{\mu\nu} C_{00} + \sum_{i,j=1}^{3} q_i^\mu q_j^\nu D_{ij}\,, \qquad (4.70)$$

$$D^{\mu\nu\rho} = \sum_{i=1}^{3} \left(g^{\mu\nu} q_i^\rho + g^{\mu\rho} q_i^\nu + g^{\mu\rho} q_i^\mu\right) D_{00i} + \sum_{l,m,n=1}^{3} q_l^\mu q_m^\nu q_n^\rho D_{lmn}\,. \qquad (4.71)$$

The rank four tensor integrals decompose as follows

$$
\begin{aligned}
D^{\mu\nu\rho\lambda} &= (g^{\mu\nu}g^{\rho\lambda} + g^{\mu\lambda}g^{\nu\rho} + g^{\mu\rho}g^{\nu\lambda}) D_{0000} \\
&+ \sum_{i,j}^{3} \big(g^{\mu\nu} q_i^\rho q_j^\lambda + g^{\mu\lambda} q_i^\nu q_j^\rho + g^{\mu\rho} q_i^\nu q_j^\lambda + g^{\rho\lambda} q_i^\mu q_j^\nu + g^{\nu\rho} q_i^\mu q_j^\lambda \qquad (4.72) \\
&+ g^{\nu\lambda} q_i^\mu q_j^\rho\big) D_{00ij} + \sum_{i,l,m,n}^{3} q_i^\mu q_l^\nu q_m^\rho q_n^\lambda D_{ilmn}\,.
\end{aligned}
$$

For the D function, the Gram matrix has size 3×3. The typical equation from which one can determine the coefficients is given by

$$G_3 \begin{pmatrix} D_1 \\ D_2 \\ D_3 \end{pmatrix} = \begin{pmatrix} R_1^D \\ R_2^D \\ R_3^D \end{pmatrix} , \tag{4.73}$$

A complete list of functions R can be found in [112][4]. In Ref. [113] one can find the generalization for higher rank tensors.

4.4 Dirac algebra in D-dimensions

4.4.1 NDR scheme

Dimensional regularization helps to avoid violation of gauge symmetries and Lorentz invariance but simultaneously provides complications in the Dirac algebra. The problems arise because γ_5 cannot be defined in D dimensions in the same way as in four dimensions. Moreover, here, D is not even a natural number. One simple solution is provided by the NDR scheme, where gamma-5 matrix is defined [114] by the anticommutation relation

$$\{\gamma^\mu, \gamma_5\} = 0 \, . \tag{4.74}$$

The metric tensor has the following properties:

$$g^{\mu\nu} = g^{\nu\mu}, \quad g^{\mu\sigma} g_\sigma{}^\nu = g^{\mu\nu}, \quad g^\mu{}_\mu = D \, . \tag{4.75}$$

All others Clifford algebra relations between γ-matrices are defined the same as in the four-dimensional case.

This scheme is very popular because of it simplicity, but it has been shown that these relations lead to algebraic inconsistencies [115, 116]. It has been shown that this scheme provides correct results in many cases [117], but the ambiguity of the Dirac traces like $\mathrm{tr}(\gamma^\mu\gamma^\nu\gamma^\lambda\gamma^\rho\gamma_5)$ cannot be solved. There are also problems for expressions which contain two ore more γ_5 matrices.

4.4.2 't Hooft - Veltman - Maison - Breitenlohner scheme

Another way to evaluate Dirac structure with an arbitrary number of γ_5 matrices and any traces was proposed by 't Hooft and Veltman [118] and also by Akyeampong and Delbourgo [119]. Later, it was systematized by Maison and Breitenlohner [115]. The idea was to separate metric and gamma matrices to D-, 4- and -2ε - dimensional parts

$$g^{\mu\nu} = \hat{g}^{\mu\nu} + \tilde{g}^{\mu\nu}, \quad \gamma^\mu = \hat{\gamma}^\mu + \tilde{\gamma}^\mu \, , \tag{4.76}$$

where $g^{\mu\nu}$ and γ^μ, $\tilde{g}^{\mu\nu}$ and $\tilde{\gamma}^\mu$, and $\hat{g}^{\mu\nu}$ and $\hat{\gamma}^\mu$ are metric and Dirac gamma matrices in D, 4 and -2ε dimensions respectively.

All properties of four-dimensional gamma matrices remain unchanged. For the infinitesimally small -2ε-dimensional part, the properties of metric tensors are also given by

$$\hat{g}^{\mu\nu} = \hat{g}^{\nu\mu}, \quad \hat{g}^{\mu\sigma} \hat{g}_\sigma{}^\nu = \hat{g}^{\mu\nu}, \quad \hat{g}^\mu{}_\mu = -2\varepsilon \, , \tag{4.77}$$

and anti-commutation relation

$$\{\hat{\gamma}^\mu, \hat{\gamma}^\nu\} = 2\hat{g}^{\mu\nu} \, . \tag{4.78}$$

The relation between metrics from different dimensions are defined as

[4] In this thesis a slightly different notation has been used.

$$\hat{g}^{\mu\sigma} g_\sigma{}^\nu = \hat{g}^{\mu\nu}, \quad \tilde{g}^{\mu\sigma} g_\sigma{}^\nu = \tilde{g}^{\mu\nu} . \tag{4.79}$$

All relations between 4- and -2ε-dimensional objects are trivial

$$\hat{g}^{\mu\sigma} \tilde{g}_\sigma{}^\nu = 0, \quad \hat{\gamma}^\mu \tilde{\gamma}_\mu = 0, \quad \hat{g}^{\mu\sigma} \tilde{\gamma}_\sigma = 0, \quad \tilde{g}^{\mu\sigma} \hat{\gamma}_\sigma = 0 , \tag{4.80}$$

implying

$$\{\hat{\gamma}^\mu, \tilde{\gamma}^\nu\} = 0 . \tag{4.81}$$

The properties of the γ_5 matrix in this scheme is given by

$$(\gamma_5)^2 = 1, \quad \{\tilde{\gamma}^\mu, \gamma_5\} = 0, \quad [\hat{\gamma}^\mu, \gamma_5] = 0 , \tag{4.82}$$

where γ_5 for the -2ϵ-dimensional part satisfies the commutation relation. This follows from the consistency of chiral vertices [120]

$$\frac{1}{2}(1+\gamma_5)\gamma^\mu(1-\gamma_5) = \tilde{\gamma}^\mu(1-\gamma_5) . \tag{4.83}$$

This scheme is implemented in *FeynCalc* and it was widely used for the calculations discussed in the next chapters.

4.5 FeynCalc

The techniques which are described in the previous sections are very powerful but in the case when the number of diagrams becomes too large an automatization is very helpful. There are many packages which provide automatic[5] and semiautomatic[6] evaluation for loop integrals. In this Section, the *FeynCalc* package will be discussed. This package is widely used in the research presented in the next chapters.

Fully automatic and semiautomatic tools have their own pros and cons. The first class of tools requires lower skills to start performing a calculation. But very often, in this class of tools, it is impossible to check some aspect of the calculation or change something in the input. The second class is not so user friendly, the performance and quality of output are very dependent on user skills in the semiautomatic tools. At the same time, it is easy to take the finger on the pulse and extract results at any step for further modification or control. One of the advantages of *FeynCalc* is the integration of a large number of tools for the loop evaluation from many other packages that are present on the market. The most important tools, like the library of all analytic results for the Passarino-Veltman functions which are implemented in *Package-X*, are connected to the *FeynCalc* through the add-on *FeynHelpers*. An interface to the powerful tools for the IBP reduction is also implemented. This function is a part of the package *FIRE* [126].

4.5.1 Basic principle

FeynCalc is a *Mathematica* open-source package that can be installed on any operational system which supports *Mathematica*. *FeynCalc* provides all necessary tools and objects for the construction and evaluation of amplitudes.

For example, the amplitude, which was given in Eq.4.7 as example in Sec.4.2, is introduced in the *FeynCalc* language as

[5] e.g. *FormCalc* [121], *CalcHEP* [122], *GRACE* [123].
[6] e.g. *HRPMath* [124], *Package X* [125], *FeynCalc*.

```
In[1]:= VUs*Conjugate[VUd]*Spinor[Momentum[p1, D], SMP["m_d"], 1].
        GAD[μ].GA[7].(mU + GSD[k]).GSD[Polarization[p, I, Transversality -> True]].
        (mU + GSD[k - p1 - p2]) . GAD[μ].GA[7]. Spinor[-Momentum[p2, D], SMP["m_s"], 1]
        FAD[k, mU[, k-p1, SMP["m_W"], k-p1-p2, mU]/(3*SMP["sin_W"]^2)
```

$$\text{Out[1]}= \frac{e^3 \text{VUs VUd}^\star(\varphi(\text{p1},\text{m}_\text{d}))\cdot\gamma^\mu\cdot\bar{\gamma}^7\cdot(\gamma\cdot\text{k}+\text{mU})\cdot(\gamma\cdot\varepsilon(\text{p}))\cdot(\gamma\cdot(\text{k-p1-p2})+\text{mU})\cdot\gamma^\mu\cdot\bar{\gamma}^7\cdot(\varphi(\text{p2},\text{m}_\text{s}))}{3\ (\sin\ (\theta_W))^2\ (\text{k}^2-\text{mU}^2)((\text{k-p1})^2-\text{m}_W{}^2)((\text{k-p1-p2})^2-(\text{mU})^2)}$$

The Dirac spinors are represented in *FeynCalc* by the operator `Spinor`. The first argument of this operator is the momentum of the particle, while the second argument is particle mass. The function `SMP` has strictly aesthetic goals, this operator provides a nice output form for all the SM parameters. The object `GA` represents the Dirac spinor in four-dimension, in output, these spinors are displayed with the line over. For the loop integrals evaluation, dimensional regularization is used, so, for this regularization, D-dimensional objects are required. *FeynCalc* manifestly works with D-dimensional objects and four-dimensional objects have been introduced for different kinds of approximations. It is possible to provide a D-dimensional object if one knows how to provide a four-dimensional one in short notation. The D-dimensional object is defined the same as four-dimensional but with an additional `D` in the name of the function. For example, a D-dimensional Dirac gamma matrix is defined by the `GAD` operator. `GSD` is a useful function that describes any four-vector contracted with the Dirac gamma matrix. And the last important ingredient is the propagator's denominator which is described by the operator `FAD`.

All diagrams in *FeynCalc* can be introduced by hand and can be modified by theory requirements, but it is not necessary to provide all diagrams by hand. In *FeynCalc*, the package *FeynArts* is implemented for the amplitude generation. For using the *FeynArts* inside of *FeynCalc*, it is enough to switch the parameter `LoadFeynArts` to `True` before the *FeynCalc* starts

```
In[2]:= $LoadFeynArts = True;
        << FeynCalc`
```

To generate the necessary diagrams, one firstly needs to generate diagrams topology. In *FeynArts*, the SM topology is described by the generic model `Lorenz.gen`. This generic model is activated by default when the SM class model is loaded

```
In[3]:= LoadModel[SMQCD]
        diags = InsertFields[
           CreateTopologies[1, 1 -> 2], {V[1]} -> {F[4,{1}], -F[4,{2}]},
           InsertionLevel -> {Classes}, Model -> "SMQCD"];
```

There are two levels of field insertion: classes and fields. By classes one understands sets of fields with common properties e.g. behaviour under charge conjugation. For example the amplitude in Eq. 4.7 from the Sec. 4.2 can be represented by three diagrams with virtual u, c and t quarks. But all these three diagrams with particles can be represented by one diagram of the up-type quarks class. In the definition of particles, the first number indicate the class of fields, e.g. `F[1,{2}]`, the first class of fermions is defined as all left-handed neutrinos.

The next steps are to generate mathematical expressions for the amplitudes, which can be done by the *FeynArts* function `CreateFeynAmp`, and to transform these expressions in *FeynCalc* notation, which is provided by the function `FCFAConvert`

```
In[4]:= amps = FCFAConvert[CreateFeynAmp[diags, PreFactor -> 1],
           IncomingMomenta -> {p},
           OutgoingMomenta -> {p1, p2}, LoopMomenta -> {k}, List -> True,
           ChangeDimension -> D,
           DropSumOver -> True, SMP -> True, UndoChiralSplittings -> True,
           TransversePolarizationVectors -> {p},
           FinalSubstitutions -> {FCGV["EL"] -> e,
             CKM[Index[Generation, 4], 1] -> VUd,
             CKM[Index[Generation, 4], 2] -> VUs,
             MQU[Index[Generation, 4]] -> mU}];
```

Here, all necessary input parameters and physical properties have been set. Most of these options are intuitively clear. Other functions are: `List`, if this parameter set to be true, each diagram will be written as separate entries in a list, `DropSumOver` implements Einstein convention, `TransversePolarizationVectors` defines the polarization vector as transverse, `SMP` enables standard notation for all the SM parameters, and `FinalSubstitutions` is needed for the replacement of remaining objects with more readable form.

The generated diagrams can be illustrated with the function `Paint`,

```
In[5]:= Paint[diags, ColumnsXRows -> 3, 5, Numbering -> Simple,
          SheetHeader -> None, ImageSize -> 1000, 800];
```

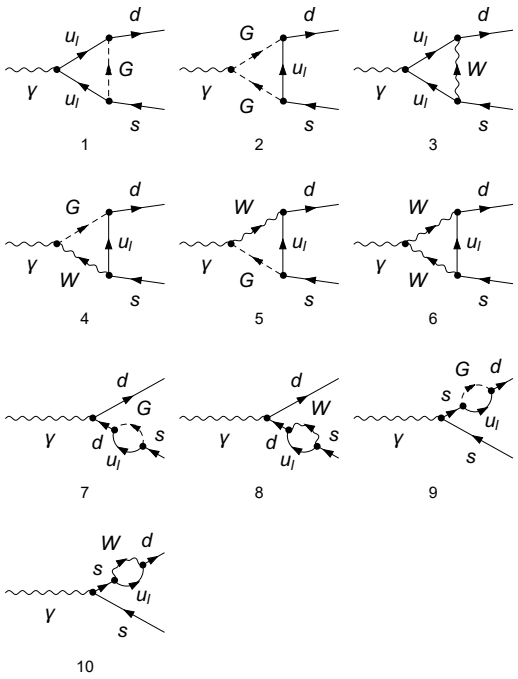

Figure 4.3: Diagrams generated by *FeynArts* for the process $b \to s\gamma$. Diagrams with u_l represent the class of diagrams with up-type quarks from all families.

From Fig. 4.3, one can see that the amplitude in Eq. 4.7 is represented by the diagram numbered "3". To calculate this diagram, the entries "3" from the list `amps` need to be chosen

```
In[6]:= amps[[3]]
```

That provides a bit different code if compared with code which has been given in the input In[1], namely

```
In[7]:= amp3=(VUs*Conjugate[VUd]*Spinor[Momentum[pE1, D], SMP["m_d"], 1].
            DiracGamma[LorentzIndex[Lor3, D], D].DiracGamma[7].
            (mU + DiracGamma[Momentum[k, D], D]).
            DiracGamma[Momentum[Polarization[p, I, Transversality -> True], D], D].
            (mU + DiracGamma[Momentum[k - p1 - p2, D], D]).DiracGamma[LorentzIndex[Lor3, D], D].
            DiracGamma[7].Spinor[-Momentum[p2, D], SMP["m_s"], 1]*
```

```
FeynAmpDenominator[PropagatorDenominator[Momentum[k, D], mU],
 PropagatorDenominator[Momentum[k - p1, D], SMP["m_W"]],
 PropagatorDenominator[Momentum[k - p1 - p2, D], mU]]*SMP["e"]^3*
SUNFDelta[SUNFIndex[Col2], SUNFIndex[Col3]])/(3*SMP["sin_W"]^2)
```

but after contraction with all repeated indices and simplification one obtains almost[7] the same output

In[8]:=
```
res2 = diag3//Contract//Simplify
```

Out[8]=
$$\frac{e^3 \text{VUs VUd}^{\star}\ \delta_{\text{Col2 Col3}}(\varphi(\text{p1},\text{m}_\text{d}))\cdot\gamma^{\text{Lor3}}\cdot\bar{\gamma}^7\cdot(\gamma\cdot\text{k+mU})\cdot(\gamma\cdot\varepsilon(\text{p}\gamma))\cdot(\gamma\cdot(\text{k-p1-p2})+\text{mU})\cdot\gamma^{\text{Lor3}}\cdot\bar{\gamma}^7\cdot(\varphi(\text{p2},\text{m}_\text{s}))}{3\ (\sin\ (\theta_W))^2\ (\text{k}^2-\text{mU}^2)((\text{k-p1})^2-\text{m}_W{}^2)((\text{k-p1-p2})^2-(\text{mU})^2)}$$

One of these notations is short and user friendly, the second is used as internal *FeynCalc* language. The definitions of "short" external and "long" internal notation are not fully interchangeable, *FeynCalc* does not operate with expressions which are defined with "mixed" notation where all objects are defined partially in "short" and partially in "long" notation. But *FeynCalc* provides automatic translation of all objects in "short" external notation with `FCE` operator, and the operator `FCI` turns all objects in "long" internal notation.

For the simplification of expressions, it is very useful to set a kinematic relation before the evaluation. These relations follow from the on-shell conditions for the process. During the evaluation, it is necessary to replace all four-momentum squares and all four-momentum products with masses and kinematics variables. The function `SPD` helps to set up these relations in *FeynCalc*. In the example for the $d \to s\gamma$ process, the relations have the form

In[8]:=
```
FCClearScalarProducts[]
SPD[p1] = 0;
SPD[p2] = SMP["m_s"]^2;
SPD[p] = 0;

SPD[p1, p2] = SMP["m_s"]^2/2;
SPD[p, p1] = -SMP["m_s"]^2/2;
SPD[p2, p] = SMP["m_s"]^2/2;
```

The function `FCClearScalarProducts` removes all early defined scalar products from the memory. It is possible to provide one or two arguments. Single argument reads as repeated, e.g. `SPD[p1] = SPD[p1, p1]`. Additional simplification, for this example, is provided by orthogonality conditions, which reads as

In[8]:=
```
Pair[Momentum[p, D],Momentum[Polarization[p, -I, Transversality -> True], D]] = 0;
```

4.5.2 Dirac algebra evaluation

Computer algebra calculations are divided into two sub-tasks: for the one-loop integrals tasks are the same as for the calculations by hand. *FeynCalc* includes all important instruments for the Dirac structure evaluation.

The most important functions for the evaluation of Dirac structures is `DiracSimplify`, which provides full possible simplification for the Dirac structures in many cases . `DiracSimplify` performs all Dirac traces, minimizes the number of Dirac gamma matrices applying (anti-)commutation relation, and enforces the Dirac equation. This function contains 28 parameters[8]. The most important from these parameters are `DiracGammaCombine`, `DiracOrder`, `DiracSubstitute5`, `DiracSubstitute67`, and `DiracTrace`. All of these parameters can be set to `True` or `False`.

The first simple example helps to understand how the parameter `DiracGammaCombine` impacts the result

[7] Colour algebra has been dropped in the Input In[1].

[8] This is true for the version of *FeynCalc 9.4*, in others revisions the number of parameters can be different.

```
In[9]:= exampDirac1 = Spinor[Momentum[p1, D], SMP["m_d"],
          1].(GSD[p1] + GSD[p2] + mU).Spinor[-Momentum[p2, D], SMP["m_s"], 1]

Out[9]= φ(p1,m_d).(mU + γ·p1 + γ·p2).φ(-p2,m_s)
```

If one applies `DiracSimplify` to this expression with `DiracGammaCombine` set to `False`, the function `DiracSimplify` will apply also the Dirac equation to the expression and return masses

```
In[10]:= exampDirac1 // DiracSimplify[#, DiracGammaCombine -> False] &

Out[10]= mU φ(p1,m_d).φ(-p2,m_s) + m_d φ(p1,m_d).φ(-p2,m_s) - m_s φ(p1,m_d).φ(-p2,m_s)
```

`DiracGammaCombine`, which is set to `True`, reduces the number of gamma matrices which are contracted with all kind of four-vectors and which appears in sums. In the example `examp1`, this enabled parameter replaces the sum of two Dirac gamma matrices contracted by four-vectors with one gamma matrix which is contracted by the sum of four-vectors

```
In[10]:= exampDirac1 // DiracSimplify[#, DiracGammaCombine -> True] &

Out[10]= mU φ(p1,m_d).φ(-p2,m_s) + φ(p1,m_d).(γ·(p1 + p2)).φ(-p2,m_s)
```

In this case, the relation from the Dirac equation cannot be applied because the argument of four-vector is `p1+p2`, and the function understands this sum is a completely new object without any association with `p1` and `p2`.

An another useful options is `DiracOrder`. With default settings, `DiracSimplify` reduces the expression, trying to obtain the smallest number of terms. But the smallest number of terms does not mean that an expression has the simplest form. There are situations when the number of terms is not important, but the simplest Dirac structure is required. For instant, some contributions from box diagrams which contain three gamma matrices can be canceled with contributions from triangle diagrams which have only one gamma matrix

```
In[10]:= exampDirac2 = GAD[μ,ν,σ,ρ,μ]

Out[10]= γ^μ.γ^ν.γ^σ.γ^ρ.γ^μ

In[10]:= exampDirac2//DiracSimplify[#, DiracOrder -> False]&//Simplify

Out[10]= (4-D)γ^ν.γ^σ.γ^ρ - 2 γ^ρ.γ^σ.γ^ν
```

but if one set the parameter `DiracOrder` to the `True` only one term with three Dirac gamma matrices will be obtained

```
In[10]:= exampDirac2//DiracSimplify[#, DiracOrder -> True]&//Simplify

Out[10]= (D-6)γ^ν.γ^ρ.γ^σ - (2D-8) γ^ν.g^ρσ + 4 γ^σ.g^ρν - 4 γ^ρ.g^σν
```

This trick is useful, for instance, if one needs to determine the Ward identity structure.

The option `DiracSubstitute5`, which is set to `True`, performs the substitution $\gamma_5 = P_R - P_L$. Unfortunately, one needs to replace scalar matrix elements by hand. `DiracSubstitute67` replaces all left-hand projector operators P_L which are represented in *FeynCalc* as γ_7 with $(1-\gamma_5)/2$, and replaces all right-hand projector operators P_R which is represented in *FeynCalc* as γ_6 with $(1+\gamma_5)/2$.

The operator `DiracSimplfy` evaluates and simplifies the Dirac traces automatically. The option `DiracTrace` allows us to disable any evaluation with Dirac trace. Keeping the trace without evaluation is very useful in some situations in order to reduce the number of terms.

The second most important operator for the Dirac structure evaluation is `Contract`. This function contracts repeated Lorentz indices of metric tensors, four-vectors, and Levi-Civita tensors, and it rewrites the expression in a simpler form for the evaluation and also for reading

```
In[11]:= FVD[q, μ] FVD[q, μ] // Contract // FCE
         % // StandardForm

Out[11]= q^2

Out[12]= SPD[q, q]
```

`ExpandScalarProduct` is a widely used function for the simplification of the Dirac algebra. This function expands scalar products of sums of momenta

```
In[13]:= exampDirac3 = SPD[k,p-k]
         exampDirac3//ExpandScalarProduct

Out[13]= k·(p-k)
         k·p-k^2
```

This function is needed for the substitution of four-momenta's scalar products using the definition of the kinematics rules. *FeynCalc* cannot automatically recognize that the scalar product of a sum of two four-vectors contracted with a four-vector $(p_1 + p_2) \cdot q$ is the same as sum of two contraction $p_1 \cdot q + p_2 \cdot q$. This function is inverse to the enabled option `DiracGammaCombine`[9].

The diagram which is taken as the example is simple and standard settings are enough for the evaluation. The operator `Contract` has been applied before, and for the Dirac structure evaluation, one needs to apply `DiracSimplfy` with the default settings

```
In[12]:= res3 = res2//DiracSimplify//Simplify;
```

The result became quite large and hardly readable after these operations. One can use isolation to see the Dirac structure of the expression. Isolation is provided by the function `Collect2`

```
In[13]:= res2x = res2 // Collect2[#, DiracSpinor, IsolateNames -> FF] &

Out[13]= - 2/3 FF(2972)(φ(p1,m_d)).(γ·ε(p)).(γ·k).γ̄^6.(φ(-p2,m_s))
         + 2/3 FF(2973)(φ(p1,m_d)).(γ·ε(p)).(γ·k).γ̄^7(φ(-p2,m_s))
         - 1/3 FF(2978)(φ(p1,m_d)).(γ·k).(γ·ε(p)).γ̄^6.(φ(-p2,m_s))
         + 1/3 FF(2979)(φ(p1,m_d)).(γ·k).(γ·ε(p)).γ̄^7.(φ(-p2,m_s))
         - 2/3 FF(2985)(φ(p1,m_d)).(γ·k).γ̄^7.(φ(-p2,m_s))
         - 1/3 FF(2983)(φ(p1,m_d)).(γ·ε(p)).γ̄^7.(φ(-p2,m_s))
```

This function will be discussed in greater details in Sec. 4.5.5.

4.5.3 Tensor integral evaluation

The next step in amplitude evaluation is the transformation of the tensor integrals into scalar ones and the reduction of the scalar integrals into basic ones. The analytic form has been shown in Sec. 4.3. Many tools are able to use the basic functions A_0, B_0, C_0 and D_0 for the further numerical or analytic evaluation. *FeynCalc* has all important tools to perform such kind of decomposition. The most important operators for the evaluation of Feynman integrals will be discussed in this section.

The key function which provides the decomposition is `TID`. In many simple cases, it is enough to only apply this function and obtain a final result which can be used in other packages for analytic or numerical evaluation. The first argument of the function is the expression that one wants to evaluate, the second argument is always the loop momentum or momenta[10]

[9] `DiracGammaCombine` also can be used as a separate function independently from `DiracSimplify`.

[10] The function `TID` is able to decompose higher-loops functions.

```
In[14]:= FCClearScalarProducts[]
         SPD[p1] = 0;
         SPD[p2] = m1^2;
         SPD[p1, p2] = m1^2;

         exampTID1a = FVD[k, μ]FAD[{k, m0},{k + p1, m1},{k + p2, m1}]//TID[#, k]&
```

$$\text{Out[14]=} -\frac{\text{m0}^2\text{p1}^\mu - (\text{m0}-\text{m1})(\text{m0}+\text{m1})\text{p1}^\mu + (\text{m0}-\text{m1})(\text{m0}+\text{m1})\text{p2}^\mu}{2\,\text{m1}^2\left(\text{k}^2 - \text{m0}^2\right)\left((\text{k} - \text{p1})^2 - \text{m1}^2\right)\left((\text{k} - \text{p2})^2 - \text{m1}^2\right)} - \frac{\text{p1}^\mu - \text{p2}^\mu}{2\,\text{m1}^2\left(\text{k}^2 - \text{m0}^2\right)\left((\text{k} - \text{p2})^2 - \text{m1}^2\right)}$$
$$+ \frac{\text{p1}^\mu}{2\,\text{m1}^2\left(\text{k}^2 - \text{m0}^2\right)\left((\text{k} - \text{p1})^2 - \text{m1}^2\right)} - \frac{\text{p2}^\mu}{2\,\text{m1}^2\left(\text{k}^2 - \text{m1}^2\right)\left((\text{k} - \text{p1} + \text{p2})^2 - \text{m1}^2\right)}$$

In simple cases, the `TID` operator provides the result using the Passarino-Veltman basis automatically, but in the case of more complicated functions, this needs to be enforced by enabling **ToPaVe** option

```
In[15]:= exampTID1b = FVD[k,μ]FAD[{k,m0},{k + p1,m1}, {k + p2,m1}]//
         TID[#, k, ToPaVe -> True]&
```

$$\text{Out[15]=} -\frac{\text{i}\pi^2\text{C}_0\left(-\text{m1}^2,\text{m1}^2,0,\text{m1}^2,\text{m1}^2,\text{m0}^2\right)\left(\text{m0}^2\text{p1}^\mu - (\text{m0}-\text{m1})(\text{m0}+\text{m1})\text{p1}^\mu + (\text{m0}-\text{m1})(\text{m0}+\text{m1})\text{p2}^\mu\right)}{2\,\text{m1}^2}$$
$$- \frac{\text{i}\pi^2\text{B}_0\left(\text{m1}^2,\text{m0}^2,\text{m1}^2\right)\left(\text{p1}^\mu - \text{p2}^\mu\right)}{2\,\text{m1}^2} - \frac{\text{i}\pi^2\text{p1}^\mu\text{B}_0\left(0,\text{m0}^2,\text{m1}^2\right)}{2\,\text{m1}^2} - \frac{\text{i}\pi^2\text{p2}^\mu\text{B}_0\left(-\text{m1}^2,\text{m1}^2,\text{m1}^2\right)}{2\,\text{m1}^2}$$

Very often, it is useful to have a more compact result for further evaluation and to keep the smaller number of large functions. For this purpose, the option `UsePaVeBasis` is very useful

```
In[16]:= exampTID1b = FVD[k,μ]FAD[{k,m0},{k + p1, m1},{k + p2, m1}]//
         TID[#, k, UsePaVeBasis -> True]&
```

$$\text{Out[16]=} \text{i}\pi^2\text{p1}^\mu\text{C}_1\left(0,-\text{m1}^2,\text{m1}^2,\text{m0}^2,\text{m1}^2,\text{m1}^2\right) + \text{i}\pi^2\text{p2}^\mu\text{C}_2\left(0,-\text{m1}^2,\text{m1}^2,\text{m0}^2,\text{m1}^2,\text{m1}^2\right)$$

If the result needs to be expressed in terms of basic functions, the operator `PaVeReduce` will be helpful. The option `A0toB0` set to `True` expresses all A_0 functions in terms of B_0 functions.

The analytic result for the functions C and D is very complicated. Before applying the operator `TID`, it is possible to reduce some of them into simpler ones, if these functions contain two or more propagators with identical momenta. For instance, the reduction of one of the functions B into A looks like

$$\frac{1}{\left(k^2 - m_1^2\right)\left(k^2 - m_2^2\right)} = \frac{1}{m_1^2 - m_2^2}\left(\frac{1}{k^2 - m_2^2} - \frac{1}{k^2 - m_2^2}\right). \tag{4.84}$$

In *FeynCalc*, this decomposition is realized by the function `ApartFF`. This function is also able to redefine momenta properly in such a way that only linearly independent propagators remain. As example

```
In[17]:= exampTID2 = FVD[k, μ] FAD[{k + p1,m1}, {k + p1,m2}]//ApartFF[#, {k}]&
```

$$\text{Out[17]=} \frac{\text{p1}^\mu}{(\text{m1}-\text{m2})(\text{m1}+\text{m2})\left(\text{k}^2 - \text{m2}^2\right)} - \frac{\text{p1}^\mu}{(\text{m1}-\text{m2})(\text{m1}+\text{m2})\left(\text{k}^2 - \text{m1}^2\right)}$$

The result which can be evaluated numerically or analytically needs to be written without four-momenta in terms of masses and Mandelstam variables. This is obtained by the definition of all possible pairs of contractions of momenta. But the denominator in *FeynCalc* is written as square of the sum of four-momenta, and the program does not perform automatically the further evaluation, because this is only the form which is necessary for the decomposition. After the tensor integral decomposition, the square of sum should be rewritten in terms of contracted pairs of four-momenta. This is possible to realize with operator `PropagatorDenominatorExplicit`. The result without this function reads

```
In[17]:= exampTID3a = FAD[{k + p1, m1}, {k + p1 + p2, m2}]//TID[#, k]&

Out[17]= 1/((k^2 - m1^2)((k - p2)^2 - m2^2))
```

and the same example with rewritten denominator

```
In[17]:= exampTID3b = FAD[{k + p1, m1}, {k + p1 + p2, m2}]//TID[#, k]&//
         PropagatorDenominatorExplicit

Out[17]= 1/((k^2 - m1^2)(k^2 - 2k·p2 + p2^2 - m2^2))
```

where p_2^2 is substituted with the mass square or Mandelstam variable if the rule for this is defined.

The evaluation of the diagram for the process $s \to d\gamma$ looks like

```
In[17]:= res3a = res2/.mU -> x SMP["m_W"]//Expand//SelectNotFree[#, x]&//Simplify;
         res3b = res3a/.SMP["m_d"] -> 0//TID[#, k, UsePaVeBasis -> True, ToPaVe -> True]&//
             PropagatorDenominatorExplicit//Collect2[#, DiracSpinor, Factoring -> Simplify]&//
             Simplify;

Out[17]= - 1/(3(sin(θ_W))^2) i π^2 VUs VUd* e^3
(2(φ(p1)).(γ·p1).γ̄^7.(φ(-p2,m_s)) (C_0(0,m_s^2,2 m_s^2,x^2m_W^2,m_W^2,x^2m_W^2) (p1·ε(p)-p2·ε(p))+
        (p1·ε(p))(D C_1(0,2 m_s^2,m_s^2,m_W^2,x^2m_W^2,x^2m_W^2) + (D-2)C_11(0,2 m_s^2,m_s^2,m_W^2,x^2m_W^2,x^2m_W^2))-
        (p2·ε(p))(2 C_1(0,2 m_s^2,m_s^2,m_W^2,x^2m_W^2,x^2m_W^2) + (D-2)C_2(0,2 m_s^2, m_s^2,m_W^2,x^2m_W^2,x^2m_W^2)+
                C_12(0,2 m_s^2,m_s^2,m_W^2,x^2m_W^2,x^2m_W^2))) - 2(φ(p1)).(γ·p1).γ̄^7.(φ(-p2,m_s))
        ((p1·ε(p))(2 C_2(0,2 m_s^2, m_s^2,m_W^2,x^2m_W^2,x^2m_W^2) + (D-2)C_12(0,2 m_s^2, m_s^2,m_W^2,x^2m_W^2,x^2m_W^2))-
        (p2·ε(p))(2 C_2(0,2 m_s^2,m_s^2,m_W^2,x^2m_W^2,x^2m_W^2) + (D-2)C_22(0,2 m_s^2, m_s^2,m_W^2,x^2m_W^2,x^2m_W^2)))+
(D-4)(φ(p1)).(γ·p1).(γ·ε(p)).γ̄^6.(φ(-p2,m_s))
(C_0(0,m_s^2,2 m_s^2,x^2m_W^2,m_W^2,x^2m_W^2) + C_1(0,2 m_s^2, m_s^2,m_W^2,x^2m_W^2,x^2m_W^2))m_s +
(φ(p1)).(γ·ε(p)).(γ·p1).γ̄^6.(φ(-p2,m_s))
(C_0(0,m_s^2,2 m_s^2,x^2m_W^2,m_W^2,x^2m_W^2) + C_1(0,2 m_s^2, m_s^2,m_W^2,x^2m_W^2,x^2m_W^2))m_s -
(D-4)(φ(p1)).(γ·p2).(γ·ε(p)).γ̄^6.(φ(-p2,m_s))( C_2(0,2 m_s^2, m_s^2,m_W^2,x^2m_W^2,x^2m_W^2)) m_s -
2(φ(p1)).(γ·ε(p)).(γ·p2).γ̄^6.(φ(-p2,m_s)) C_2(0,2 m_s^2, m_s^2,m_W^2,x^2m_W^2,x^2m_W^2)m_s -
(φ(p1)).(γ·ε(p)).γ̄^7.(φ(-p2,m_s))(-4C_0(0,m_s^2,2 m_s^2,x^2m_W^2,m_W^2,x^2m_W^2)m_s -
        D x^2 C_0(0,m_s^2,2 m_s^2,x^2m_W^2,m_W^2,x^2m_W^2)m_W^2 + 6 x^2 C_0(0,m_s^2,2 m_s^2,x^2m_W^2,m_W^2,x^2m_W^2)m_W^2
        D C_0(0,m_s^2,2 m_s^2,x^2m_W^2,m_W^2,x^2m_W^2)m_W^2 - 6 C_0(0,m_s^2,2 m_s^2,x^2m_W^2,m_W^2,x^2m_W^2)m_W^2
        2 B_0 (0, m_W^2,x^2 m_W^2) + 2 B_0(m_s^2,m_W^2,x^2 m_W^2) - D B_0(2m_s^2,x^2 m_W^2,x^2 m_W^2) -
                6 B_0(2m_s^2,x^2 m_W^2,x^2 m_W^2) -
        2 D C_00(0,2 m_s^2, m_s^2,m_W^2,x^2m_W^2,x^2m_W^2) + 4 C_00(0,2 m_s^2, m_s^2,m_W^2,x^2m_W^2,x^2m_W^2)))δ_Col2 Col3
```

Here, the masses of all quarks, except the bottom and top quarks, are neglected and the GIM mechanism is applied - all terms, which are not proportional to mU, cancel due to the unitarity of the CKM matrix. A new variable $x = mU/m_W$ is chosen for convenience. The result consists of a set of Passarino-Veltman functions and is ready for further numerical or analytic evaluation.

4.5.4 Analytic result

In many cases, it is important to check the properties of amplitudes analytically or numerically. *FeynCalc* itself does not contain any tool for providing an analytic or numeric result for the Passarino-Veltman function, but *FeynCalc* is linked via *FeynHelpers* to the *Package-X* which contains a library of analytic results for the basic Passarino-Veltman functions and is able to

match properly the result in the library with the corresponding function with specified arguments.

`PaXEvaluate` is used for the substitution of the Passarino-Veltman function by the analytic result. By default for simplicity, `PaXEvaluate` substitutes the result without the factor $(2\pi)^{-D}$. To obtain correct result, one needs to use the option `PaXImplicitPrefactor -> 1/(2 Pi)^D`. The analytic results for the C and D functions are very long and `PaXEvaluate` with default settings ignores these functions. The settings `PaXC0Expand` and `PaXD0Expand` substitute the analytic results for C and D functions respectively when set to `True`.

The result can be more compact if approximations are used. One possible approximation at this step is an expansion in Taylor series. An option `PaXSeries` provides this expansion. `PaXEvaluate` with default settings cannot expand the Passarino-Veltman function near Landau singularities [127][11], but the enabled option `PaXAnalytic` provides an expansion also for functions with Landau singularities. For example, an expansion for the C_{11} function looks like

```
In[17]:= x = PaVe[1, 1, 0, 0, SMP["m_s"]^2, SMP["m_s"]^2, 0, SMP["m_W"]^2,
            PaVeAutoOrder -> True, PaVeAutoReduce -> False]
```

Out[17]= $C_{11}\left(0,0,\text{m\_s}^2,\text{m\_s}^2,0,\text{m\_W}^2\right)$

```
In[17]:= x // PaXEvaluate[#, PaXSeries -> {{SMP["m_s"], 0, 0}},PaXC0Expand -> True,
          PaXAnalytic -> True,PaXImplicitPrefactor -> 1/(2 Pi)^D]&//Simplify
```

Out[17]= $$\frac{\varepsilon(11-6\gamma + 6\ \log(4\pi)) + 6\ \varepsilon\ \log\left(\frac{\mu^2}{\text{m\_W}^2}\right)+6}{288\pi^4\ \varepsilon\ \text{m\_W}^2}$$

The result would be much longer and contain complicated polylogarithmic functions without expansion. The analytic result for the selected diagram from the process $s \to d\gamma$ is obtained by applying the next code

```
In[17]:= res4 = res3b // FCReplaceMomenta[#, {p2 -> p - p1}] & //
          ExpandScalarProduct//DiracSimplify//PaXEvaluate[#, PaXSeries -> {{SMP["m_s"], 0, 0}},
          PaXC0Expand -> True, PaXAnalytic -> True,PaXImplicitPrefactor -> 1/(2 Pi)^D]&//
          Factor2//Simplify//
          Collect2[#, DiracSpinor, Epsilon, SUNFDelta, Factoring -> FullSimplify] &
```

Out[17]=
$$\frac{\text{i e}^3\ \text{VUs VUd}^*\ \delta_{\text{Col2 Col3}}\ (\varphi(\text{p1})).(\gamma\cdot\varepsilon(\text{p})).\bar{\gamma}^7.(\varphi(-\text{p2},\text{m}_s))}{48\ \pi^2\varepsilon(\sin(\theta_W))^2} - \frac{\text{i e}^3\ \text{VUs VUd}^*\ \delta_{\text{Col2 Col3}}}{96\ \pi^2(\text{x}^2\text{-1})^2(\sin(\theta_W))^2}$$
$$\left(\left(\text{x}^2\text{-1}\right)\left(-2\left(\text{x}^2\text{-1}\right)\log\left(\frac{\pi\ \mu^2}{\text{x}^2\ \text{m}^W{}_2}\right)+2\gamma\left(\text{x}^2\text{-1}\right)+\text{x}^2(-(1+\log(16)))-1+\log(16)\right)+\left(2-4\text{x}^2\right)\log\left(\frac{1}{\text{x}^2}\right)\right)$$
$$(\varphi(\text{p1})).(\gamma\cdot\varepsilon(\text{p})).\bar{\gamma}^7.(\varphi(-\text{p2},\text{m}_s)) +$$
$$\frac{\text{i e}^3\ \text{VUs VUd}^*\left(4\text{x}^6\text{-21x}^4\text{+24 x}^2\text{+(6-12x}^2)\left(\frac{1}{\text{x}^2}\right)\text{-7}\right)\delta_{\text{Col2 Col3}}(\text{p1}\cdot\varepsilon(\text{p}))(\varphi(\text{p1})).(\gamma\cdot\text{p}).\bar{\gamma}^7.(\varphi(-\text{p2},\text{m}_s))}{144\ \pi^2\ \left(\text{x}^2\text{-1}\right)^4(\sin(\theta_W))^2\ \text{m}^W{}_2}$$

4.5.5 Useful tricks

Many useful *FeynCalc* functions were presented in previous section. Another important function is `Collect2`. Without this function, many complicated calculations could not be performed. This function is used for the evaluation of Dirac structures and Feynman integrals. This function has the same purpose as the native *Mathematica* function `Collect`, but *FeynCalc* function is much more elaborated and flexible. `Collect2` allows one to collect the class of an object, which is not possible in the case of `Collect`. For example, one can collect all Dirac structures in separate terms. After this operation, the terms which have been collected with unique structure appear in the results only once

[11] For review, e.g. [128].

```
In[17]:= exampleTrick = a Spinor[p].GAD[μ, ν].Spinor[q] + b^2 Spinor[p].GAD[μ, ν].Spinor[q] +
           b^2 Spinor[p].GAD[ν, μ].GA[5].Spinor[q]
```

Out[17]= $b^2(\varphi(p)).\gamma^\nu.\gamma^\mu.\bar{\gamma}^5.(\varphi(q)) + a\ (\varphi(p)).\gamma^\mu.\gamma^\nu.(\varphi(q)) + b^2(\varphi(p)).\gamma^\mu.\gamma^\nu.(\varphi(q))$

```
In[17]:= exampleTrick//Collect2[#, Spinor]&
```

Out[17]= $b^2(\varphi(p)).\gamma^\nu.\gamma^\mu.\bar{\gamma}^5.(\varphi(q)) + (a + b^2)\ (\varphi(p)).\gamma^\mu.\gamma^\nu.(\varphi(q))$

```
In[17]:= exampleTrick//Collect2[#, b]&
```

Out[17]= $b^2\left((\varphi(p)).\gamma^\nu.\gamma^\mu.\bar{\gamma}^5.(\varphi(q)) + \varphi(p)).\gamma^\mu.\gamma^\nu.(\varphi(q))\right) + a\ (\varphi(p)).\gamma^\mu.\gamma^\nu.(\varphi(q))$

`Collect2` allows to provide as many segregations as is needed in one operation. One can specify in one operation all goals of segregation, dividing the objects of collection with commas. The collection is performed in the order of appearing these objects as arguments.

`Collect2` allows one to do each manipulation with prefactors, which objects of collection have. The option `Factoring` is responsible for this, where the operation which needs to be performed under each prefactor, is used as a parameter.

```
In[17]:= exampleTrick//Collect2[#, Spinor, Factoring->Simplify]&;
```

In the example above, the simplification is applied for each prefactor. In many cases, it is very useful if prefactors are isolated. This is possible to obtain with the option `IsolateNames`

```
In[17]:= exampleTrick // Collect2[#, Spinor, IsolateNames -> FF] &
```

Out[17]= $\texttt{FF(58)}(\varphi(p)).\gamma^\nu.\gamma^\mu.\bar{\gamma}^5.(\varphi(q)) + \texttt{FF(57)}\ (\varphi(p)).\gamma^\mu.\gamma^\nu.(\varphi(q))$

The numbers, which appear as an argument of the new function `FF`, are completely random and are changed in every next session. The expressions, which are associated to each isolated function, are saved in the memory and will be lost after the end of the session. The function `FRH` reveals isolated expression back. It can be applied for all isolated functions or for one selected

```
In[17]:= FF[58]//FRH
```

Out[17]= b^2

Indeed, the prefactor of $\varphi(p)\gamma^\nu\gamma^\mu\bar{\gamma}^5\varphi(q)$ is b^2.

In some situations, the option `IsolateFast`, which is set to `True`, allows to save some time. If it does not help, the option `TimeConstrained` will stop all operations after the timer runs out, and it will return the actual result. As a parameter, one needs to set a time in seconds.

Other useful *FeynCalc* functions are `SelectFree` and `SelectNotFree`, which return that part of the initial expression which is free or not free of any occurrence of the selected variables

```
In[17]:= exampleTrics2 = a + a^2 + a b + 6 b + b^2
```

Out[17]= $a + a^2 + a\ b + 6\ b + b^2$

```
In[17]:= res1 = SelectNotFree[exampleTrics2, a]
```

Out[17]= $a + a^2 + a\ b$

```
In[17]:= res2 = SelectFree[exampleTrics2, a]
```

Out[17]= $6\ b + b^2$

```
In[17]:= res1 + res2 - exampleTrics2
```

Out[17]= 0

The last function which will be mentioned in this section is `FCReplaceMomenta`. This function is not as important as the previous ones, but it will be widely used in further calculations. Very often, it is important to replace four-momenta everywhere but not in the arguments of the spinors. This function realizes such kind of replacements.

Chapter 5

The SM Higgs decay into two leptons and photon

5.1 Motivation

The SM Higgs sector has been constructed minimally with only one Higgs doublet. But solutions to many problems suggest that the theory looks more natural with at least one more Higgs doublet. A 2HDM can be one explanation of the baryogenesis phenomena. A possible way to confirm the hypothesis about an extended scalar sector in the SM is to find a deviation in the SM prediction from experiments.

The decay rate $h \to l\bar{l}$ is suppressed by the Yukava couplings in all orders of the expansion. Meanwhile $h \to l\bar{l}\gamma$ can be the process without parity flipping and $h \to l_{L(R)}\bar{l}_{L(R)}\gamma$ provides the leading order contribution at the one-loop level. Higgs decay into electrons dominantly happens via this process with additional emission of a photon. For muons, the amplitudes of $h \to l\bar{l}\gamma$ and $h \to l\bar{l}$ processes are of the same order of magnitude, and for tau-leptons the one-loop contribution is negligible.

5.2 Calculation

Diagrams and input

This process is described by 436 diagrams which were generated with *FeynArts* [130]. In these calculations, small values of the Yukawa couplings were neglected. This allowed to reduce the number of diagrams with non-zero contributions almost by a factor of four. These diagrams are divided into 13 classes:

- Class 1. Box-diagrams. (Fig.A.1)
- Class 2. External leg radiation diagrams. (Fig.A.2)
- Class 3. 4-point vertex with k-independent[1] γ propagator type 4. (Fig.A.3)
- Class 4. 4-point vertex with k-independent Z-boson propagator type 4. (Fig.A.4)
- Class 5. Triangle diagrams with with k-independent photon propagator. (Fig.A.5)
- Class 6. Triangle diagrams with k-independent Z-boson propagator. (Fig.A.6)

[1] A loop momentum is denoted with k throughout this Thesis.

- Class 7. 4-point vertex with k-independent γ-propagator type 1. (Fig.A.7)
- Class 8. 4-point vertex with k-independent Z-boson propagator type 1. (Fig.A.8)
- Class 9. 4-point vertex with k-independent γ propagator type 2. (Fig.A.9)
- Class 10. 4-point vertex with k-independent Z-boson propagator type 2. (Fig.A.10)
- Class 11. Higgs-photon mixing and external leg radiation. (Fig.A.11)
- Class 12. Higgs-Z-boson mixing and external leg radiation. (Fig.A.12)
- Class 13. 4-point vertex with k-independent Z-boson propagator type 3. (Fig.A.13)

Only two classes of these diagrams, diagrams with Higgs and Z/γ mixing (Fig.A.11 and Fig.A.12), are gauge independent[2]. The gauge parameters cancellation happens only if all other classes of diagrams are summed up together.

The Mandelstam notation is the most convenient choice of kinematic variables. Parameters s, t and u are chosen as squares of the four-momenta sum of the leptons, the first lepton with the photon, and the second lepton with the photon, respectively

$$\begin{aligned} (p_1 + p_2)^2 &= s\,, \\ (p_1 + p_\gamma)^2 &= t\,, \\ (p_2 + p_\gamma)^2 &= u\,. \end{aligned} \tag{5.1}$$

The four-momentum of the Higgs particle is expressed through the sum of all other momenta $p_H = p_1 + p_2 + p_\gamma$ according to momentum conservation. In loop amplitudes, the top quark, W- and Z-boson masses are dominant, all other masses including lepton masses are ignored. Applying on-shell conditions, one will obtain scalar products of the external momenta

$$\begin{aligned} p_1 \cdot p_2 &= s/2\,, \\ p_1 \cdot p_\gamma &= t/2, \\ p_1 \cdot p_\gamma &= (m_H^2 - s - t)/2\,, \end{aligned} \tag{5.2}$$

where $u = m_H^2 - s - t$ has been substituted according to the relation

$$s + t + u = \sum_{i=1}^{3} m_i^2\,, \tag{5.3}$$

where i runs over all masses of real particles which are involved in the process.

5.2.1 Tools

These diagrams are calculated using *FeynCalc* [131, 132]. For checks *Package-X* [125] is used, which is connected to *FeynCalc* via *FeynHelpers* [133]. The most convenient way to create diagrams for the further evaluation in *FeynCalc* is the *FeynArts* package[3]. The process of amplitudes generation is divided into three stages: 1) creation of topologies, 2) substitution of all vertices and propagators 3) substitution of all appropriate parameters.

[2] Also subclasses of Classes 3 and 4 with fermion loops are trivially gauge independent.

[3] Both are *Mathematica* packages.

The topology has been created using the Lorentz generic vertex function `Lorentz.gen`, which describes how to create the correct topology structure for the SM processes. The tadpole topology for this process does not provide a non-vanishing contribution and for simplicity has been excluded. Amplitudes were created according to the *FeynArts* SM model `SM.mod`. Only the masses of the top quark m_t, Higgs, W and Z bosons m_H, m_W, m_Z respectively are kept in the one-loop amplitudes.Furthermore, all Yukawas couplings for b-quarks and lighter fermions in the loop amplitudes are ignored. In the code `mH`, `mW`, `mZ`, `mt` are used as the masses of Higgs boson, $W^{\pm}$ and Z bosons, and top quark respectively. `cosW` and `sinW` denote cosine and sine of the Weinberg mixing angle parameter. `pE1`, `pE2`, `pPh`, `pH` are four-momenta of the first and second lepton, photon and Higgs boson respectively, `k` denotes the loop four-momentum.

A few of the amplitudes contain more than one gamma-5 matrix. This is the reason that the NDR gamma matrices scheme is not applicable. For all diagrams except the box diagrams Fig. A.1, the 't Hooft - Veltman - Maison - Breitenlohner scheme have been used[4]. The box diagrams do not contribute divergent $1/\varepsilon$ terms, hence it is safe to apply the NDR scheme for these diagrams. For the one-loop UV-finite process, if all four-momenta corresponding to the dimension -2ε, $\hat{p}_i^{\mu}$ are set to zero the result will not be changed:

```
In[1]:= $BreitMaison = True;
        Momentum[pE1 | pE2 | pPh | pH, D - 4] = 0;
        Momentum[Polarization[pPh, __], D - 4] = 0;
```

FeynCalc and *FeynHelpers* provide all necessary tools for the evaluation of one-loop amplitudes. The most challenging point in this evaluation was to evaluate box diagrams in a general R_{ξ} gauge. The amplitudes have been evaluated with *FeynCalc* ver. 9.2 one by one using the following code

```
In[2]:= expresSec[exp_] :=
         Block[step0, step1, step2, step3, step4, step5, step6, step7[,
          step0 = (Collect2[
              exp // DiracSimplify // Contract // DotSimplify //
                 DiracEquation // PowerExpand // Expand, cosW, mW,
              DiracSpinor, Factoring -> Simplify]) // Simplify;
          step1 =
           step0 // FeynAmpDenominatorSimplify[#, k] & //
            Collect2[#, mW, mZ, cosW, FAD, DiracSpinor,
              Factoring -> Simplify] &;
          step2 = ApartFF[step1, k];
          step3 =
           step2 //
             Collect2[#, FAD, mW, sinW, DiracSpinor,
               Factoring -> Simplify] & // Simplify;
          step4 =
           TID[step3, k, UsePaVeBasis -> True, ToPaVe -> True] //
                  PropagatorDenominatorExplicit[#] & // DiracEquation //
                DiracSimplify // Contract // DotSimplify // Expand //
             Collect2[#, PaVe, A0, B0, C0, D0, IsolateNames -> KK,
               Factoring -> Simplify] & // Simplify;
          step5 = step4 // PaVeReduce // Simplify;
          step6 =
           step5 // FRH // DiracSimplify //
             Collect2[#, PaVe, A0, B0, C0, D0, Factoring -> Simplify] & //
            Simplify;
          step7 =
           step6 /. cosW -> Sqrt[1 - sinW^2] /.
                 Spinor[Momentum[pE1, D], 0, 1] .
                       DiracGamma[Momentum[Polarization[pPh, -I,
```

[4]More details in Sec.4.4.2.

```
                Transversality -> True], D], D] .
            Spinor[-Momentum[pE2, D], 0, 1] ->
          Spinor[Momentum[pE1, D], 0,
                  1] . DiracGamma[Momentum[Polarization[pPh, -I,
                      Transversality -> True], D], D] .
               DiracGamma[6] . Spinor[-Momentum[pE2, D], 0, 1] +
           Spinor[Momentum[pE1, D], 0,
                  1] . DiracGamma[Momentum[Polarization[pPh, -I,
                      Transversality -> True], D], D] .
               DiracGamma[7] . Spinor[-Momentum[pE2, D], 0, 1] //
        PowerExpand // Expand // DotSimplify // DiracSimplify //
     Collect2[#, PaVe, A0, B0, C0, D0, Factoring -> Simplify] & //
    Simplify;
  Print[i++ "This one is good!"];
  step7]
```

This code is not universal. It was optimized for the calculation of box diagrams in the $h \to l\bar{l}\gamma$ process with propagators in general R_ξ gauge. For the diagrams with three and two propagators, the structure of this code is overabundant and very often not optimal. This code can be taken as a basis for the calculation of similar processes , but the structure of the code requires reorganization and optimization. Based on this experience Vladyslav Shtabovenko implemented many optimizations and additional functions in the new version of *FeynCalc 9.3* [134], which make preparation steps more simple.

In `"step0"` the simplification of the Dirac algebra is performed using the *FeynCalc* functions `DiracSimplify`, `Contract`, `DotSimplify` and `DiracEquation`. Every operation produces a lot of additional terms and standard *Mathematica* tools cannot simplify its. An effective reduction of the number of terms can be performed using a *FeynCalc* function `Collect2`. One needs this function for collecting together terms which have a dependence of the selected variable. As an example, the function `Collect2[exp, cosW, mW]` collects together terms which are not free of any dependence of `cosW` and `mW`. It is very important to use the parameter `Factoring` which applies the chosen operation to each prefactor of the collected terms.

In `"step1"` the function `FeynAmpDenominatorSimplify` has been applied. This function simplifies each propagator denominator `FAD` in a canonical way. As an example how it does work

```
In[3]:= a = SPD[k, k] FAD[k, m1[, k + p1, m2, k + p1 + p2, m1 + m2]
```

$$\text{Out[3]=} \quad \frac{k^2}{(k^2 - m1^2)((k+p1)^2 - m2^2)\ ((k + p1 + p2)^2 - (m1+m2)^2)}$$

```
In[4]:= b = FeynAmpDenominatorSimplify[a, k]]
```

$$\text{Out[4]=} \quad \frac{k^2 + 2\ (k \cdot p) + p1^2}{(k^2 - m2^2)((k+p1)^2 - m2^2)\ ((k - p2)^2 - (m1+m2)^2)}$$

This helps to reduce the number of Passarino-Veltman functions and arguments of these functions in further evaluation. In `"step2"` the *FeynCalc* function `ApartFF` performs decomposition of B, C and D Passarino - Veltman functions into A, B and C if the parameters of these functions provide such simplification. More detail in Sec. 4.5.3

In the next `"step3"` important sorting is performed. The number of terms became tremendously huge without this step. In `"step4"`, tensor integral decomposition is performed. This is realized by the function `TID`. After tensor integral decomposition, the Dirac structure needs to be simplified once more. For simple diagrams, the function `TID` can be applied in the first step, but usually further analytical evaluations without preparation steps are not possible for the more complicated amplitudes which contain C and D Passarino - Veltman functions. Usage of `IsolateNames` is another trick how to perform a simplification before further analytical evaluation. At the end of this step, the Passarino-Veltman function is isolated for further transformation. The function `TID` in `"step4"` produces as output non reduced Passarino - Veltman

functions like C_{01} or D_{111}. In `"step5"` and `"step6"` the reduction of those complex Passarino - Veltman functions into elementary A_0, B_0, C_0, D_0, as well as further simplification of the coefficients in front of these functions, is performed. This reduction is the only way to see much of analytic dependence like gauge parameter cancellation or symmetry in the Ward identity coefficients.

During the evaluation, *FeynCalc* produces scalar, pseudoscalar, and also chiral Dirac structures as an output: $\bar{l}l$, $\bar{l}\gamma_5 l$, $\bar{l}P_L l$, and $\bar{l}P_R l$[5]. The scalar and pseudoscalar matrix elements need to be transformed in chiral form for future simplification. In the last `"step7"`, before the summation of the diagrams, this transformation is performed - all operators $\bar{l}l$ and $\bar{l}\gamma_5 l$ are replaced with $\bar{l}P_L l$ and $\bar{l}P_R l$ as

$$(\bar{l}l) = (\bar{l}P_L l) + (\bar{l}P_R l)\,, \tag{5.4}$$

$$(\bar{l}\gamma_5 l) = (\bar{l}P_L l) - (\bar{l}P_R l)\,. \tag{5.5}$$

Also in this step, the cosine of the electroweak mixing angle is replaced with the sine function using trigonometrical identities, this is an important step for further simplification. The vector Dirac structures come in chiral form only and the replacement is not necessary. In the intermediate steps, some structures contain three gamma matrices, but all these contributions cancel after the amplitude's summation.

5.2.2 Gauge dependence and Ward identity

The cancellation of the gauge parameters ξ is a very important check of the evaluation before producing numerical results. In this process, there are two types of massive propagators for gauge bosons

$$iG^{\mu\nu}_{Z(W)}(p,\ \xi) = -\frac{1}{p^2 - m^2_{Z(W)}}\left(g^{\mu\nu} - (1-\xi_{Z(W)})\frac{p^\mu p^\nu}{(p^2 - \xi_{Z(W)} m^2_{Z(W)})}\right)\,, \tag{5.6}$$

and one type of massless propagators

$$iG^{\mu\nu}_{A}(p,\ \xi) = -\frac{1}{p^2}\left(g^{\mu\nu} - (1-\xi_A)\frac{p^\mu p^\nu}{p^2}\right)\,. \tag{5.7}$$

The gauge parameters ξ_W and ξ_Z also appear in Goldstone boson propagators for charged and neutral particles correspondingly

$$iG_{G^\pm(G^0)}(p,\ \xi) = -\frac{1}{p^2 - \xi_{W(Z)} m^2_{W(Z)}}\,. \tag{5.8}$$

All other propagators are gauge independent. The parameters ξ_A, ξ_W and ξ_Z are nonphysical and in real physical processes they must vanish. The cancellation of the gauge parameters ξ_A and ξ_Z is straightforward. These parameters cancel analytically after the summation of all one-loop diagrams and manipulation of Dirac structures. The direct analytic cancellation of the ξ_W parameter had not been obtained within this investigation, but the amplitude is gauge independent. The cancellation also has been checked numerically, the contribution for fixed external kinematic parameters is the same. An important condition for the analytic gauge parameter cancellation is the relation between masses of Z and $W^\pm$ bosons:

$$m_W = m_Z \cos\theta_W\,. \tag{5.9}$$

[5]In *FeynCalc*, the operators P_L and P_R are denoted as γ_7 and γ_6, correspondingly.

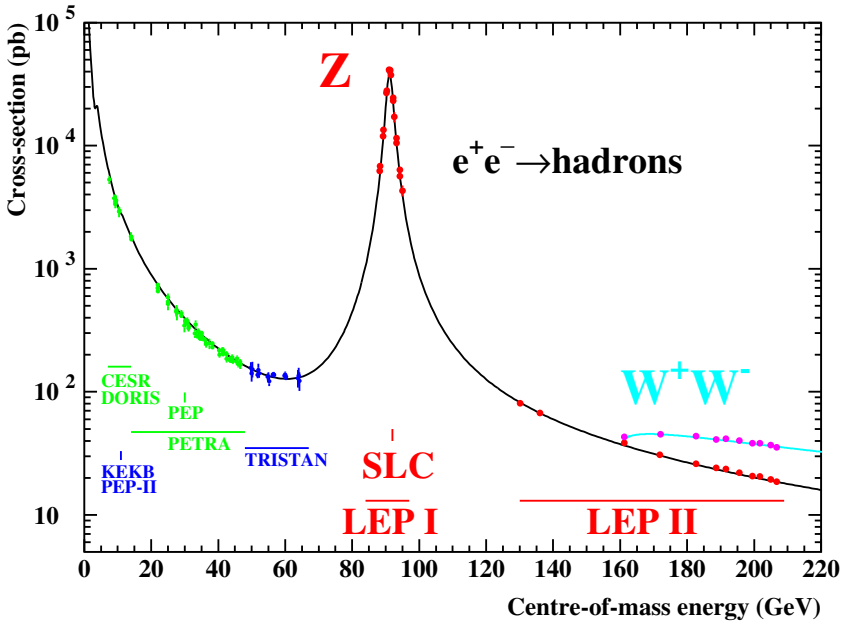

Figure 5.1: The hadronic cross-section as a function of the centre-of-mass energy. (from the LEP EWWG [135])

This condition is important for the cancellation because there are contributions proportional to $\sim \xi_W m_Z^2/(k^2 - m_W^2)$. These contributions are produced because $W^\pm - G^\pm - Z$ vertices are proportional to the mass of the Z boson m_Z, while the gauge dependent parameter ξ_W is a part of $W^\pm$ boson propagator $G_W(p)$. So, in this process the contribution from $W^\pm - G^\pm - Z$ vertices partially cancel with the contribution from that part of propagator which is proportional to $\sim \xi_W m_W^2/(\sin\theta_W)^2(k^2 - m_W^2)$.

Another very important check for this calculation is that the amplitude satisfies the Ward identity. The Ward identity follows from the Ward-Takahashi identities. The Ward-Takahashi identities provides a relation between the fermion n-point function and the $n+1$-point QED function. E.g. one of the Ward-Takahashi identities implies that there are relations between two point fermion function (self-energy) and the fermion-fermion-photon vertex.

The requirement to be gauge invariant provides the Ward identity, for one incoming or outgoing photon it can be written as

$$p_\gamma^\mu \mathcal{A}_\mu(p_\gamma) = 0\,. \tag{5.10}$$

This relation can be generalized to an arbitrary number of photons. Following from this, a two-point function is represented in the most general form as

$$\begin{aligned}\epsilon^{\star\mu}(p_\gamma)\mathcal{A}_\mu(p_\gamma) \;=\; & [((p_\gamma)q_\nu - g_{\mu\nu}p\cdot q)\,\bar{u}(p_2)\big(a\gamma^\nu P_R + b\gamma^\nu P_L\big)v(p_1) \\ & + i\epsilon_{\mu\nu\alpha\beta}(p_\gamma)^\alpha q^\beta \bar{u}(p_2)\big(c\gamma^\nu P_R + d\gamma^\nu P_L\big)v(p_1)]\epsilon^{\star\mu}(p_\gamma)\,,\end{aligned} \tag{5.11}$$

where q is an outgoing momentum, and a, b, c and d are arbitrary coefficients.

For the process $h \to l\bar{l}\gamma$ there are a couple of diagrams which potentially provide the contribution with the antisymmetric tensor. First of all these are the diagrams with fermion loop and Z-boson propagator (the diagrams 1 and 2 in the first row of Fig. A.6). These diagrams contain

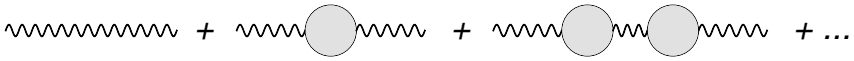

Figure 5.2: Bosonic propagator at all orders. Filled blobs represent one-particle irreducible corrections

---

Dirac traces of five Dirac gamma matrices, one of which is a γ_5 matrix. The result of this trace is the totally antisymmetric epsilon tensor

$$\mathrm{tr}(\gamma^\mu\gamma^\nu\gamma^\rho\gamma^\lambda\gamma_5) = 4i\epsilon^{\mu\nu\rho\lambda}\,. \tag{5.12}$$

In the process $h \to l\bar{l}\gamma$ there are two diagrams which provide a contribution with the antisymmetric epsilon tensor which arises from the Dirac trace. These two diagrams look almost the same, the only difference is in the direction of the fermion line in the loop. Both diagrams provide a non-zero contribution, but the antisymmetric parts of the contributions exactly compensate each other.

The second possible source of the Levi-Civita tensor are diagrams with three Dirac gamma matrices like Fig.A.1. The Chisholm identity suggests the decomposition using the totally antisymmetric tensor

$$\gamma^\mu\gamma^\nu\gamma^\rho = g^{\mu\nu}\gamma^\rho - g^{\mu\rho}\gamma^\nu + g^{\rho\nu}\gamma^\mu + i\epsilon^{\mu\nu\rho\lambda}\gamma^\lambda\gamma_5\,. \tag{5.13}$$

The total sum of all contributions which contain three Dirac gamma matrices in matrix structures for this process is equal zero.

The amplitude with symmetric part only has been obtained within this investigation of the process $h \to l\bar{l}\gamma$

$$\begin{aligned}\mathcal{A}_\mu(p_\gamma) &= \big[((p_\gamma)_\nu\, p_{1\mu} - g_{\nu\mu}\, p_\gamma\cdot p_1)\bar{u}(p_2)\big(a(p_1,p_2)\gamma^\nu P_R + b(p_1,p_2)\gamma^\nu P_L\big)v(p_1)\\ &+ ((p_\gamma)_\nu\, p_{2\mu} - g_{\mu\nu}\, p_\gamma\cdot p_2)\bar{u}(p_2)\big(a(p_2,p_1)\gamma^\nu P_R + b(p_2,p_1)\gamma^\nu P_L\big)v(p_1)\big]\,.\end{aligned} \tag{5.14}$$

where the coefficients $a(p_l)$ and $b(p_l)$ are functions of the lepton momenta p_1 and p_2, and photon momentum p_γ, and also of the masses of the particles involved in the process. All other dependence is not shown in the notation. After evaluation of the amplitude, the coefficients a for p_1 and p_2 are present explicitly in the resulting expression and can be extracted. Analytically the extracted coefficients $a_1(p_1)$ and $a_2(p_2)$ do not look the same, but numerically it is a very good test to check that $a_1(p_1) = a_2(p_1)$ and $a_1(p_2) = a_2(p_2)$. The same holds for the coefficient $b(p)$. In a numerical check one indeed sees that these coefficients are the same.

5.2.3 Breit-Wigner propagator

In this process, at the one-loop level most of the diagrams have propagators that are singular at some kinematic points. As an example, the triangle diagrams with photon or Z-boson propagator without loop momentum Fig.A.5 and Fig.A.6 can be given. The diagrams with Z-boson propagator are proportional to

$$\mathcal{A} \sim \frac{1}{s - m_Z^2}\,. \tag{5.15}$$

It is clear, that for $s = m_Z^2$ all of these diagrams are divergent. Experiments indicate a resonance in the regions around 90 GeV for processes which involve a Z-boson propagator without loop

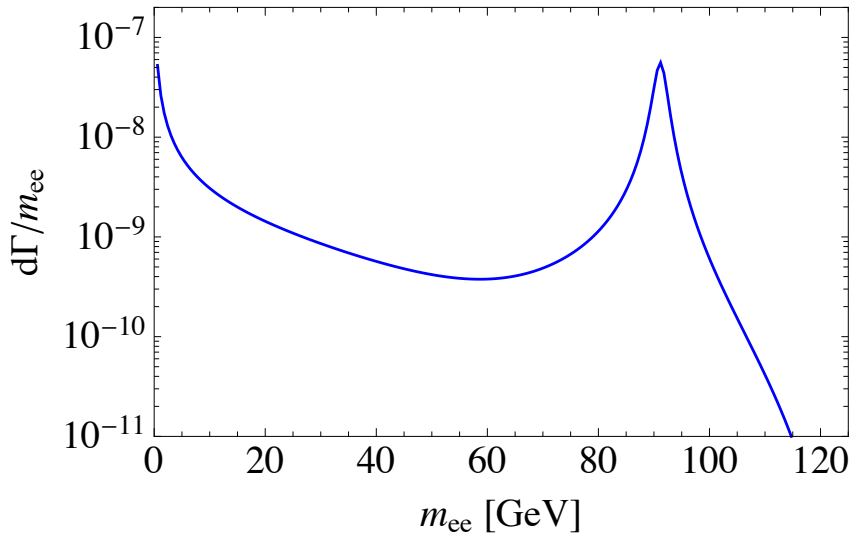

Figure 5.3: Differential decay rate with respect to the invariant dilepton mass $\sqrt{s}$ for electrons. The one-loop is denoted by the blue line. The tree level contribution is negligible in this process. The cuts $E_{\gamma,\,\mathrm{min}} = 5\,\mathrm{GeV}$ have been used.

---

momenta, but this resonance has a finite contribution (Fig. 5.1). This phenomena is explained by a strong influence of nonperturbative effects in the energy region around the Z-boson pole mass. The contributions from all orders of perturbation theory need to be resummed to understand how these effects resolve the problem.

The bosonic propagator expanded to all orders is shown in Fig. 5.2. Filled blobs contain corrections of all orders and ellipsis means summation up to infinity. Every next order provides a smaller correction. In the kinematic region which is far away from the resonance higher order contributions can be ignored. The extra contribution starts to play the dominant role if the propagator's momentum square is very close to the propagator's particle pole mass square.

To obtain the effective propagator, all the diagrams on Fig. 5.2 should be resumed according to the geometric series relation

$$\begin{aligned} G_Z(p) &= \frac{i}{s-m_Z^2} + \frac{i}{s-m_Z^2} i\Sigma(s) \frac{i}{s-m_Z^2} \\ &+ \frac{i}{s-m_Z^2} i\Sigma(s) \frac{i}{s-m_Z^2} i\Sigma(s) \frac{i}{s-m_Z^2} + \dots \\ &= \frac{i}{s-m_Z^2} \left(1 + i\Sigma(s) \frac{i}{s-m_Z^2} + \left(i\Sigma(s) \frac{i}{s-m_Z^2} \right)^2 + \dots \right) \\ &= \frac{i}{s-m_Z^2+\Sigma(s)}\,, \end{aligned} \tag{5.16}$$

where $\Sigma(s)$ denotes the one-particle irreducible corrections.

It is possible to divide the correction $\Sigma(s)$ into three sub-parts. The most general form of the contribution $\Sigma(s)$ is

$$\Sigma(s) = Z^{-1}s + B(s) + i\gamma(s)\,, \tag{5.17}$$

where Z^{-1} is the field renormalization constant, and $B(s)$ and $\gamma(s)$ are real functions which need to be determined. The constant and the functions depend on the renormalization scheme. The on-shell scheme is the most convenient choice, because only the function $\gamma(s)$ is nontrivial.

To determine the value or structure of the $\gamma(s)$ function in the on-shell scheme one must require that the inclusive decay width should be reproduced with $\gamma(s) = m_Z\Gamma(Z \to l\bar{l})$. To obtain this, all $\Gamma(Z \to f\overline{f})$ where $m_Z^2 \geq 4m_f$ need to be summed up according to the optical theorem.

To avoid the divergence around the kinematic region where $s = m_Z^2$, one needs to replace the perturbative propagator with a Breit-Wigner propagator where nonperturbative effects are included

$$\frac{i}{s - m_Z^2} \to \frac{i}{s - m_Z^2 + im_Z\Gamma_Z} \tag{5.18}$$

The theory which is considered in this chapter contains a general R_ξ gauge. The resummation can be generalized for gauge dependent theories [136] as

$$G^{\mu\nu}_{tot,\ Z} = iG_Z^{\mu\nu}(s,\ \xi) + iG_Z^{\mu\rho}(s,\ \xi)i\Sigma_{\rho\sigma}(s)iG_Z^{\sigma\nu}(s,\ \xi) + \ldots = \frac{i}{(G_Z^{\mu\nu}(s,\ \xi))^{-1} + \Sigma^{\mu\nu}(s)}\,, \tag{5.19}$$

where $G_Z^{\mu\nu}(s,\ \xi)$ is the Z-boson propagator in general R_ξ gauge which is given in Eq.(5.6). The inverse function of Z-boson propagator is a two-point function

$$(G_Z^{\mu\nu}(s,\ \xi))^{-1} = g^{\mu\nu}p_Z^2 - \left(1 - \frac{1}{\xi_Z}\right)p_Z^\mu p_Z^\nu\,, \tag{5.20}$$

but in this case the replacement of the propagator is not enough, also vertices should be modified[6]. These modifications produce a lot of additional terms that significantly complicate the evaluation. A much wiser strategy is to obtain gauge cancellation first and then use the replacement for the 't Hooft - Feynman gauge (Eq.5.18).

The value of the decay width Γ_Z is fitted [51] as

$$\Gamma_Z = 2.4952 \pm 0.0023\,\text{GeV}\,. \tag{5.21}$$

5.2.4 Complex-Mass scheme

The Breit-Wigner scheme is very powerful to avoid perturbative divergences which appear in a perturbative QFT and which are not observed in experiments. But the Breit-Wigner scheme has at least two problems. The first problem with the Breit-Wigner scheme is that outside of the resonance region the extra term in denominator $-im\Gamma$ provides an incorrect contribution [138]. The second problem with the Breit-Wigner scheme is the violation of gauge invariance [139].

The Complex-Mass scheme is an alternative approach that does not break gauge invariance and remains valid in the full phasespace region. In this scheme, all masses in amplitudes are replaced, not only the mass in the propagator like in the Breit-Wigner scheme (Eq. 5.18)

$$m^2 \to \mu^2 = m^2 - im\Gamma\,. \tag{5.22}$$

This provides that all coupling constants which are related to the mass are complex. The Complex-Mass Scheme is not a panacea, with restoring the gauge invariance it breaks perturbative unitarity. This means that Cutkosky cutting rules are not valid anymore and cannot be used to verify unitarity [138].

[6]For details see e.g. [136].

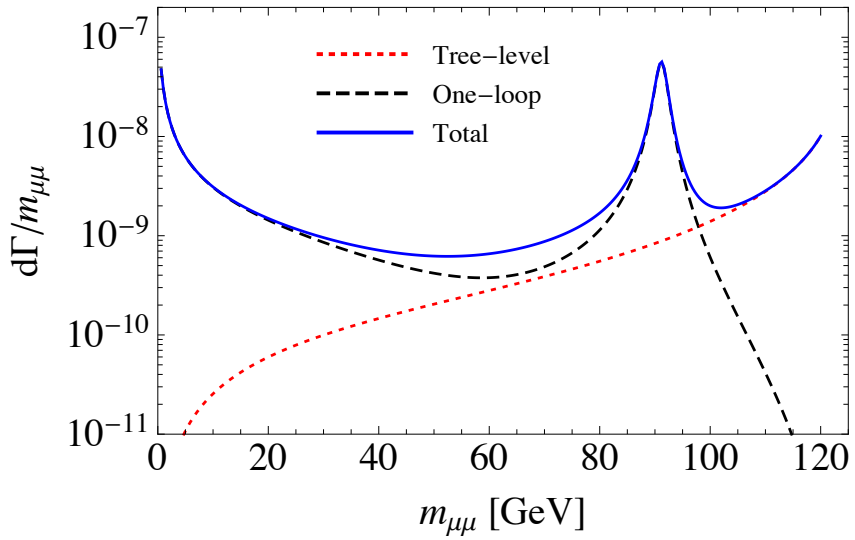

Figure 5.4: Differential decay rate with respect to the invariant dilepton mass $\sqrt{s}$ for muons. The tree level, one-loop, and total contributions are denoted by red dotted, black dashed lines, and solid blue lines, respectively. The cuts $E_{\gamma,\,\mathrm{min}} = 5\,\mathrm{GeV}$ have been used.

The Breit-Wigner scheme is much easier for the implementation in *FeynCalc*, and for the process $h \to l\bar{l}\gamma$, the propagator replacement has been implemented at the step where the gauge parameter $\xi_{Z(W,A)}$ dependence vanishes. It is impossible to check whether the gauge dependent contributions from all diagrams are canceled out before the propagator replacement if the Feynman gauge is used. If the replacement happens before the cancellation this will provide an incorrect result. The Complex-Mass scheme is much safer with the Feynman gauge than the Breit-Wigner method.

Within this research, the results have been compared in both Breit-Wigner and Complex-Mass scheme approximations. The numerical difference is negligible between the differential decay width with respect to the invariant dilepton mass $d\Gamma(h \to l\bar{l}\gamma)/d\sqrt{s}$ in these approaches.

5.3 Results

The total decay rate consists of two main contributions from the tree and one-loop level Γ_{tree} and Γ_{loop}. The interference between tree and one-loop level is negligible and has been ignored. The differential decay rate with respect to ds and dt for the tree and for the loop level contribution are

$$\begin{aligned}\frac{d^2\Gamma_{\mathrm{tree}}}{ds\,dt} &= \mathcal{N}\Big[\frac{9m_l^4 + m_l^2(-2s+t-3u) + t\,u}{(t-m_l^2)^2} + \frac{9m_l^4 + m_l^2(-2s+u-3t) + t\,u}{(u-m_l^2)^2} \\ &+ \frac{34m_l^4 - 2m_l^2(8s+5(t+u)) + 2(s+t)(s+u)}{(t-m_l^2)(u-m_l^2)}\Big]\,, \end{aligned} \tag{5.23}$$

where the constant factor $\mathcal{N}$ is

$$\mathcal{N} = \frac{e^4 m_l^2}{256\,\pi^3 \sin^2\theta_W m_W^2 m_H^3}\,, \tag{5.24}$$

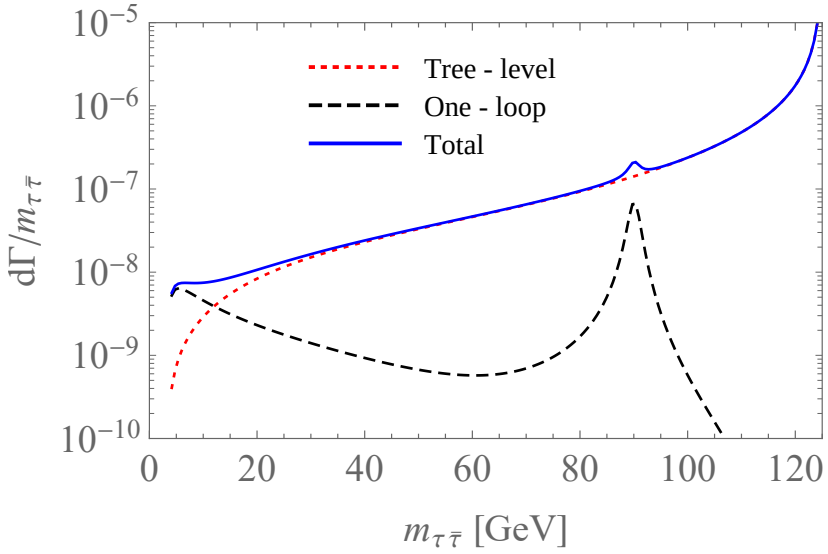

Figure 5.5: Differential decay rate with respect to the invariant dilepton mass $\sqrt{s}$ for tau leptons. The tree level, one-loop, and total contributions are denoted by red dotted, black dashed lines, and solid blue lines, respectively. The cuts $E_{\gamma,\,\mathrm{min}} = 5\,\mathrm{GeV}$ have been used. The contribution from the loop level is recognizable in the photon and Z-boson resonance region only.

---

and,

$$\frac{d^2\Gamma_{\mathrm{loop}}}{ds\,dt} = \frac{s}{512\pi^3 m_H^3}\left[t^2(|a(p_1,p_2)|^2 + |b(p_1,p_2)|^2) + u^2(|a(p_2,p_1)|^2 + |b(p_2,p_1)|^2)\right], \tag{5.25}$$

$a(p_x,p_y)$, $b(p_x,p_y)$ are coefficients from the Ward identity (Eq. 5.14), where

$$
\begin{aligned}
a(p_1,p_2) = \frac{e^4}{(2\pi)^2}\Bigg[& \frac{8m_t^2\big((D-4)m_H^2-(D-2)s\big)B_0(m_H^2,m_t^2,m_t^2)}{3m_W\sin\theta_W(D-2)s(m_H^2-s)^2} + \frac{16m_t^2B_0(s,m_t^2,m_t^2)}{3m_W\sin\theta_W(D-2)(m_H^2-s)^2} \\
& - \frac{\big(2(D-1)m_W^2+m_H^2\big)\big((D-4)m_H^2-(D-2)s\big)B_0(m_H^2,m_W^2,m_W^2)}{2\,m_W\sin\theta_W(D-2)s(m_H^2-s)^2} \\
& - \frac{\big(2(D-1)m_W^2+m_H^2\big)B_0(s,m_W^2,m_W^2)}{m_W\sin\theta_W(D-2)(m_H^2-s)^2} \\
& - \frac{2m_t^2\big(-2m_H^2+2s+8m_t^2\big)C_0(0,m_H^2,s,m_t^2,m_t^2,m_t^2)}{3\,m_W\sin\theta_W\,s(m_H^2-s)} \\
& + \frac{m_W\big(-3m_H^2+6m_W^2+4s\big)C_0(0,m_H^2,s,m_W^2,m_W^2,m_W^2)}{\sin\theta_W\,s(m_H^2-s)} \\
& + \frac{m_Z\sin\theta_W}{\cos^3\theta_W}\big(D_{23}(0,u,0,t,0,m_H^2,0,m_Z^2,0,m_Z^2)+(D_{23}\to D_{33})\big) \\
& + \frac{1}{s-m_Z^2+im_Z\Gamma_Z}\Bigg(\frac{(4\cos\theta_W^2-1)m_ZC_0(0,m_H^2,s,m_W^2,m_W^2,m_W^2)}{\cos\theta_W\sin\theta_W} \\
& + \frac{(5-8\cos\theta_W^2)m_t^2C_0(0,m_H^2,s,m_t^2,m_t^2,m_t^2)}{6\cos^2\theta_W\sin\theta_Wm_W} + \frac{2(8\cos\theta_W^2-5)m_t^2C_{12}(0,m_H^2,s,m_t^2,m_t^2,m_t^2)}{3\cos^2\theta_W\sin\theta_Wm_W} \\
& - \frac{\big(2m_W^2(6\cos^2\theta_W-1)+(2\cos^2\theta_W-1)m_H^2\big)C_{12}(0,m_H^2,s,m_W^2,m_W^2,m_W^2)}{2\,\cos^2\theta_W\sin\theta_Wm_W}\Bigg)\Bigg],
\end{aligned}
\tag{5.26}
$$

here, the explicit kinematic dependence is hidden into functions s,t,u which depend on p_1 and p_2 (Eq.5.1) for shortness. The coefficient $a(p_2,p_1)$ can be obtained by interchanging t with u in $a(p_1,p_2)$

$$
a(p_2,p_1) = a(p_1,p_2)|_{t\leftrightarrow u}, \tag{5.27}
$$

and

$$
\begin{aligned}
b(p_1,p_2) = \frac{e^4}{(2\pi)^2}\Bigg[& \frac{8\big((D-4)m_H^2-(D-2)s\big)B_0(m_H^2,m_t^2,m_t^2)m_t^2}{3\,m_W\sin\theta_W(D-2)(m_H^2-s)^2 s} + \frac{16B_0(s,m_t^2,m_t^2)m_t^2}{3m_W\sin\theta_W(D-2)(m_H^2-s)^2} \\
& - \frac{(m_H^2+2(D-1)m_W^2)B_0(s,m_W^2,m_W^2)}{m_W\sin\theta_W(D-2)(m_H^2-s)^2} \\
& - \frac{\big(m_H^2+2(D-1)m_W^2\big)\big((D-4)m_H^2-(D-2)s\big)B_0(m_H^2,m_W^2,m_W^2)}{2\,m_W\sin\theta_W(D-2)(m_H^2-s)^2 s} \\
& + \frac{2\big(2m_H^2-8m_t^2-2\,s\big)C_0(0,m_H^2,s,m_t^2,m_t^2,m_t^2)m_t^2}{3m_W\sin\theta_W(m_H^2-s)s} \\
& + \frac{m_W\big(-3m_H^2+6m_W^2+4\,s\big)C_0(0,m_H^2,s,m_W^2,m_W^2,m_W^2)}{\sin\theta_W\,(m_H^2-s)s} \\
& - \frac{m_W D_0(m_H^2,0,0,0,s,t,m_W^2,m_W^2,m_W^2,0)}{2\sin^3\theta_W} - \frac{m_W D_1(0,t,m_H^2,s,0,0,m_W^2,0,m_W^2,m_W^2)}{2\,\sin^3\theta_W} \\
& + \frac{m_W D_3(0,u,m_H^2,s,0,0,m_W^2,0,m_W^2,m_W^2)}{2\,\sin^3\theta_W} - \frac{m_W D_3(0,t,m_H^2,s,0,0,m_W^2,0,m_W^2,m_W^2)}{2\,\sin^3\theta_W} \\
& + \frac{m_W D_{12}(0,t,m_H^2,s,0,0,m_W^2,0,m_W^2,m_W^2)}{2\,\sin^3\theta_W} \\
& + \frac{m_Z(1-2\cos^2\theta_W)^2 D_{23}(0,u,0,t,0,m_H^2,0,m_Z^2,0,m_Z^2)}{4\,\cos^3\theta_W\sin^3\theta_W} \\
& + \frac{m_W D_{23}(0,u,m_H^2,s,0,0,m_W^2,0,m_W^2,m_W^2)}{2\sin^3\theta_W} \\
& + \frac{m_W D_{23}(0,t,m_H^2,s,0,0,m_W^2,0,m_W^2,m_W^2)}{2\sin^3\theta_W} \\
& + \frac{m_Z(1-2\cos^2\theta_W)^2 D_{33}(0,u,0,t,0,m_H^2,0,m_Z^2,0,m_Z^2)}{4\cos^3\theta_W\sin^3\theta_W} \\
& - \frac{1}{s-m_Z^2+im_Z\Gamma_Z}\Bigg(\frac{(2\cos^2\theta_W-1)(4\cos^2\theta_W-1)m_Z C_0(0,m_H^2,s,m_W^2,m_W^2,m_W^2)}{2\cos\theta_W\sin^3\theta_W} \\
& + \frac{(5-8\cos^2\theta_W)(2\cos^2\theta_W-1)m_t^2 C_0(0,m_H^2,s,m_t^2,m_t^2,m_t^2)}{12\,\cos^2\theta_W\sin^3\theta_W m_W} \\
& - \frac{(2\cos^2\theta_W-1)\big(2m_W^2(6\cos^2\theta_W-1)+(2\cos^2\theta_W-1)m_H^2\big)C_{12}(0,m_H^2,s,m_W^2,m_W^2,m_W^2)}{4\cos^2\theta_W\sin^3\theta_W m_W} \\
& + \frac{(2\cos^2\theta_W-1)(8\cos^2\theta_W-5)m_t^2 C_{12}(0,m_H^2,s,m_t^2,m_t^2,m_t^2)}{3\,\cos^2\theta_W\sin^3\theta_W m_W}\Bigg)\Bigg]. \qquad (5.28)
\end{aligned}
$$

The second coefficient $b(p_2,p_1)$ can be obtained from $b(p_1,p_2)$ in the same way as $a(p_2,p_1)$ from $a(p_1,p_2)$.

The lepton mass m_l is neglected in the loop amplitude, however it plays a crucial role in the tree-level contribution. For the numerical result, s and t were restricted by the upper and lower limit as

$$
\begin{aligned}
s_{\min} = 4\,m_\ell^2\,, \quad s_{\max} = m_H^2\,, \\
t_{\min(\max)} = \frac{1}{2}\left(m_H^2 - s + 2m_\ell^2 \mp (m_H^2-s)\sqrt{1-4m_\ell^2/s}\right). \qquad (5.29)
\end{aligned}
$$

Here are all parameters which have been used to obtain numerical results

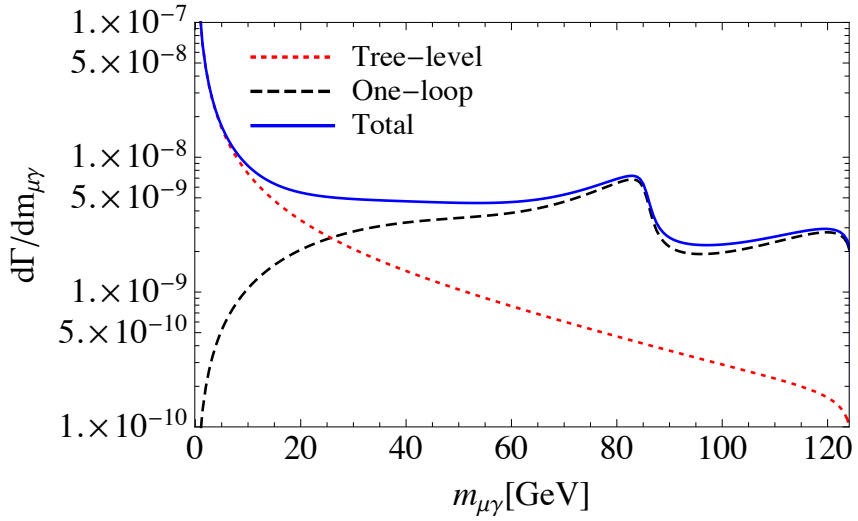

Figure 5.6: Differential decay rate with respect to the invariant mass $\sqrt{t}$ of the muon-photon pair. The tree level, one-loop, and their sum are denoted by red dotted, black dashed lines, and solid blue lines, respectively. No cuts on s have been introduced.

$$
\begin{gathered}
m_W = 80.379\,\mathrm{GeV}\,, \qquad m_Z = 91.1876\,\mathrm{GeV}\,, \qquad \sin^2\theta_W = 1 - \frac{m_W^2}{m_Z^2} = 0.223013\,, \\
m_t = 173.1\,\mathrm{GeV}\,, \qquad m_H = 125.1\,\mathrm{GeV}\,, \qquad m_e = 5.110 \times 10^{-4}\,\mathrm{GeV}\,, \qquad m_\mu = 0.106\,\mathrm{GeV}\,, \\
G_F = 1.1663787 \times 10^{-5}\,\mathrm{GeV}^{-2}\,, \qquad \alpha^{-1} = \frac{\pi}{\sqrt{2} G_F m_W^2 \sin^2\theta_W} = 132.184\,,
\end{gathered}
\tag{5.30}
$$

where m_W and m_Z are the W and Z bosons masses, θ_W is the mixing Weinberg angle, m_t is the top quark mass, m_H is the mass of the SM Higgs boson, m_e and m_μ are masses of electron and muon respectively, G_F is the Fermi coupling constant, and $\alpha = e^2/(4\pi)$ is the fine structure constant. The structure constant α in this calculation strongly depends on the fundamental parameters of the SM, as e.g. in Ref. [137]. Higher orders of radiative corrections provide a more known value for the structure constant $\alpha \simeq 1/128$, but this also requires higher order corrections for the other inputs.

Moreover, the kinematical cuts of Ref. [140, 141], have been implemented for the evaluation of the full decay rates:

$$
s, t, u > (0.1\, m_H)^2\,, \qquad E_\gamma > 5\,\mathrm{GeV}\,, \qquad E_1 > 7\,\mathrm{GeV}\,, \qquad E_2 > 25\,\mathrm{GeV}\,. \tag{5.31}
$$

The results do not change if the cuts on E_1 and E_2 are interchanged.

The total decay rates are

$$
\Gamma^{(e)} = 0.237\,\mathrm{keV}\,, \quad \Gamma^{(\mu)} = 0.262\,\mathrm{keV}. \tag{5.32}
$$

The difference between $\Gamma^{(e)}$ and $\Gamma^{(\mu)}$ comes from the larger Yukawa coupling in the case of the decay into muons.

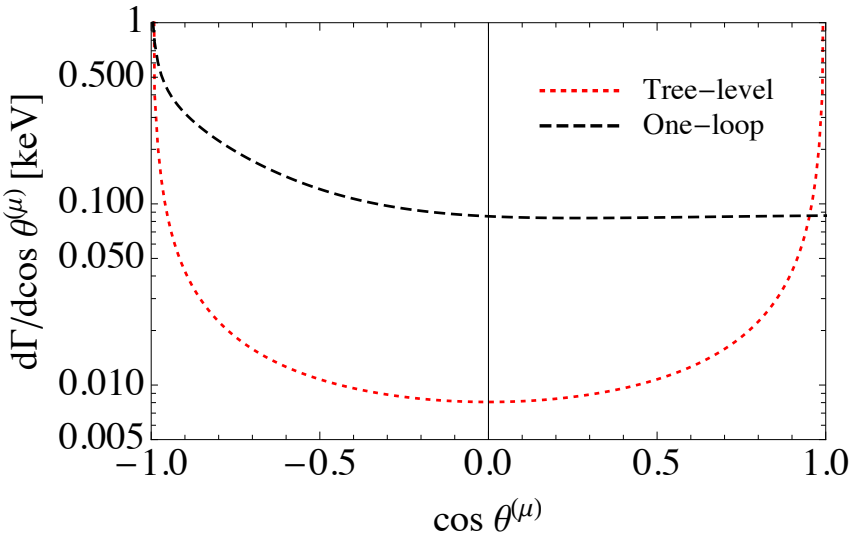

Figure 5.7: Differential decay rate with respect to $\cos\theta^{(\mu)}$, here $\theta^{(\mu)}$ is the angle between the lepton and the photon in the rest frame of the Higgs boson. For the integration over $m_{\mu\mu}$ the cuts $m_{\mu\mu} > 0.1 m_H$ and $E_{\gamma,\min} = 5\,\text{GeV}$ have been applied.

The differential decay rate for electrons with respect of the invariant mass $\sqrt{s}$ of dilepton pair is presented in Fig. 5.3, differential decay rate for muon with respect of the invariant mass of dilepton pair $\sqrt{s}$ and muon-photon pair $\sqrt{t}$ are presented in Figs. 5.4 and 5.6.

5.3.1 Forward-backward asymmetry

As a part of this analysis the θ_l angular dependence of the differential decay distribution has been studied, where θ_l is the angle between lepton and photon in the Higgs boson rest frame. The Mandelstam variable t has this dependence according to the definition Eq.5.1

$$t = E_\gamma(E_1 - |\vec{p}_1|\cos\theta_{(l)}). \tag{5.33}$$

The distribution for the muon case has been presented in Fig. 5.7, where cuts $m_{\mu\mu} > 0.1 m_H$ and $E_\gamma > 5\,\text{GeV}$ [7] have been introduced.

The forward-backward asymmetry with respect to θ_l is defined as

$$\mathcal{A}_{l,\text{FB}} = \frac{\int_{-1}^{0} \frac{d\Gamma}{d\cos\theta_l} - \int_{0}^{1} \frac{d\Gamma}{d\cos\theta_l}}{\int_{-1}^{0} \frac{d\Gamma}{d\cos\theta_l} + \int_{0}^{1} \frac{d\Gamma}{d\cos\theta_l}}, \tag{5.34}$$

which provides the results for the electronic and muonic decays

$$\mathcal{A}_{e,\text{FB}} = 0.342\,, \quad \mathcal{A}_{\mu,\text{FB}} = 0.255\,. \tag{5.35}$$

The difference in the numerical result between $\mathcal{A}_{e,\text{FB}}$ and $\mathcal{A}_{\mu,\text{FB}}$ is more pronounced than the difference between Γ_e and Γ_μ in Eq. 5.32, because different cuts are used in these two cases.

[7] There are no cuts on leptons energy $E_{1,2}$.

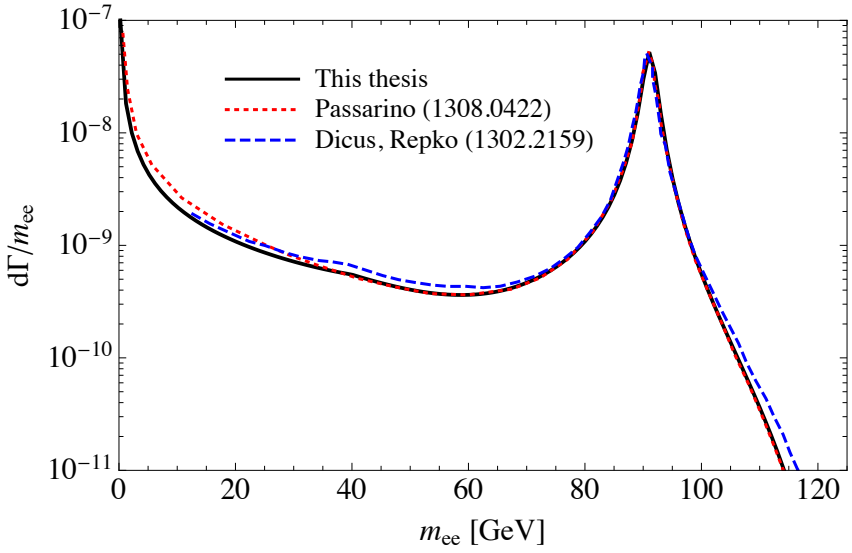

Figure 5.8: Differential decay rate with respect to the invariant dielectron mass. In all compared results the same cuts were implemented. The result, which was obtained within this Thesis, is denoted by the black solid line, while the results of Refs. [140] and [141] are denoted by blue long-dashed lines and red short-dashed, respectively. The cuts $s, t, u > (0.1\, m_H)^2$, $E_\gamma > 5\,\text{GeV}$, $E_1 > 7\,\text{GeV}$, $E_2 > 25\,\text{GeV}$ have been used.

5.4 Comparison with previous results

In this section the discrepancies with respect to previous evaluations in the literature will be discussed. Only in two papers [142, 143] the analytic result was provided. In the first paper, the Ward structure contains only the symmetric part, while the second paper also suggests the term that involves the completely antisymmetric Levi-Civita tensor in the final result for the amplitude. The result that was obtained within this study does not confirm the presence of this term. Numerical evaluation of the result from the first paper[8] in some regions provides quantitative agreement, meanwhile, it also provides significant disagreement in others regions. The plots in Refs. [140] and [141] for $d\Gamma(h \to l\bar{l}\gamma)/dm_{ee}$ were digitalized. The same, as in these references, cuts for the result obtained during the PhD project were implemented. These results were compared in Fig. 5.8. In previous manuscripts, the results differ up to 30%. The result, which was obtained in this investigation, is close to the result obtained by Passarino in the region $m_{ee} > 40\,\text{GeV}$ in Ref. [141]. For smaller values of the dielectron invariant mass, the results are notably different.

The choice of the fine structure constant α can make the difference smaller, especially in the region with $m_{ee} > 35\,\text{GeV}$. The value of the fine structure constant inverse $\alpha^{-1} = 128$ cannot completely resolve the disagreement. Numerical integration over t eventually also provides a difference in the shape of the distribution. The differential distributions have been integrated over the Mandelstam variable t with different tools, in order to cross-check the result. The total rate $\Gamma^{(e)} = 0.237\,\text{keV}$ reasonably agrees with the result $\Gamma^{(e)} = 0.233\,\text{keV}$ provided in Ref. [141]. In the same work, a disagreement with this investigation of the tree-level contribution to the process $h \to \mu\bar{\mu}\gamma$ by a factor of 2 has been found.

Different cuts have been chosen to obtain the decay rate for the same process $h \to l\bar{l}\gamma$ in

[8]The typo, which was reported in Ref. [140], was taken into account.

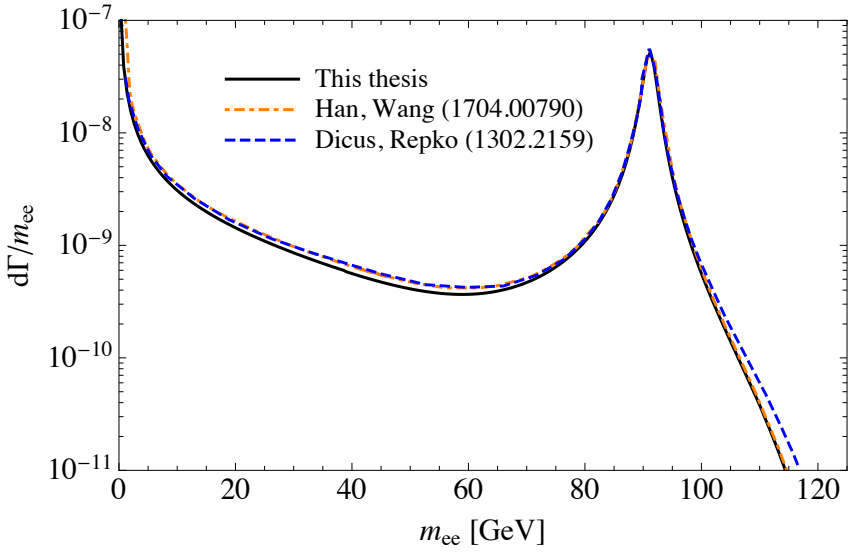

Figure 5.9: Differential decay rate with respect to the invariant dielectron mass. The result, which was obtained within this Thesis is denoted by the black solid line, the results of Refs. [144] and [140] are denoted by orange dash-dotted and blue dashed lines, respectively.

Ref. [144]

$$\Delta R_{\gamma e^+} > 0.4\,, \qquad \Delta R_{\gamma e^-} > 0.4\,, \tag{5.36}$$

where $\Delta R_{\gamma f} = (\Delta\eta^2 + \Delta\phi^2)^{1/2}$ indicates the rapidity-azimuthal angular separation. The result of Han and Wang was also compared with this investigation: the cuts which are shown in Eq. 5.36 do not provide a large influence on the loop-induced contribution. Comparing results without cuts (Fig. 5.9), one finds a good agreement between Refs. [140] and [144] in the energy region below the Z peak. For the region $m_{\mu\bar{\mu}} > m_Z$, Ref. [144] shows good agreement with this investigation.

5.5 Comparison with approximate results

From the plot in Fig. 5.3 one observes that the largest contribution to the total decay rate comes from the region near the Z-peak. Also, one notes the effect of the photon peak rising towards the small values of the dielectron invariant mass $m_{ee} < 10\,\text{GeV}$ but this region is hardly accessible in accelerator experiments because of the high level of background radiation. To avoid the calculation of complicated box diagrams and in order to sufficiently reduce the number of diagrams, one can approximate the process $h \to l\bar{l}\gamma$ as an one-loop contribution $h \to Z\gamma$ with on-shell Z boson and further decay $Z \to l\bar{l}$. In this approximation, the Z-boson propagator is replaced with the Breit-Wigner propagator

$$\mathcal{A} \sim \frac{C(hZ\gamma)}{s - m_Z^2 + i m_Z \Gamma_Z}\,, \tag{5.37}$$

where $C(hZ\gamma)$ is the decay amplitude of the $h \to Z\gamma$ process. In this approximation, the result is gauge independent, but for the full kinematic region, Z-boson is assumed to be on-shell, what is not true.

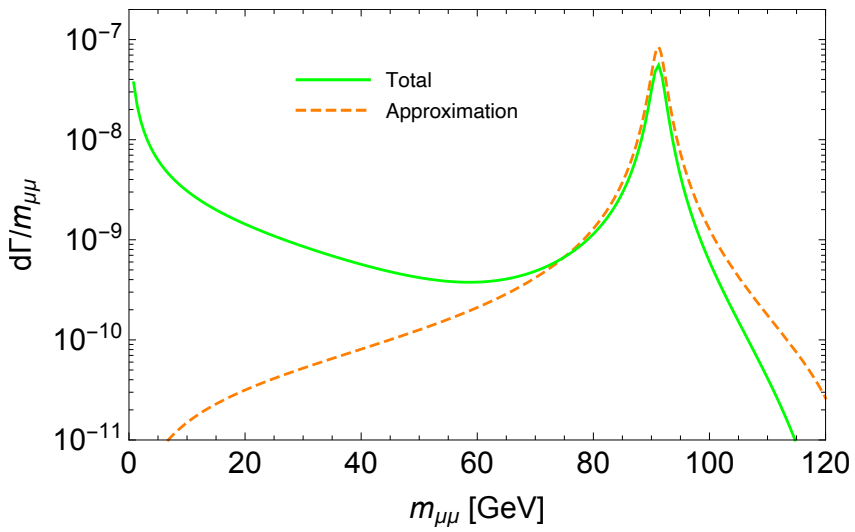

Figure 5.10: Differential decay rates with respect to the invariant dielectron mass. The full result is denoted by green solid line, the approximate result for the process $h \to Z\gamma[Z \to l\bar{l}]$ is denoted by orange dashed line, respectively.

From the plot, which is shown in Fig. 5.10, there are a few observations: first, the total decay rate is dependent on the integration limit. In the region $80\,\text{GeV} < m_{ee} < 100\,\text{GeV}$ the agreement is reasonably well. Meanwhile, in all other regions, the result differs significantly. The second observation, although the full result and approximation agree in shape, the total result is lower in the region $m_{ee} > 80\,\text{GeV}$, because of interference contributions. These conclusions are consistent with the results found in Figure 2 of Ref. [141].

Chapter 6

B to $K^{(\star)}$ plus missing energy

6.1 Introduction

Studying of the rare process $b \to s\phi$ could provide some hints about properties and interactions of particles in the Dark Sector. Here ϕ is a scalar mediator which connects the DM sector with the SM. This mediator is coupled to the SM through the Higgs portal. It is convenient to consider this process in the physical mass eigenbasis. In this basis, the model has two physical states - for sufficiently small mixing angle the first h_1 is a heavy state, which corresponds to the 125 GeV excitation observed in *LHC* experiments [67, 145], and the second h_2 is light.

In this chapter the calculation of the loop-induced amplitude $b \to sh_2$ will be revisited. The result, which can be found in the literature, is derived from the SM $h\bar{s}b$ vertex, where the Higgs boson is off-shell [147]. But the gauge dependence for this vertex is not canceled [146]. This observation was a reason to revisit $\bar{s}bh_2$ vertex. The calculations were performed in an arbitrary R_ξ gauge. This was done in order to provide additional investigation of the standard approach and also to clarify the cancellation of the gauge parameter ξ in physical observables. In this chapter, first, the model will be briefly reviewed[1], also the details about mass matrix diagonalization will be provided. Later, the mechanism of the gauge cancellation for different simple DM models will be discussed. And finally, a benchmark for the experiment *Belle II* will be proposed. The light scalar h_2, if it exists, will decay back to SM particles. In some scenarios it can be observed as displaced vertices in collider experiments.

6.2 Model

The model with an extra scalar boson, which serves as a mediator to the Dark sector, is described by the Lagrangian

$$\mathcal{L} = \mathcal{L}'_{SM} - V, \tag{6.1}$$

where $\mathcal{L}'_{SM}$ is the SM Lagrangian without scalar potential. The scalar potential V, which substitutes the standard V_H (Eq. 2.24), is

$$V \;=\; V_H + V_{H\phi} + V_\phi + \text{h.c.}\,, \tag{6.2}$$

where

[1] Review of the BSM scalar sector can be found in Chapter 3.

$$\begin{aligned} V_H &= -\mu^2 H^\dagger H + \frac{\lambda}{4}(H^\dagger H)^2\,, \\ V_{H\phi} &= \frac{\alpha_2}{2}\,\phi(H^\dagger H)\,, \\ V_\phi &= \frac{m^2}{2}\phi^2 + \frac{\kappa_4}{4}\phi^4\,, \end{aligned} \tag{6.3}$$

and where H is the SM Higgs doublet

$$H = \begin{pmatrix} G^+ \\ (v + h + iG^0)/\sqrt{2} \end{pmatrix}. \tag{6.4}$$

The term $\sim \phi^2 H^\dagger H$ is not included in the scalar potential (Eq. 6.2), because this term does not change the low-energy phenomenology which is related to the considered process. This term provides an additional contribution to the self-interactions that is not relevant in this investigation.

To obtain new Feynman rules in terms of physical states h_1 and h_2 observables, one needs to diagonalize a mass matrix M

$$M^2 = \begin{pmatrix} \mu_h^2 & \mu_{h\phi}^2/2 \\ \mu_{h\phi}^2/2 & \mu_\phi^2 \end{pmatrix}, \tag{6.5}$$

where the explicit form of the mass matrix elements will be determined later.

According to the algebraic relations, which are valid for any invertible matrix M, there is an identity

$$\varphi^\dagger U U^{-1} M U U^{-1} \varphi = (U^{-1}\varphi)^\dagger M_{diag} (U^{-1}\varphi) = \varphi'^\dagger M_{diag} \varphi', \tag{6.6}$$

where U is a unitary transformation, $\varphi^\dagger = (h \;\; \phi)^T$, and the new state is defined as $\varphi' = (h_1 \;\; h_2)^T$. The diagonal mass matrix, which corresponds to the mass matrix (Eq. 6.5), is determined as

$$M_{diag} = \begin{pmatrix} \frac{1}{2}\left(\mu_h^2 + \mu_\phi^2 - K\right) & 0 \\ 0 & \frac{1}{2}\left(\mu_h^2 + \mu_\phi^2 + K\right) \end{pmatrix}, \tag{6.7}$$

where $K = \sqrt{\mu_h^4 + 2\mu_\phi^2\mu_h^2 + \mu_\phi^4 + \mu_{h\phi}^4}$ is introduced for convenience.

This matrix will be obtained if one applies the unitary matrix, which is represented by

$$U = \begin{pmatrix} \dfrac{1}{\sqrt{\left(\mu_\phi^2 - \mu_h^2 + K\right)^2/\mu_{h\phi}^4 + 1}} & \dfrac{\mu_h^2 - \mu_\phi^2 - K}{\sqrt{\left(\mu_\phi^2 - \mu_h^2 + K\right)^2 + \mu_{h\phi}^4}} \\ \dfrac{1}{\sqrt{\left(\mu_h^2 - \mu_\phi^2 + K\right)^2/\mu_{h\phi}^4 + 1}} & \dfrac{\mu_h^2 - \mu_\phi^2 + K}{\sqrt{\left(\mu_h^2 - \mu_\phi^2 + K\right)^2 + \mu_{h\phi}^4}} \end{pmatrix}. \tag{6.8}$$

Since this matrix is orthogonal, it can be parametrized as:

$$U = \begin{pmatrix} \cos\theta & -\sin\theta \\ \sin\theta & \cos\theta \end{pmatrix}. \tag{6.9}$$

The mass eigenstate fields are denoted by h_1 and h_2. They are expressed in terms of the fields ϕ and h as

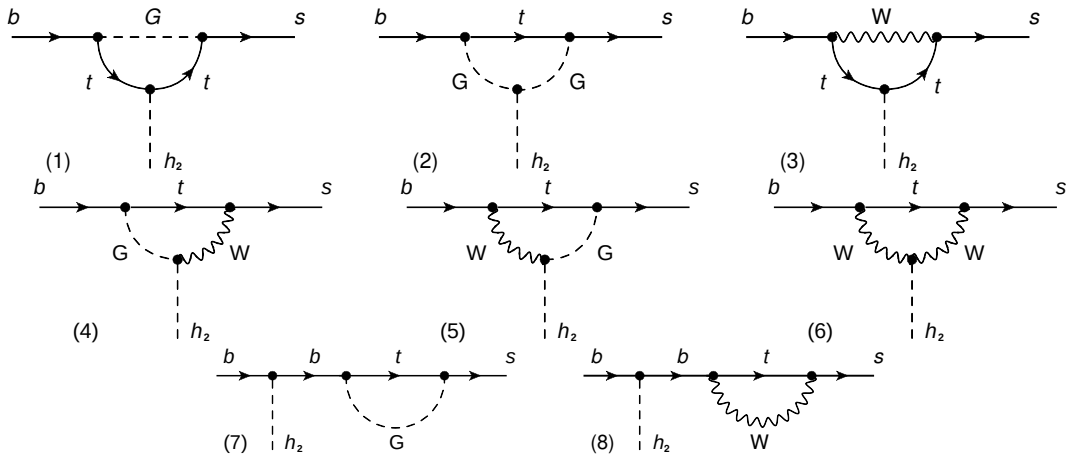

Figure 6.1: One-loop diagrams contributing to $b \to s h_2$ in R_ξ gauge.

$$\begin{aligned} h_1 &= h\cos\theta + \phi\sin\theta, \\ h_2 &= -h\sin\theta + \phi\cos\theta. \end{aligned} \tag{6.10}$$

One can check that both definitions of $\cos\theta$ and $\sin\theta$ in Eq. 6.8 are equivalent.

6.3 Gauge dependence

In the next step, the model parameters μ and m need to be expressed in terms of physical *vev* v and v_ϕ. This is important in order to find Feynman rules in the new parameterisation. To perform this one can write down the Lagrangian in the massdiagonal basis. The mass matrix elements are defined as

$$\begin{aligned} \mu_h^2 &\equiv \frac{\partial^2 V}{\partial h^2} = \frac{\lambda v^2}{2}, \\ \mu_{h\phi}^2 &\equiv \frac{\partial^2 V}{\partial h \partial \phi} = \frac{\alpha_2 v}{2}, \\ \mu_\phi^2 &\equiv \frac{\partial^2 V}{\partial \phi^2} = 2\kappa_4 v_\phi^2 - \frac{\alpha_2 v^2}{4 v_\phi}. \end{aligned} \tag{6.11}$$

The *vev* v_ϕ appears even if mass squared m^2 has the "correct" sign in the potential of the model in general R_ξ gauge, $m^2 > 0$.

A bit more work has to be performed to obtain the Feynman rules for the process $b \to s h_2$ in a general R_ξ gauge. Reading the Lagrangian, which is written in terms of observables, one can find the expression for the required vertices

$$\begin{aligned} G^+G^-h_1 : &\quad -i\frac{e m_{h_1}^2 \cos\theta}{2 m_W \sin\theta_W}, \\ G^+G^-h_2 : &\quad i\frac{e m_{h_2}^2 \sin\theta}{2 m_W \sin\theta_W}. \end{aligned} \tag{6.12}$$

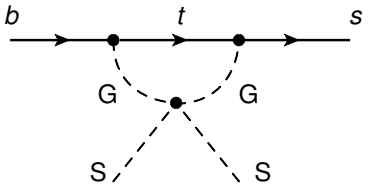

Figure 6.2: One-loop diagram which cancels gauge dependence in the model where the DM is represented by scalar particle.

These vertices are simply a rescaling of the corresponding SM Higgs vertex with additional replacement of m_h to m_{h_1} or m_{h_2} in the case of $G^+G^-h_1$ or $G^+G^-h_2$, respectively.

The diagram contributions $\mathcal{A}_i$ have been decomposed as $\mathcal{A}_i = \tilde{\mathcal{A}}_i + \mathcal{A}_i^{(\xi)}$, where $\tilde{\mathcal{A}}_i$ is the gauge independent part of the contribution and $\mathcal{A}_i^{(\xi)}$ is the contribution which depends on the W gauge parameter ξ. The expressions for $\tilde{\mathcal{A}}_i$ will be discussed in Sec. 6.5. The gauge dependent part for the summed diagrams is

$$\begin{aligned}\sum_i \mathcal{A}_i^{(\xi)} &= \sin\theta \frac{\lambda_t m_t^2 m_b}{8\pi^2 v^3 (m_b^2 - p_{h_2}^2)} (p_{h_2}^2 - m_{h_2}^2) \Big(B_0(p_{h_2}^2, m_W^2\xi, m_W^2\xi) - B_0(m_b^2, m_t^2, m_W^2\xi) \\ &+ (p_{h_2}^2 - m_b^2 + m_t^2 - m_W^2\xi)\, C_0(0, m_b^2, p_{h_2}^2, m_W^2\xi, m_t^2, m_W^2\xi) \Big)\, \bar{s} P_R b, \end{aligned} \tag{6.13}$$

where $\lambda_t = V_{tb}V_{ts}^\star$ is a short notation for the product of two *CKM* matrix elements. The contribution in the gauge dependent piece of the amplitude Eq. 6.13 is proportional to the mass squared $m_{h_2}^2$ comes from the diagram with two Goldstone bosons[2] in Fig. 6.1. All other diagrams provide a contribution which is proportional to the momentum square p_{h_2}.

For the on-shell case, the difference $(p_{h_2}^2 - m_{h_2}^2)$ vanishes, and the full expression, which is proportional to this difference, also disappears. But for the case when the mediator particle cannot be on-shell, the situation is a bit more complicated - one needs to include additional diagrams, which cancel this gauge dependence.

To cancel the gauge dependence in the case when the mediator couple to the pair stable scalars, which is described by the Lagrangian

$$\mathcal{L}_S = \kappa_S \phi S^2, \tag{6.14}$$

one needs to remember about an extra diagram which is shown in Fig. 6.2.

For the case when the scalar is coupled to the fermionic DM, which is represented by the Lagrangian

$$\mathcal{L}_\chi = \lambda_\chi \phi \overline{\chi}\chi\,, \tag{6.15}$$

the cancellation happens if one takes into account also the diagrams corresponding to $b \to s\, h_1[\to \overline{\chi}\chi]$ (Fig. 6.17) involving the heavy state h_1 which corresponds to the 125 GeV excitation. The amplitudes, which involve the h_2 and h_1 propagators, are proportional to $\sim -\sin\theta$ and to $\sim \cos\theta$, respectively:

$$\mathcal{A}_{b\text{-}s\text{-}h2} \sim -\sin\theta, \qquad \mathcal{A}_{b\text{-}s\text{-}h1} \sim \cos\theta, \tag{6.16}$$

[2]The first row, middle diagram in Fig.6.1.

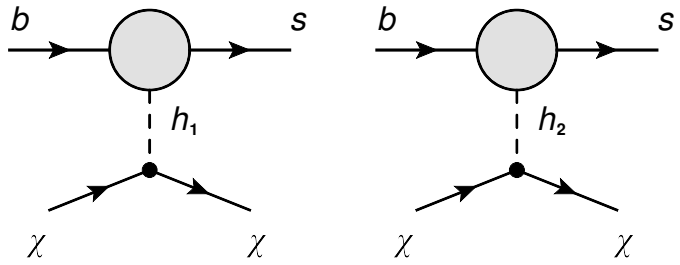

Figure 6.3: Gauge independent set of diagrams for the models with fermionic DM. Here, the blob represents all possible one-loop diagrams corresponding to the process $b \to s h_1$ in the first case and $b \to s h_2$ in the second case.

---

if the vertices $\mathcal{V}_{h_1\chi\chi}$ and $\mathcal{V}_{h_2\chi\chi}$, which involve the coupling of the DM fermion to the scalar bosons λ_χ, depend on the parameter θ as $\mathcal{V}_{h_1\chi\chi} \sim \sin\theta$ and $\mathcal{V}_{h_2\chi\chi} \sim \cos\theta$. The $b \to s\ h_1[\to \overline{\chi}\chi]$ amplitude $\mathcal{A}_{h_1}$ and $b \to s\ h_2[\to \overline{\chi}\chi]$ amplitude $\mathcal{A}_{h_2}$ can be written as

$$\mathcal{A}_{h_2} = -\lambda_\chi \sin\theta\cos\theta \left(F(\xi, p^2) + \frac{G(p^2)}{p^2 - m_{h_2}^2} \right), \tag{6.17}$$

$$\mathcal{A}_{h_1} = \lambda_\chi \sin\theta\cos\theta \left(F(\xi, p^2) + \frac{G(p^2)}{p^2 - m_{h_1}^2} \right), \tag{6.18}$$

where p^2 is the square of the momentum transferred to the fermion pair. The sum of these terms is free of the gauge dependent part $F(\xi, p^2)$.

To obtain a gauge independent process for the SM matter final states, like $b \to s\mu\mu$, which involves the light scalar particle h_2, one needs to add not only the diagrams involving heavy h_1 states but also box diagrams like the ones shown in Ref. [146] for the SM case.

The Wilson coefficient for the gauge independent amplitude $\sum_i \tilde{\mathcal{A}}_i$ is similar to what one can find in the literature Refs. [43] and [147], and up to the sign in the Ref. [41]

$$\mathcal{L}_{\text{eff}} = C_{sbh_2}\, h_2\, \overline{s} P_R b + \text{h.c.}\,, \tag{6.19}$$

$$C_{sbh_2} = -\frac{3\, \sin\theta\, \lambda_t\, m_b\, m_t^2}{16\, \pi^2\, v^3}\,, \tag{6.20}$$

where $v \simeq 246\,\text{GeV}$ is the *vev* of the SM Higgs doublet.

The procedure of searching the $\overline{s}bh_2$ vertex, where the SM result for the $\overline{s}bh$ vertex is multiplied by $-\sin\theta$, is not correct for the general R_ξ gauge[3] because of the subtlety with the $G^\pm G^\mp h_1$ and $G^\pm G^\mp h_2$ vertices which were mentioned as a comment on Eq. 6.12. Nevertheless, the missing terms do not contribute to the effective dimension-4 Lagrangian from Eq. 6.19. Their contribution is suppressed by higher powers of $m_{h_2}^2/m_W^2$.

6.4 Evaluation

For this investigation, as for the process $h \to l\bar{l}\gamma$, all diagrams were generated by *FeynArts* and evaluated by *FeynCalc*, the analytic result was obtained with *Package-X* which is connected to *FeynCalc* via *FeynHelpers* add-on.

[3]This also is not correct for the special cases of the $\xi = 0$ Landau or $\xi = 1$ Feynman gauges.

The code that is used to create the diagrams is

```
In[1]:= amps = FCFAConvert[
          CreateFeynAmp[diags, PreFactor -> 1/(2 Pi)^4, GaugeRules -> {}],
          IncomingMomenta -> {p} ,
          OutgoingMomenta -> {pH, l}, LoopMomenta -> {k}, List -> True,
          ChangeDimension -> D,
          DropSumOver -> True, SMP -> False, UndoChiralSplittings -> True,
          FinalSubstitutions -> {FCGV["EL"] -> EL, FCGV["SW"] -> sinW,
            FCGV["CW"] -> cosW, FCGV["MS"] -> 0, FCGV["MH"] -> mH,
            FCGV["MB"] -> mB, FCGV["MW"] -> mW,
            CKM[Index[Generation, 4], 3] -> VUb,
            CKM[Index[Generation, 4], 2] -> VUs,
            MQU[Index[Generation, 4]] -> mU}] //
         ReplaceAll[#, pH -> p - l] &;
```

where `p` is momentum of the b quark, `l` is momentum of the s quark, `pH` is momentum of the light scalar particle p_{h_2} and, `k` is the loop momentum. For the generation of the gauge dependent and gauge independent parts of the amplitudes different code has been used. The structure of the code is very similar for both cases, it differs only in the output variable. As an example here is presented the code for the generation of gauge dependent amplitudes:

```
In[2]:= ClearAll[ampExpandFree];
        ampExpandFree[exp_] :=
         Block[{ tmp0, tmp1, tmp2, tmp3, tmp4, diagA, diagAresX, ckm,
           diagAres5, diagAresFin, diagAresFin2, diagAresFin3NotFree,
           diagAresFin3Free, diagAres, diagAres4} ,
          tmp0 = ApartFF[exp, {k} ]//DotSimplify//DiracSimplify//
            DiracEquation;
          tmp1 = TID[tmp0, k, ToPaVe -> True, UsePaVeBasis -> True]//
             PropagatorDenominatorExplicit//DiracSimplify;
          tmp2 = tmp1//PowerExpand//DiracSubstitute5//DotSimplify//
              DiracSimplify//PaVeReduce//Simplify;
          diagA =
           Collect2[tmp2//DiracSubstitute5//DotSimplify // ReplaceAll[#,
                 Spinor[Momentum[l, D], 0, 1].Spinor[Momentum[p, D], mB, 1] :>
                   Spinor[Momentum[l, D], 0, 1].DiracGamma[6].Spinor[
                     Momentum[p, D], mB, 1] +
                   Spinor[Momentum[l, D], 0, 1].DiracGamma[7].Spinor[
                     Momentum[p, D], mB, 1] ] & // DotSimplify, Spinor,
             Factoring -> Simplify] // Simplify;
          diagAres = (diagA /. mU -> Sqrt[x] mW)//PowerExpand;
          diagAres4 = SelectNotFree2[diagAres, x];
          diagAresX = SelectFree2[diagAres, x];
          check1 = diagAresX + diagAres4 - diagAres // Simplify;
          ckm[1, b] := Vub; ckm[2, b] = Vcb; ckm[3, b] = Vtb;
          ckm[1, s] := Vus; ckm[2, s] = Vcs; ckm[3, s] = Vts;
          check2 =
           Sum[diagAresX/.x -> mU^2/mW^2/.{ VUb -> ckm[i, b],
                   VUs -> ckm[i, s], mU -> mU[i]} , { i, 1,
                  3} ]/.{ Vcb Conjugate[Vcs] -> -Vtb Conjugate[Vts] -
                   Vub Conjugate[Vus]} /. mU[3] -> mt /. mU[2] -> 0 /.
             mU[1] -> 0 // Simplify;
          diagAres5 =
           Sum[diagAres4/.x -> mU^2/mW^2/.{ VUb -> ckm[i, b],
                   VUs -> ckm[i, s], mU -> mU[i]}, { i, 1,
                  3} ] /. { Vcb Conjugate[Vcs] -> -Vtb Conjugate[Vts] -
                   Vub Conjugate[Vus]}/. mU[3] -> mt/. mU[2] -> 0/.
             mU[1] -> 0//Simplify;
          diagAresFin =
           diagAres5/. mt -> mW*Sqrt[x]/.mB -> mb//PaVeOrder//
            Collect2[#, A0, B0, C0, PaVe, Factoring -> Simplify] &;
```

```
diagAresFin2 =
 diagAresFin/.{ Spinor[Momentum[l, D], 0, 1].DiracGamma[6].Spinor[
       Momentum[p, D], mb, 1] ->
     Spinor[Momentum[l, D], 0, 1].DiracGamma[6].
     Spinor[Momentum[p, D], mBB, 1], Spinor[Momentum[l, D], 0, 1].DiracGamma[7].
     Spinor[Momentum[p, D], mb, 1] ->
     Spinor[Momentum[l, D], 0, 1].DiracGamma[7].Spinor[Momentum[p, D], mBB, 1]}//Simplify;
diagAresFin3NotFree =
 diagAresFin2//SelectNotFree2[#, GaugeXi]&//Simplify;
diagAresFin3Free =
 diagAresFin2//SelectFree2[#, GaugeXi]&//Simplify;
check3 =
 diagAresFin3NotFree + diagAresFin3Free - diagAresFin2//Simplify;
If[check1 == 0, Print[ "Check 1 is ", check1, ", and this is OK"],
 Print[ "Check 1 FAILD (is ", check1, ")"]];
If[check2 == 0, Print[  "Check 2 is ", check2, ", and this is OK"],
 Print[ "Check 2 FAILD (is ", check2, ")"]];
If[check3 == 0, Print[  "Check 3 is ", check3, ", and this is OK"],
 Print[ "Check 3 FAILD (is ", check3, ")"]];
Print[i, "- This one is good!"];
Clear[check1, check2, check3];
diagAresFin3Free
]
```

In many aspects this code is similar to that used in Chapter 5, also a lot of details one can find in Chapter 4. It is important to comment, that part of the code which is responsible for the evaluation of the Feynman integrals is much simpler and hardly handles box diagrams. During the evaluation, for every diagram the *GIM* mechanism was applied, which is described in Sec. 2.3. For the self-consistency three different checks are used: the first and second checks ensure that the GIM mechanism was applied correctly. The third check examines the completeness in the separation procedure into gauge dependent and gauge independent parts.

6.5 The results

The mass of the mediator m_{h_2} can be determined from the decay kinematics. The second important parameter of the model θ could be determined from the branching ratio $Br(B \to K\, h_2)$. For the more massive scalar particle h_2 more decay channels are open, for certain parameters decays can be observed in the *Belle II* experiment. In this section, such an analysis will be provided.

Signatures of the Higgs-portal at B factories have been widely studied [41, 43, 44, 148–151]. Within this thesis: Will be briefly revisited the recent analyses of Refs. [43, 44]. There, an analysis of $B \to K^\star(892) h_2$ in comparison to $B \to K h_2$ was presented. Highlighted the number of events, which can be observed in *Belle II* experiment, in the process $B \to K h_2[\to f]$, which are a function of the relevant $B \to K h_2$ and $h_2 \to f$ branching ratios. At the end, the benefits of the lifetime information will be discussed. The lifetime information can be obtained from the data of displaced vertices.

The gauge independent contributions of $\tilde{\mathcal{A}}_i$ to the diagrams shown in Fig. 6.1 reads:

$$\tilde{\mathcal{A}}_{(1)} = -\sin\theta\, \frac{\lambda_t\, m_b m_t^2}{8\pi^2 v^3}\, \frac{p_{h_2}^2 - 2m_t^2}{m_b^2 - p_{h_2}^2}\, B_0(p_{h_2}^2, m_t^2, m_t^2)\,.$$

The second diagram has a purely gauge dependent contribution, namely

$$\tilde{\mathcal{A}}_{(2)} = 0\,. \tag{6.21}$$

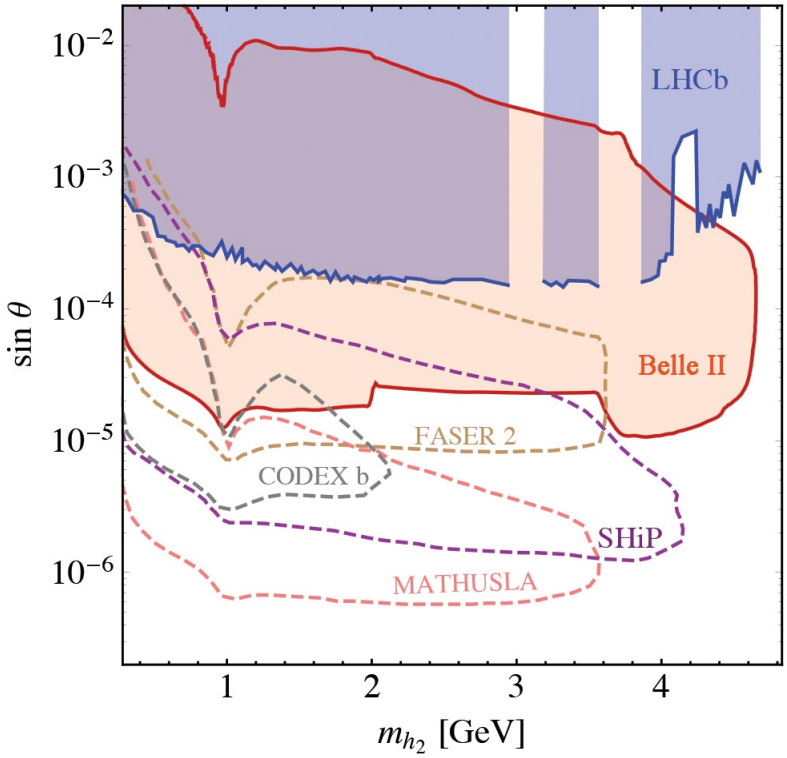

Figure 6.4: Sensitivity of the *Belle II* experiment to the decay h_2 into SM particles, including both $B \to K h_2$ and $B \to K^* h_2$ and decays of h_2 to $(\pi\pi + KK), \mu^+\mu^-, \tau^+\tau^-$ are shown with the filled red region, and compared to the search limit of *LHCb* [152] (shaded blue) and projected sensitivities by other future experiments: *CODEX b* [153] (gray), *FASER 2* [154] (brown), *Mathusla* [155] (pink), and *SHiP* [156] (purple). Here the regions where at least three events are produced at *Belle II* with the 50 ab^{-1} data at the *Belle II* experiment were displayed.

All other results are

$$\begin{aligned}\tilde{\mathcal{A}}_{(3)} = &-\sin\theta \frac{\lambda_t\, m_t^2}{16\,\pi^2\, m_b v^3} \frac{1}{m_b^2 - p_{h_2}^2} \times \\ &\Big\{ \big[-m_b^2 \big(m_W^2(4D + 5x - 9) + p_{h_2}^2\big) + 3m_b^4 + m_W^2 p_{h_2}^2 (x-1)\big] B_0(m_b^2, m_t^2, m_W^2) \\ &+ 2m_b^2 m_W^2 \big[m_b^2(2-x) + 2m_W^2(x-1)(2+x) - p_{h_2}^2\big] C_0(0, m_b^2, p_{h_2}^2, m_t^2, m_W^2, m_t^2) \\ &- 4(D-2) m_b^2 m_W^2 B_0(p_{h_2}^2, m_t^2, m_t^2) + \frac{2m_W^2(m_b^2 - p_{h_2}^2)}{D-2} B_0(0, m_W^2, m_W^2) \Big\}, \end{aligned} \tag{6.22}$$

$$\tilde{\mathcal{A}}_{(4)} = -\sin\theta \frac{\lambda_t\, m_b}{8\pi^2 v^3} \big((m_t^2 - 2m_W^2) B_0(0, m_t^2, m_W^2) + 2m_W^2 B_0(0, 0, m_W^2) \big), \tag{6.23}$$

$$\begin{aligned}\tilde{\mathcal{A}}_{(5)} = &\sin\theta \frac{\lambda_t\, m_t^2}{16\pi^2 (D-2) m_b v^3 (m_b^2 - p_{h_2}^2)} \Big\{ 2m_W^2 (m_b^2 - p_{h_2}^2) B_0(0, m_W^2, m_W^2) \\ &- (D-2)\big(m_b^4 - m_b^2(m_t^2 + m_W^2 + 3p_{h_2}^2) + p_{h_2}^2(m_t^2 - m_W^2)\big) B_0(m_b^2, m_t^2, m_W^2) \Big\}, \end{aligned} \tag{6.24}$$

$$\begin{aligned}\tilde{\mathcal{A}}_{(6)} = &-\sin\theta\,\frac{\lambda_t\, m_b}{8\pi^2\, v^3(m_b^2-p_{h_2}^2)}\Big\{m_W^2\big(2(2-D)m_W^2+2m_b^2-m_t^2\big)B_0(m_b^2,m_t^2,m_W^2)\\ &-2m_W^2\big(m_b^2-(D-2)m_W^2\big)B_0(m_b^2,0,m_W^2)+m_t^2(2m_W^2+p_{h_2}^2)B_0(p_{h_2}^2,m_W^2,m_W^2)\\ &+\big[m_t^2(2m_W^4-m_W^2p_{h_2}^2+p_{h_2}^4)-4m_W^6+2m_b^4m_W^2-m_b^2\big(m_t^2(2m_W^2+p_{h_2}^2)\\ &+2m_W^2p_{h_2}^2\big)+m_t^4(2m_W^2+p_{h_2}^2)+2m_W^4p_{h_2}^2\big]C_0(0,m_b^2,p_{h_2}^2,m_W^2,m_t^2,m_W^2)\\ &-2m_W^2(-2m_W^4+m_b^4-m_b^2p_{h_2}^2+m_W^2p_{h_2}^2)C_0(0,m_b^2,p_{h_2}^2,m_W^2,0,m_W^2)\Big\}\,,\end{aligned}\tag{6.25}$$

$$\tilde{\mathcal{A}}_{(7)} = -\sin\theta\,\frac{\lambda_t m_t^4}{4\,\pi^2(D-2)m_b v^3}B_0(0,m_t^2,m_t^2)\,,\tag{6.26}$$

$$\begin{aligned}\tilde{\mathcal{A}}_{(8)} = &\sin\theta\,\frac{\lambda_t\, m_W^2}{8\,\pi^2 m_b v^3}\Big\{m_W^2(x-1)(D+x-2)B_0(0,m_t^2,m_W^2)\\ &+\frac{2\,m_t^2}{D-2}\,B_0(0,m_W^2,m_W^2)+(D-2)\,m_W^2B_0(0,0,m_W^2)\\ &-2\,m_t^2B_0(0,m_t^2,m_t^2)\Big\}\,,\end{aligned}\tag{6.27}$$

where B_0 and C_0 are Passarino-Veltman functions, and these functions and their properties are described in the Sec. 4.3. The total amplitude, where the m_{h_2} mass is small and the mass of the b-quark m_b[4] is treated as small, is given by the Eq. 6.19.

The branching ratio of $B\to Kh_2$ is written as

$$Br(B\to Kh_2)=\frac{\tau_B}{32\pi m_B^2}|C_{h_2sb}|^2\left(\frac{m_B^2-m_K^2}{m_b-m_s}\right)^2 f_0(m_{h_2}^2)^2\frac{\lambda(m_B^2,m_K^2,m_{h_2}^2)^{1/2}}{2m_B}\,,$$

where $\lambda(a,b,c)=a^2+b^2+c^2-2(ab+ac+bc)$. The corresponding matrix element is parameterised in terms of the form-factor $f_0(q^2)$ as

$$\langle K|\bar{s}b|B\rangle=\frac{m_B^2-m_K^2}{m_b-m_s}\,f_0(q^2)\,,\tag{6.28}$$

where $q=p_B-p_K$. For this form factor the QCD lattice result of Ref. [157][5] have been used.

To obtain the number of events, an analisys of the *Belle II* detector geometry has been performed[6]. All particles which are produced in the collision are boosted, this is a feature of the *Belle II* collider. The boost is induced by the asymmetric electron $E_-=7\,\text{GeV}$ and positron $E_+=4\,\text{GeV}$ beam energies, and the boost is determined by $\beta_B\gamma_B=(E_--E_+)/2\sqrt{E_-E_+}=0.28$, $\gamma_B=1.04$. To obtain the decay probability of the h_2 particle inside the detector layers, the Lorentz transformation from the rest frame of the scalar particle h_2 to the laboratory frame need to be considered $\mathcal{B}_1\mathcal{R}\mathcal{B}_0$, where $\mathcal{R}\mathcal{B}_0$ is the transformation from the rest frame of h_2 to the rest frame of the B meson:

$$\mathcal{R}\mathcal{B}_0\begin{pmatrix}m_{h_2}\\0\\0\\0\end{pmatrix}=\begin{pmatrix}E_{h_2}\\0\\|\vec{p}_{h_2}|\sin\vartheta_0\\|\vec{p}_{h_2}|\cos\vartheta_0\end{pmatrix}\,,\tag{6.29}$$

[4]The mass of b-quark m_b cannot be completely ignored, because this process is proportional to this mass.
[5]See Ref. [158] as alternative.
[6]In Ref. [44] there is a similar study.

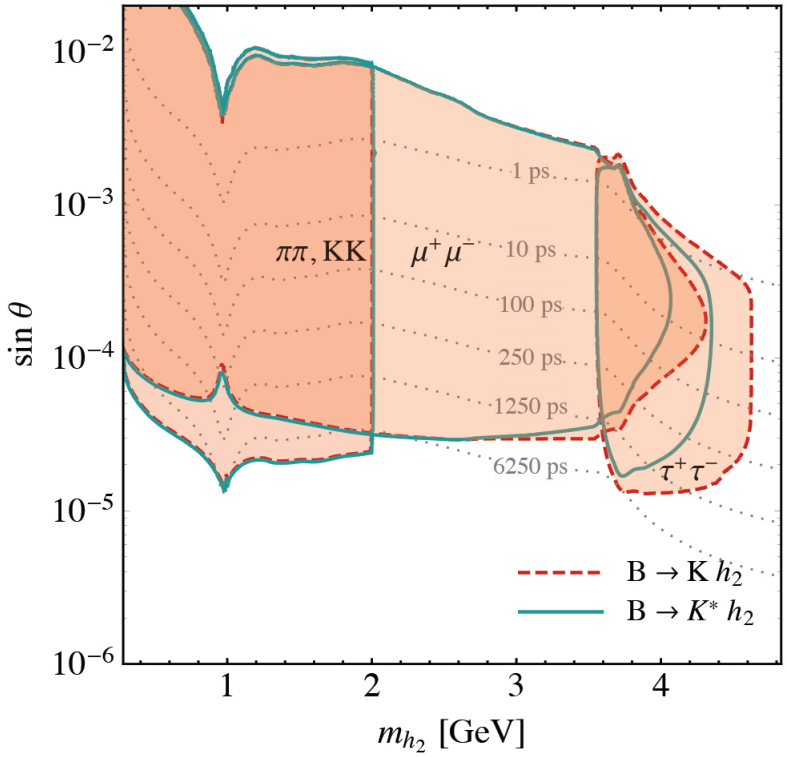

Figure 6.5: Parameter regions with three and more events of $B \to Kh_2\,(\to f)$, $f = (\pi\pi + KK), \mu^+\mu^-, \tau^+\tau^-$ are bounded by the dashed red contours and shaded in red. Dark green contours represent the same regions for $B \to K^\star h_2$ process. The number of events was summed over in the decays of B^+, B^-, B^0, and $\bar{B}^0$. The dotted lines denote contours of constant h_2 proper lifetime.

---

here $\mathcal{B}_1$ is the boost from the Υ resonance rest frame to the laboratory frame. The Υ resonance is produced by B meson decay. A small boost from the Υ rest frame to the B rest frame is neglected.

The momentum magnitude and the energy of h_2 in the B meson rest-frame are:

$$E_{h_2} = \frac{m_B^2 + m_{h_2}^2 - m_{K^{(\star)}}^2}{2m_B}, \quad |\vec{p}_{h_2}| = \sqrt{E_{h_2}^2 - m_{h_2}^2}. \tag{6.30}$$

In the rest frame of the mediator, the decay occurs at $(c\tau, 0, 0, 0)$. In the laboratory frame, the decay length comes from the Lorentz transformation

$$\begin{aligned}
\begin{pmatrix} ct_{\text{lab}} \\ x_{\text{lab}} \\ y_{\text{lab}} \\ z_{\text{lab}} \end{pmatrix} &= \mathcal{B}_1\mathcal{R}\mathcal{B}_0 \begin{pmatrix} c\tau \\ 0 \\ 0 \\ 0 \end{pmatrix} = \frac{c\tau}{m_{h_2}} \begin{pmatrix} \gamma_B & 0 & 0 & \gamma_B\beta_B \\ 0 & 1 & 0 & 0 \\ 0 & 0 & 1 & 0 \\ \gamma_B\beta_B & 0 & 0 & \gamma_B \end{pmatrix} \begin{pmatrix} E_{h_2} \\ 0 \\ |\vec{p}_{h_2}|\sin\vartheta_0 \\ |\vec{p}_{h_2}|\cos\vartheta_0 \end{pmatrix} \\
&= \frac{c\tau}{m_{h_2}} \begin{pmatrix} \gamma_B E_{h_2} + \gamma_B\beta_B|\vec{p}_{h_2}|\cos\vartheta_0 \\ 0 \\ |\vec{p}_{h_2}|\sin\vartheta_0 \\ \gamma_B\beta_B E_{h_2} + \gamma_B|\vec{p}_{h_2}|\cos\vartheta_0 \end{pmatrix},
\end{aligned} \tag{6.31}$$

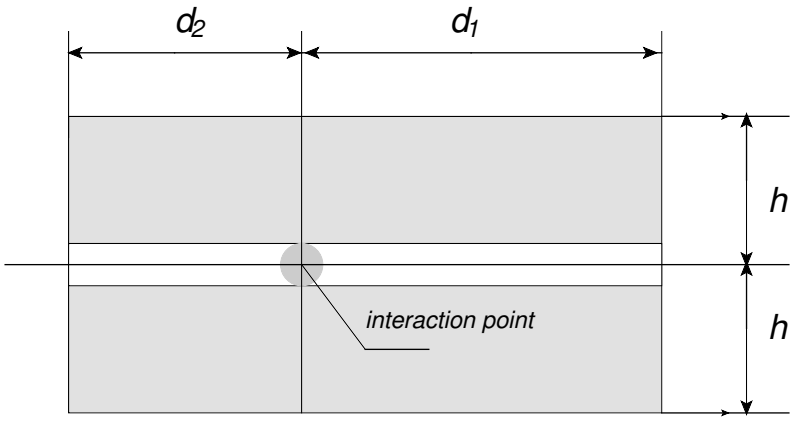

Figure 6.6: Schematic illustration of the *Belle II* detector geometry. d_1 is the dimension of the detector along the z-direction measured from the interaction point to the front side, d_2 is the dimension of the detector along the z-direction measured from the interaction point to the backside, and h is the height measured from the beam line. In the evaluation the values $d_1 = 1.5\,\mathrm{m}$, $d_2 = 0.74\mathrm{m}$, $h = 1.17\,\mathrm{m}$ have been used.

The decay length of the h_2 mediator in the laboratory frame is $d_L = \left(x_{\mathrm{lab}}^2 + y_{\mathrm{lab}}^2 + z_{\mathrm{lab}}^2\right)^{1/2}$. The relation to the corresponding angle ϑ is given by

$$y_{\mathrm{lab}} = d_L(\vartheta_0)\sin\vartheta, \quad z_{\mathrm{lab}} = d_L(\vartheta_0)\cos\vartheta. \tag{6.32}$$

The expected number of $B^\pm \to K^{(\star)\pm} h_2[\to f]$ events is

$$N_f^\pm = N_{B^+B^-}\, 2Br(B^\pm \to K^{(\star)\pm}h_2)\, Br(h_2 \to f) \int d\vartheta\, p(\vartheta) \frac{1}{d_L} \int_{r_{\min}(\vartheta)}^{r_{\max}(\vartheta)} dr \exp\left[-\frac{r}{d_L}\right], \tag{6.33}$$

where $N_{B^+B^-}$ is the total number of produced B^+-B^- meson pairs.

The differences in the lifetimes and the production asymmetry of B^+ and B^0 mesons have been included:

$$\tau_{B^+} = 1.638\,\mathrm{ps}\,, \qquad \tau_{B^0} = 1.519\,\mathrm{ps}\,, \tag{6.34}$$

$$f^{+-} \equiv Br(\Upsilon(4S) \to B^+B^-) = 0.514\,, \tag{6.35}$$

$$f^{00} \equiv Br(\Upsilon(4S) \to B^0\overline{B}^0) = 0.486\,, \tag{6.36}$$

where the numerical values have been taken from Ref. [159].

The total number of displaced vertex events, for all B^+, B^-, B^0 and $\bar{B}^0$ meson initial states, is

$$\begin{aligned} N_f^{\mathrm{tot}} &= N_{B\bar{B}} 2Br(B^\pm \to K^{(\star)\pm}h_2) Br(h_2 \to f)\left(f^{+-} + f^{00}\frac{\tau_{B^0}}{\tau_{B^+}}\right) \\ &\times \int d\vartheta\, p(\vartheta) \frac{1}{d_L} \int_{r_{\min}(\vartheta)}^{r_{\max}(\vartheta)} dr \exp\left[-\frac{r}{d_L}\right], \end{aligned} \tag{6.37}$$

where $N_{B\bar{B}} \equiv N_{B^+B^-} + N_{B^0\bar{B}^0} = 5 \times 10^{10}$ is the total number of produced B meson pairs with $50\,\mathrm{ab}^{-1}$ of data at the *Belle II* experiment [160].

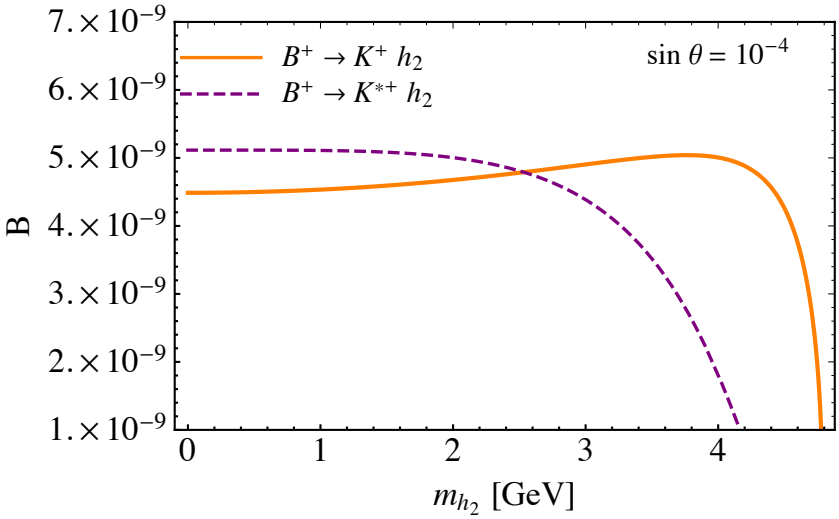

Figure 6.7: The branching fractions B of $B^+ \to K^+ h_2$ (thick orange curve) and $B^+ \to K^{\star+} h_2$ (dashed purple curve) for $\sin\theta = 10^{-4}$.

Substituting the result from the Eq. 6.36

$$\begin{aligned} N_f^{\rm tot} &= N_{B\bar{B}} 1.93\, Br(B^\pm \to K^{(\star)\pm} h_2) Br(h_2 \to f) \\ &\times \int d\vartheta\, p(\vartheta) \frac{1}{d_L} \int_{r_{\rm min}(\vartheta)}^{r_{\rm max}(\vartheta)} dr \exp\left[-\frac{r}{d_L} \right]. \end{aligned} \tag{6.38}$$

In the B meson rest frame, the angular distribution of the scalar mediator h_2 is trivial:

$$p(\vartheta_0) = \frac{1}{2} \sin\vartheta_0, \tag{6.39}$$

meanwhile, in the laboratory frame, the ϑ angular distribution is

$$p(\vartheta) = \frac{1}{2} \sin\vartheta_0 \left| \frac{d\vartheta_0}{d\vartheta} \right|, \tag{6.40}$$

where the angle ϑ_0 was expressed in terms of ϑ according to Eq. 6.38.

The detector has a cylindrical symmetry [160], and there are three ways how the scalar particle h_2 can escape from the detector: 1) Front side. The distance from interaction point to this escape point denotes $d_1 = 1.5\,\text{m}$ 2) Backside ($d_2 = 0.74\,\text{m}$), and 3) Side ($h = 1.17\,\text{m}$). These parameters are restricted by the size of the CDC.

According to these parameters, the travelling distances depending to the escape zone are

$$\begin{aligned} &\vartheta \in (0.3, \arctan\frac{h}{d_1}), \quad r_{\rm max} = \frac{d_1}{\cos\vartheta}, \\ &\vartheta \in (\frac{\pi}{2} + \arctan\frac{d_2}{h}, \frac{5\pi}{6}), \quad r_{\rm max} = -\frac{d_2}{\cos\vartheta} \\ &\vartheta \in (\arctan\frac{h}{d_1}, \frac{\pi}{2} + \arctan\frac{d_2}{h}), \quad r_{\rm max} = \frac{h}{\sin\vartheta}, , \end{aligned} \tag{6.41}$$

m_{h_2}[GeV]	τ [ps]				
	250	500	1000	2000	4000
0.3	50204	18385	5734	1614	429
0.9	972.3	465	191.8	65.7	19.6
1.5	1634.7	815.2	382.7	152.7	50.9
2.1	334.2	167.6	82.6	36.8	13.7
2.7	115.6	58	29	13.9	5.8
3.3	56.8	28.6	14.4	7.1	3.2
3.9	58.4	29.6	14.9	7.4	3.6

Table 6.1: Total number $N_f^{\rm tot}$ of displaced-vertex $B \to K^{(\star)} h_2[\to f]$ events in the detector of *Belle II* according to Eq. 6.38 for various values of the proper lifetime (columns) and mass (rows) of h_2. Here, all possible final states for the mesons K and $K^\star$ are taken into account.

---

in the first, second, and third cases, respectively.

As in Ref. [44] the minimal vertex resolution $r_{\rm min} = 500\,\mu$m has been chosen. The $r_{\rm min}$ dependence on the angle ϑ is neglected. The final formula is:

$$N_f^{\rm tot} = N_{B\bar{B}} 1.93\, Br(B^\pm \to K^{(\star)\pm} h_2) Br(h_2 \to f) \times \int d\vartheta\, \sin\vartheta_0(\vartheta) \left| \frac{d\vartheta_0(\vartheta)}{d\vartheta} \right| \left[\exp\left(- \frac{r_{\rm min}}{d_L(\vartheta)} \right) - \exp\left(- \frac{r_{\rm max}(\vartheta)}{d_L(\vartheta)} \right) \right]. \tag{6.42}$$

The number of events is obtained in both cases for K and for $K^\star$ according to this formula. In the K case, the evaluation of the sensitivities corresponds to 5×10^{10} $B\bar{B}$ meson pairs, where B includes both B^+ and B^0 mesons, at $50\,{\rm ab}^{-1}$ of data at the *Belle II* experiment [160].

The parameter regions are shown by dashed red contours in Fig. 6.4. These parameter regions correspond to three or more displaced vertex events of any of the final state signatures in $B \to K(h_2 \to f)$, $f = (\pi\pi + KK), \mu\mu, \tau\tau$ within the *Belle II* detector. By the number of events, one must understand all decays of B^+, B^0 and the corresponding charge-conjugate mesons.

Lifetime information is given on Fig. 6.5. Because of the strong dependence on m_{h_2}, this information will improve the determination of m_{h_2} deduced from the $B \to K h_2$ decay kinematics for fixed $\sin\theta$ from branching ratios.

Within this research, also the decay of B mesons into vector mesons $K^\star$ has been analysed. The branching fraction is

$$Br(B \to K^\star h_2) = \frac{\tau_B}{32\pi m_B^2} |C_{h_2 sb}|^2 \frac{A_0(m_{h_2}^2)^2}{(m_b + m_s)^2} \frac{\lambda(m_B^2, m_{K^\star}^2, m_{h_2}^2)^{3/2}}{2m_B}. \tag{6.43}$$

The form factor $A_0(q^2)$ corresponds to the pseudoscalar hadronic matrix element as

$$\langle K^\star(k,\epsilon) | \bar{s}\gamma_5 b | B(p_B) \rangle = \frac{2\, m_{K^\star}\, \epsilon^\star \cdot q}{m_b + m_s} A_0(q^2), \tag{6.44}$$

where ϵ is the polarization vector of the vector meson $K^\star$ and $q = p_B - p_\gamma$. This form factor has been obtained from the combination of lattice QCD [161] and QCD sum rules [162] results.

The branching fraction for $Br(B \to K^\star h_2)$ and $Br(B \to K h_2)$ are given in Fig.6.7. One can conclude that these branching fractions are comparable in size for masses up to $\sim 2\,$GeV. $Br(B \to K^\star h_2)$ is suppressed for the mass m_{h_2} larger than $3\,$GeV. This happens because the kinematic function in Eq.6.43 has an additional power of λ, which comes from the longitudinal

$K^\star$ polarization contribution. The reason is that by angular momentum conservation this is the only contributing polarization. The combination of the experimental data from both processes is required for the discrimination of the spin-0 vs. spin-1 hypotheses. The decay $B \to K^\star h_2$ has been studied before in Ref. [45], in which a plot is similar to the plot presented in Fig.6.7. In Ref. [45] the focus was on *LHC*, *ShiP*, and *DUNE*, the analysis for *Belle II*, which has been performed within this Thesis and published [163], is new. In Refs. [44,45] only the fully inclusive decay $B \to X_s h_2$ was studied.

The number of $B \to K^\star h_2(\tau\tau)$ events is much smaller than $B \to K h_2(\tau\tau)$. This follows from the suppression close to the endpoint. The region corresponding to $K^\star$ events is shown with the dark green contour in Fig.6.5.

In Fig.6.4 the reach of the *Belle II* experiment to displaced vertices of h_2 has been compared. The origin of displaced vertices includes both $B \to K h_2$ and $B \to K^\star h_2$ processes and decays of h_2 to $(\pi\pi + KK), \mu^+\mu^-, \tau^+\tau^-$ with the existing search limit of the *LHCb* experiment [152]. The result of Ref. [43] for the *LHCb* search limit on $B(B \to K h_2[\to \mu^+\mu^-])$ has been used. Projected sensitivities of other future experiments, *Mathusla* [155], *SHiP* [156], *CODEX b* [153] and *FASER 2* [154] has been added for the plot.

In Tab. 6.1 the total number of displaced vertex events $N_f^{\rm tot}$ for interesting values for the proper lifetime τ and mass of h_2 is shown.

Chapter 7

Conclusion

In this thesis, a new result for the process $h \to l\bar{l}\gamma$ was presented. The results previously presented in the literature for the differential decay rates $d\Gamma(H \to l\bar{l}\gamma)/dm_{l\bar{l}}$ where $l = e,\ \mu$, differ to a significant extent. Furthermore, a new result for the differential decay rate $d^2\Gamma(h \to l\bar{l}\gamma)/(ds\,dt)$, where s is the squared dilepton mass and t is the squared invariant mass of the lepton - photon pair, has been calculated. Additional attention was dedicated to the check of gauge invariance. As part of this project, the forward-backward asymmetry has been presented. This asymmetry was defined as a distribution in terms of the angle between the photon and one of the leptons. For a special choice of experimental cuts, the result was presented in analytic form.

The second project, within my PhD study, was dedicated to the process $B \to K^{(\star)}+$ invisible. The invisible particle was represented by an extra scalar ϕ which couples to the SM via mixing with the Higgs doublet. This scalar particle is considered as a mediator which connects the SM with the Dark Sector. This model has two physical states: the heavy h_1 and the light h_2 bosons. Within this project, the phenomenology for the *Belle II* detector with a novel consideration of the $B \to K^{\star}h_2$ process has been studied. The *Belle II* experiment permits the lifetime and mixing angle measurement of the light scalar h_2. Also, the number of observed displaced vertices for the process $B \to Kh_2\,, [h_2 \to ff]$ in the *Belle II* experiment has been presented.

Appendix A

Diagrams for the process $h \to l\bar{l}\gamma$

In this appendix the diagrams that are divided into 13 classes to the process $h \to l\bar{l}\gamma$ are shown[1]

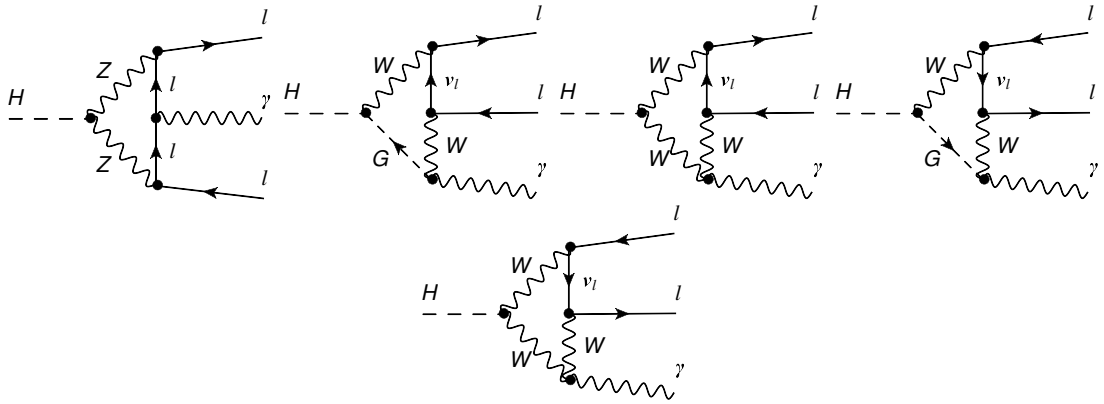

Figure A.1: Class 1. Box-diagrams for the one-loop contribution to the process $h \to l\bar{l}\gamma$

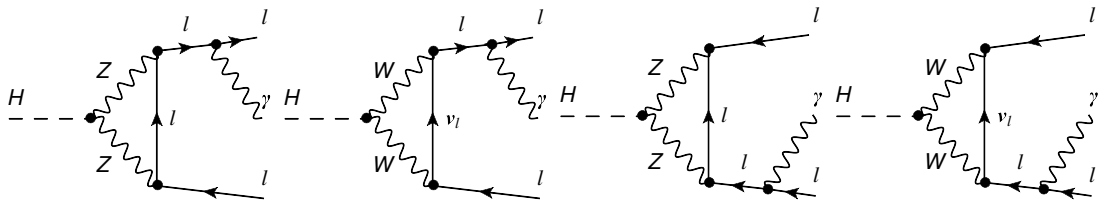

Figure A.2: Class 2. External leg radiation diagrams for the one-loop contribution to the process $h \to l\bar{l}\gamma$.

[1]Some of the following diagrams need to be counted twice because they are repeated with different momentum flow.

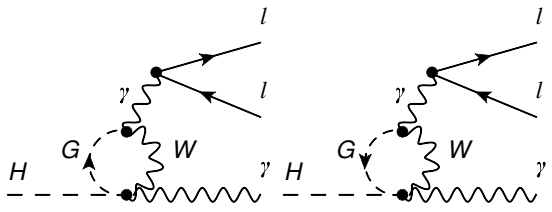

Figure A.3: Class 3. 4-point vertex with k-independent γ propagator type 4.

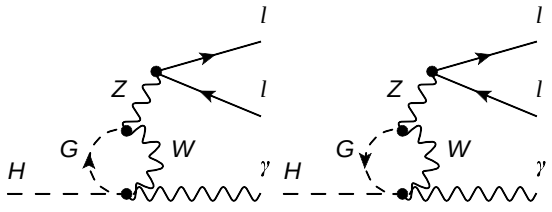

Figure A.4: Class 4. 4-point vertex with k-independent Z-boson propagator type 4.

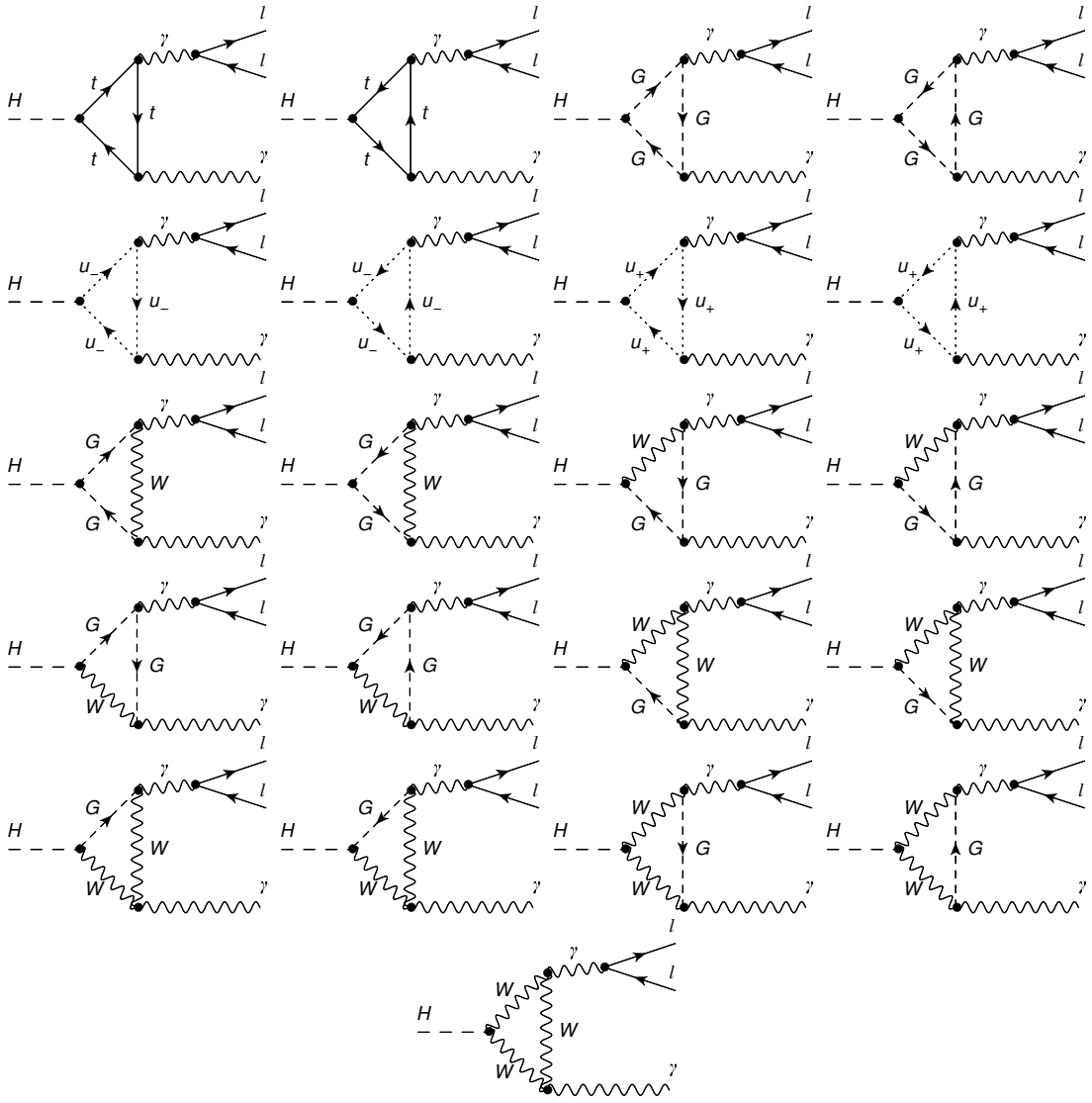

Figure A.5: Class 5. Triangle diagrams with intermediate photon propagator for the one-loop contribution to the process $h \to l\bar{l}\gamma$.

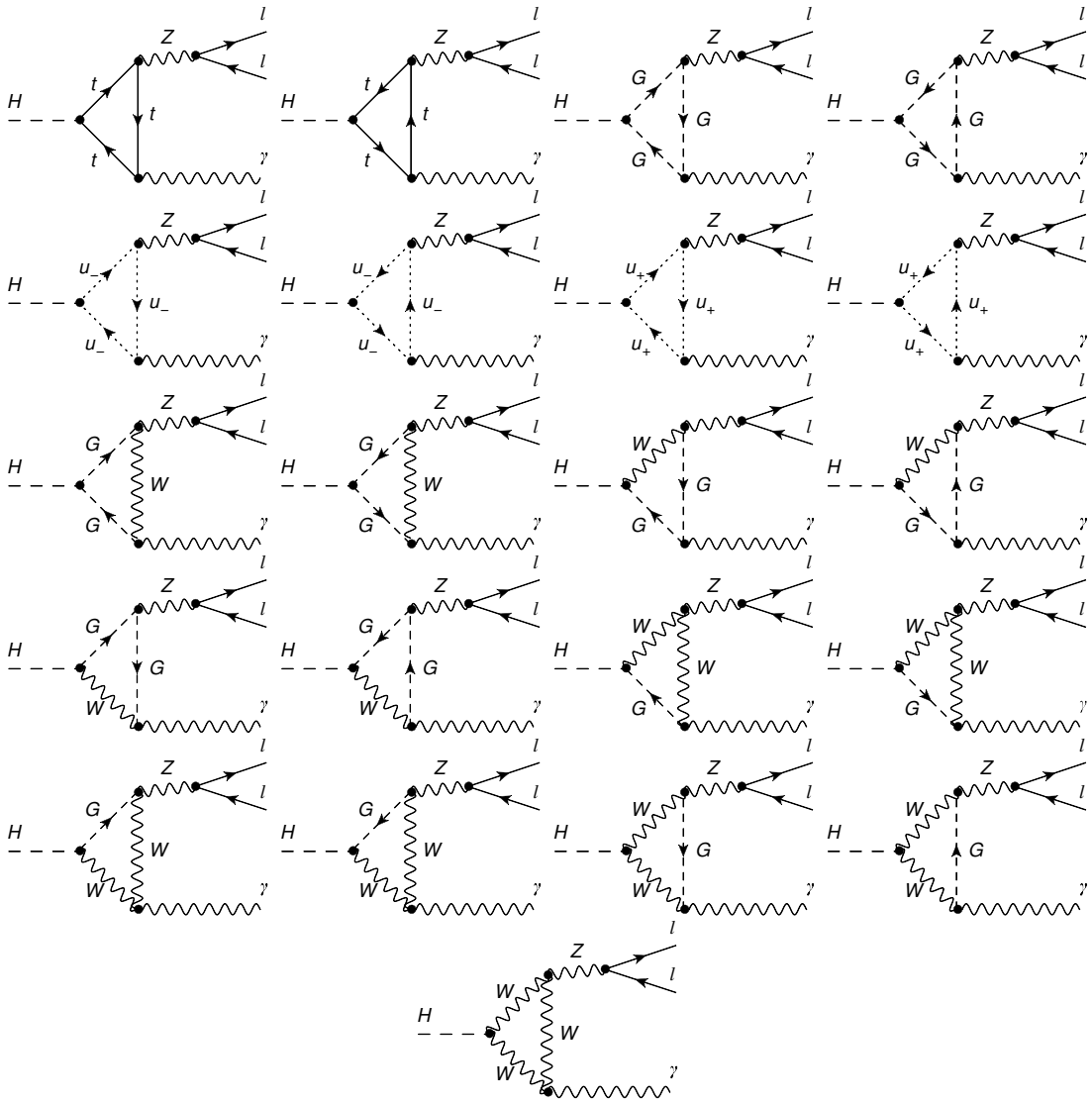

Figure A.6: Class 6. Triangle diagrams with Z-boson propagator which is not dependent on the loop momentum for the one-loop contribution to the process $h \to l\bar{l}\gamma$.

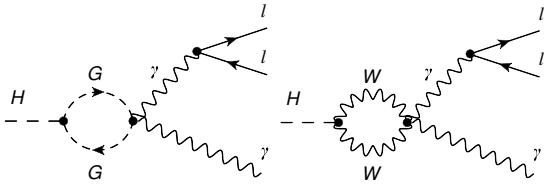

Figure A.7: Class 7. 4-point vertex with k-independent γ-propagator type 1 for the one-loop contribution to the process $h \to l\bar{l}\gamma$.

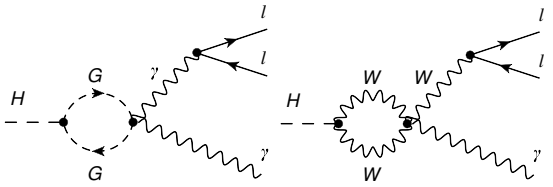

Figure A.8: Class 8. 4-point vertex with k-independent Z-boson propagator type 1 for the one-loop contribution to the process $h \to l\bar{l}\gamma$

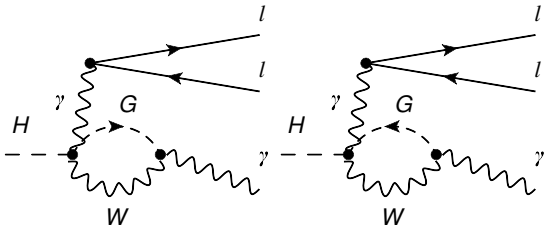

Figure A.9: Class 9. 4-point vertex with k-independent γ-propagator type 2 for the one-loop contribution to the process $h \to l\bar{l}\gamma$.

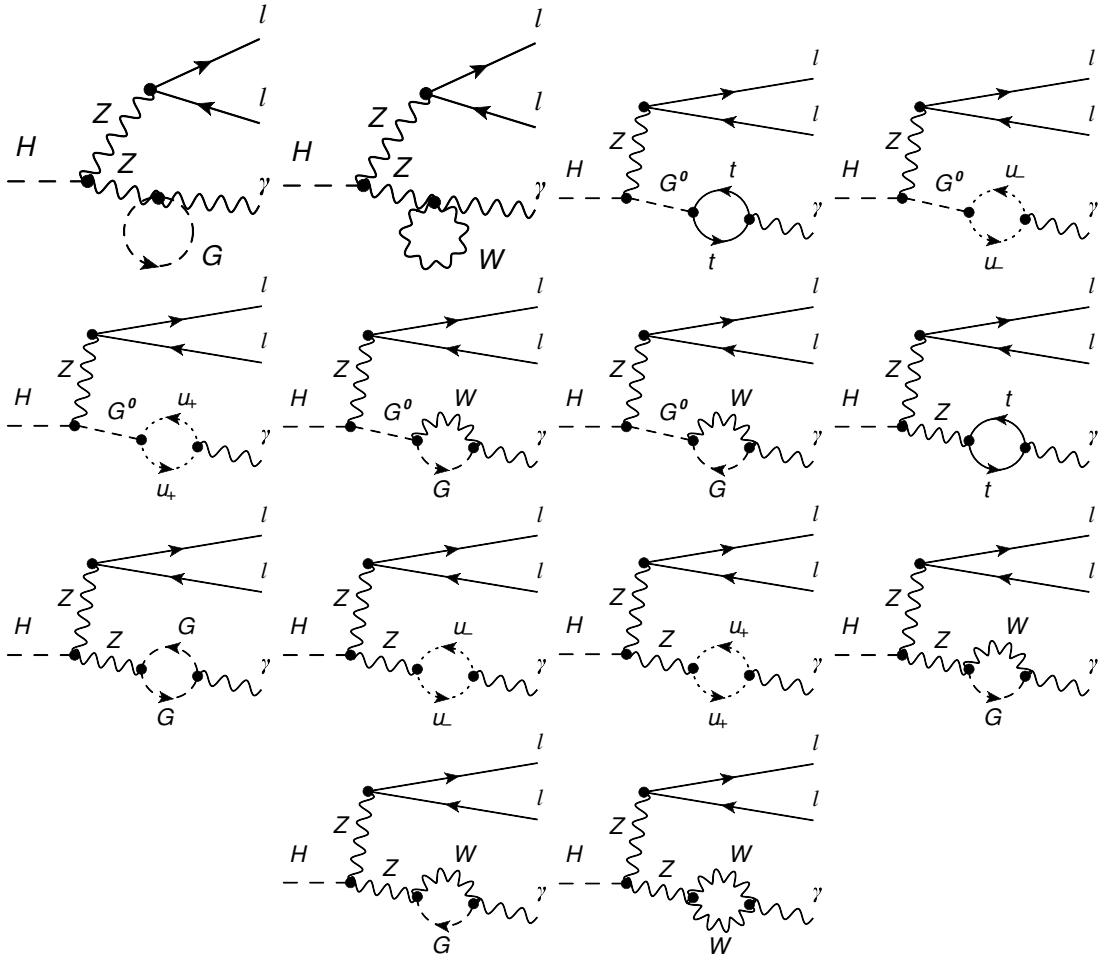

Figure A.10: Class 10. 4-point vertex with k-independent Z-boson propagator type 2 for the one-loop contribution of the process $h \to l\bar{l}\gamma$

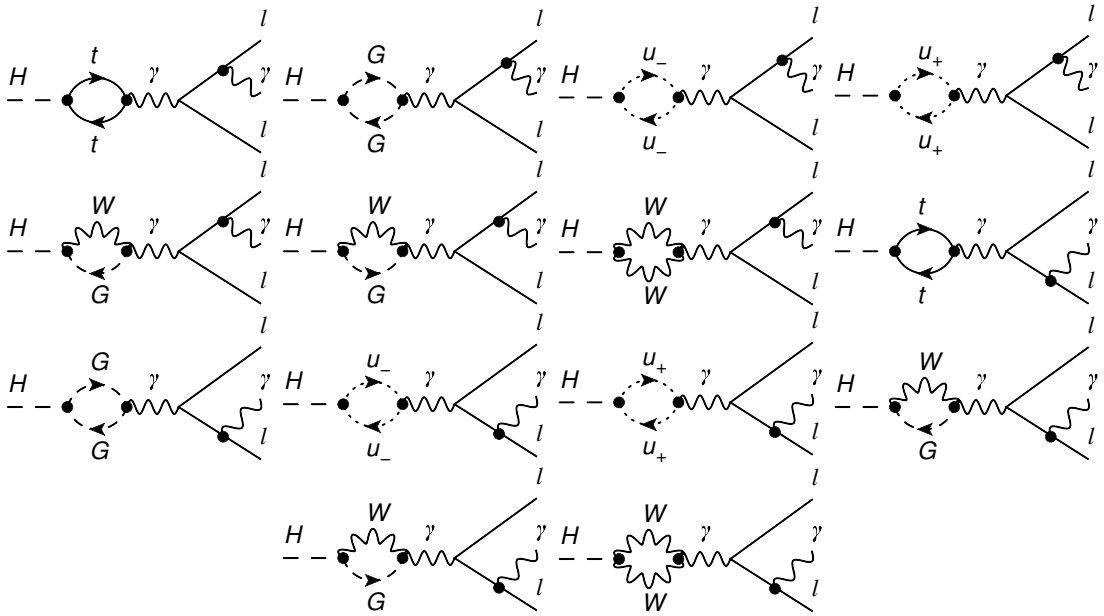

Figure A.11: Class 11. Higgs - photon mixing and external leg radiation

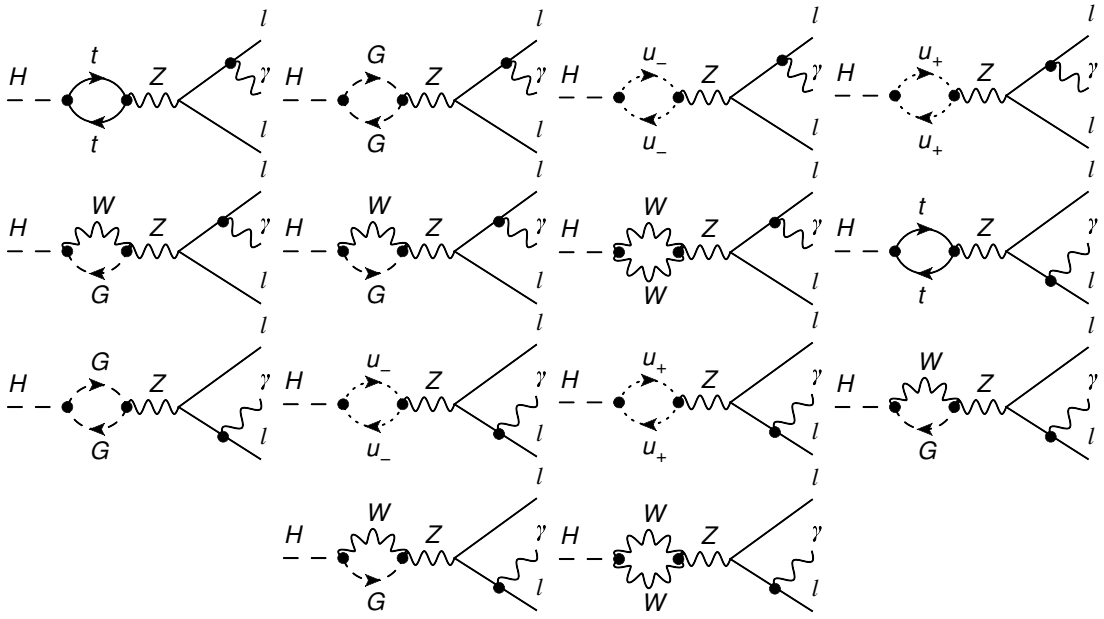

Figure A.12: Class 12. Higgs - Z-boson mixing and external leg radiation.

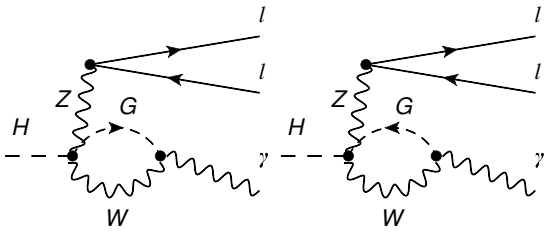

Figure A.13: Class 13. 4-point vertex with k-independent Z-boson propagator type 3.

Bibliography

[1] E. Fermi, "Tentativo di una teoria dell'emissione dei raggi beta," Ric. Sci. **4** (1933), 491-495

[2] W. Pauli, "Relativistic Field Theories of Elementary Particles," Rev. Mod. Phys. **13** (1941), 203-232

[3] H. A. Bethe, "The Electromagnetic shift of energy levels," Phys. Rev. **72** (1947), 339-341

[4] W. E. Lamb and R. C. Retherford, "Fine Structure of the Hydrogen Atom by a Microwave Method," Phys. Rev. **72** (1947), 241-243

[5] S. L. Glashow, "Partial Symmetries of Weak Interactions," Nucl. Phys. **22** (1961), 579-588

[6] P. W. Anderson, "Plasmons, Gauge Invariance, and Mass," Phys. Rev. **130** (1963), 439-442

[7] S. Weinberg, "A Model of Leptons," Phys. Rev. Lett. **19** (1967), 1264-1266

[8] F. Englert and R. Brout, "Broken Symmetry and the Mass of Gauge Vector Mesons," Phys. Rev. Lett. **13** (1964) 321.

[9] P. W. Higgs, "Broken Symmetries and the Masses of Gauge Bosons," Phys. Rev. Lett. **13** (1964) 508.

[10] G. S. Guralnik, C. R. Hagen and T. W. B. Kibble, "Global Conservation Laws and Massless Particles," Phys. Rev. Lett. **13** (1964) 585.

[11] C. Englert, A. Freitas, M. M. Muehlleitner, T. Plehn, M. Rauch, M. Spira and K. Walz, "Precision Measurements of Higgs Couplings: Implications for New Physics Scales," J. Phys. G **41** (2014), 113001 [arXiv:1403.7191 [hep-ph]].

[12] G. Aad *et al.* [ATLAS], "Evidence for the Higgs-boson Yukawa coupling to tau leptons with the ATLAS detector," JHEP **04** (2015), 117 [arXiv:1501.04943 [hep-ex]].

[13] A. M. Sirunyan *et al.* [CMS], "Observation of the Higgs boson decay to a pair of τ leptons with the CMS detector," Phys. Lett. B **779** (2018), 283-316 [arXiv:1708.00373 [hep-ex]].

[14] M. Aaboud *et al.* [ATLAS], "Cross-section measurements of the Higgs boson decaying into a pair of τ-leptons in proton-proton collisions at $\sqrt{s} = 13$ TeV with the ATLAS detector," Phys. Rev. D **99** (2019), 072001 [arXiv:1811.08856 [hep-ex]].

[15] G. Aad *et al.* [ATLAS], "Observation and measurement of Higgs boson decays to WW* with the ATLAS detector," Phys. Rev. D **92** (2015) no.1, 012006 [arXiv:1412.2641 [hep-ex]].

[16] G. Aad *et al.* [ATLAS], "Study of (W/Z)H production and Higgs boson couplings using $H \to WW^*$ decays with the ATLAS detector," JHEP **08** (2015), 137 [arXiv:1506.06641 [hep-ex]].

[17] A. M. Sirunyan *et al.* [CMS], "Measurements of properties of the Higgs boson decaying to a W boson pair in pp collisions at $\sqrt{s} = 13$ TeV," Phys. Lett. B **791** (2019), 96 [arXiv:1806.05246 [hep-ex]].

[18] A. M. Sirunyan *et al.* [CMS], "Measurements of the Higgs boson width and anomalous HVV couplings from on-shell and off-shell production in the four-lepton final state," Phys. Rev. D **99** (2019) no.11, 112003 [arXiv:1901.00174 [hep-ex]].

[19] S. Chatrchyan *et al.* [CMS], "Measurement of the Properties of a Higgs Boson in the Four-Lepton Final State," Phys. Rev. D **89** (2014) no.9, 092007 [arXiv:1312.5353 [hep-ex]].

[20] G. Aad *et al.* [ATLAS], "Fiducial and differential cross sections of Higgs boson production measured in the four-lepton decay channel in pp collisions at $\sqrt{s}$=8 TeV with the ATLAS detector," Phys. Lett. B **738** (2014), 234-253 [arXiv:1408.3226 [hep-ex]].

[21] M. Aaboud *et al.* [ATLAS], "Combined measurement of differential and total cross sections in the $H \to \gamma\gamma$ and the $H \to ZZ^* \to 4\ell$ decay channels at $\sqrt{s} = 13$ TeV with the ATLAS detector," Phys. Lett. B **786** (2018), 114-133 [arXiv:1805.10197 [hep-ex]].

[22] M. Aaboud *et al.* [ATLAS], "Observation of $H \to b\bar{b}$ decays and VH production with the ATLAS detector," Phys. Lett. B **786** (2018), 59-86 [arXiv:1808.08238 [hep-ex]].

[23] A. M. Sirunyan *et al.* [CMS], "Observation of Higgs boson decay to bottom quarks," Phys. Rev. Lett. **121** (2018) no.12, 121801 [arXiv:1808.08242 [hep-ex]].

[24] A. M. Sirunyan *et al.* [CMS], "Evidence for associated production of a Higgs boson with a top quark pair in final states with electrons, muons, and hadronically decaying τ leptons at $\sqrt{s} = 13$ TeV," JHEP **08** (2018), 066 [arXiv:1803.05485 [hep-ex]].

[25] M. Aaboud *et al.* [ATLAS], "Observation of Higgs boson production in association with a top quark pair at the LHC with the ATLAS detector," Phys. Lett. B **784** (2018), 173-191 [arXiv:1806.00425 [hep-ex]].

[26] A. M. Sirunyan *et al.* [CMS], "Measurements of Higgs boson properties in the diphoton decay channel in proton-proton collisions at $\sqrt{s} = 13$ TeV," JHEP **11** (2018), 185 [arXiv:1804.02716 [hep-ex]].

[27] M. Aaboud *et al.* [ATLAS], "Measurements of Higgs boson properties in the diphoton decay channel with 36 fb^{-1} of pp collision data at $\sqrt{s} = 13$ TeV with the ATLAS detector," Phys. Rev. D **98** (2018), 052005 [arXiv:1802.04146 [hep-ex]].

[28] O. Eberhardt, G. Herbert, H. Lacker, A. Lenz, A. Menzel, U. Nierste and M. Wiebusch, "Impact of a Higgs boson at a mass of 126 GeV on the standard model with three and four fermion generations," Phys. Rev. Lett. **109** (2012), 241802 [arXiv:1209.1101 [hep-ph]].

[29] G. Belanger, B. Dumont, U. Ellwanger, J. F. Gunion and S. Kraml, "Global fit to Higgs signal strengths and couplings and implications for extended Higgs sectors," Phys. Rev. D **88** (2013), 075008 [arXiv:1306.2941 [hep-ph]].

[30] O. Eberhardt, U. Nierste and M. Wiebusch, "Status of the two-Higgs-doublet model of type II," JHEP **07** (2013), 118 [arXiv:1305.1649 [hep-ph]].

[31] J. Baglio, O. Eberhardt, U. Nierste and M. Wiebusch, "Benchmarks for Higgs Pair Production and Heavy Higgs boson Searches in the Two-Higgs-Doublet Model of Type II," Phys. Rev. D **90** (2014) no.1, 015008 [arXiv:1403.1264 [hep-ph]].

[32] S. Kanemura, K. Tsumura, K. Yagyu and H. Yokoya, "Fingerprinting nonminimal Higgs sectors," Phys. Rev. D **90** (2014), 075001 [arXiv:1406.3294 [hep-ph]].

[33] A. Broggio, E. J. Chun, M. Passera, K. M. Patel and S. K. Vempati, "Limiting two-Higgs-doublet models," JHEP **11** (2014), 058 [arXiv:1409.3199 [hep-ph]].

[34] P. S. Bhupal Dev and A. Pilaftsis, "Maximally Symmetric Two Higgs Doublet Model with Natural Standard Model Alignment," JHEP **12** (2014), 024 [arXiv:1408.3405 [hep-ph]].

[35] D. Chowdhury and O. Eberhardt, "Global fits of the two-loop renormalized Two-Higgs-Doublet model with soft Z_2 breaking," JHEP **11** (2015), 052 [arXiv:1503.08216 [hep-ph]].

[36] J. Bernon, J. F. Gunion, H. E. Haber, Y. Jiang and S. Kraml, "Scrutinizing the alignment limit in two-Higgs-doublet models: m_h=125 GeV," Phys. Rev. D **92** (2015) no.7, 075004 [arXiv:1507.00933 [hep-ph]].

[37] H. E. Haber and O. Stal, "New LHC benchmarks for the $\mathcal{CP}$ -conserving two-Higgs-doublet model," Eur. Phys. J. C **75** (2015) no.10, 491 [arXiv:1507.04281 [hep-ph]].

[38] D. Chowdhury and O. Eberhardt, "Update of Global Two-Higgs-Doublet Model Fits," JHEP **05** (2018), 161 [arXiv:1711.02095 [hep-ph]].

[39] L. Wang, F. Zhang and X. F. Han, "Two-Higgs-doublet model of type-II confronted with the LHC run-I and run-II data," Phys. Rev. D **95** (2017) no.11, 115014 [arXiv:1701.02678 [hep-ph]].

[40] B. Patt and F. Wilczek, "Higgs-field portal into hidden sectors," [arXiv:hep-ph/0605188 [hep-ph]].

[41] G. Krnjaic, "Probing Light Thermal Dark-Matter With a Higgs Portal Mediator," Phys. Rev. D **94** (2016) no.7, 073009 [arXiv:1512.04119 [hep-ph]].

[42] S. Matsumoto, Y. L. S. Tsai and P. Y. Tseng, "Light Fermionic WIMP Dark Matter with Light Scalar Mediator," JHEP **07** (2019), 050 [arXiv:1811.03292 [hep-ph]].

[43] M. W. Winkler, "Decay and detection of a light scalar boson mixing with the Higgs boson," Phys. Rev. D **99** (2019) no.1, 015018 [arXiv:1809.01876 [hep-ph]].

[44] A. Filimonova, R. Schaefer and S. Westhoff, "Probing dark sectors with long-lived particles at BELLE II," Phys. Rev. D **101** (2020) no.9, 095006 [arXiv:1911.03490 [hep-ph]].

[45] I. Boiarska, K. Bondarenko, A. Boyarsky, V. Gorkavenko, M. Ovchynnikov and A. Sokolenko, "Phenomenology of GeV-scale scalar portal," JHEP **11** (2019), 162 [arXiv:1904.10447 [hep-ph]].

[46] S. L. Glashow, "The renormalizability of vector meson interactions," Nucl. Phys. **10** (1959), 107-117

[47] A. Salam and J. C. Ward, "Weak and electromagnetic interactions," Nuovo Cim. **11** (1959), 568-577

[48] wikipedia.org/

[49] B. Pontecorvo, "Mesonium and anti-mesonium," Sov. Phys. JETP **6** (1957), 429

[50] Z. Maki, M. Nakagawa and S. Sakata, "Remarks on the unified model of elementary particles," Prog. Theor. Phys. **28** (1962), 870-880

[51] M. Tanabashi *et al.* [Particle Data Group], "Review of Particle Physics," Phys. Rev. D **98** (2018) no.3, 030001

[52] B. Pontecorvo, "Neutrino Experiments and the Problem of Conservation of Leptonic Charge," Sov. Phys. JETP **26** (1968), 984-988

[53] E. D. Bloom, D. H. Coward, H. C. DeStaebler, J. Drees, G. Miller, L. W. Mo, R. E. Taylor, M. Breidenbach, J. I. Friedman, G. C. Hartmann and H. W. Kendall, "High-Energy Inelastic e p Scattering at 6-Degrees and 10-Degrees," Phys. Rev. Lett. **23** (1969), 930-934

[54] J. E. Augustin *et al.* [SLAC-SP-017], "Discovery of a Narrow Resonance in e^+e^- Annihilation," Phys. Rev. Lett. **33** (1974), 1406-1408

[55] J. J. Aubert *et al.* [E598], "Experimental Observation of a Heavy Particle J," Phys. Rev. Lett. **33** (1974), 1404-1406

[56] M. Kobayashi and T. Maskawa, "CP Violation in the Renormalizable Theory of Weak Interaction," Prog. Theor. Phys. **49** (1973), 652-657

[57] J. H. Christenson, J. W. Cronin, V. L. Fitch and R. Turlay, "Evidence for the 2π Decay of the K_2^0 Meson," Phys. Rev. Lett. **13** (1964), 138-140

[58] Y. Grossman, "Introduction to flavor physics," [arXiv:1006.3534 [hep-ph]].

[59] C. Amsler *et al.* [Particle Data Group], "Review of Particle Physics," Phys. Lett. B **667** (2008), 1-1340

[60] S. L. Glashow, J. Iliopoulos and L. Maiani, "Weak Interactions with Lepton-Hadron Symmetry," Phys. Rev. D **2** (1970), 1285-1292

[61] H. Fritzsch, M. Gell-Mann and H. Leutwyler, "Advantages of the Color Octet Gluon Picture," Phys. Lett. **47B** (1973) 365.

[62] M. Banner *et al.* [UA2], "Observation of Single Isolated Electrons of High Transverse Momentum in Events with Missing Transverse Energy at the CERN anti-p p Collider," Phys. Lett. B **122** (1983), 476-485

[63] P. Bagnaia *et al.* [UA2], "Evidence for $Z^0 \to e^+e^-$ at the CERN $\bar{p}p$ Collider," Phys. Lett. B **129** (1983), 130-140

[64] G. Arnison *et al.* [UA1], "Experimental Observation of Isolated Large Transverse Energy Electrons with Associated Missing Energy at s**(1/2) = 540-GeV," Phys. Lett. B **122** (1983), 103-116

[65] F. Abe *et al.* [CDF Collaboration], "Observation of top quark production in $\bar{p}p$ collisions," Phys. Rev. Lett. **74** (1995) 2626 [hep-ex/9503002].

[66] S. Abachi *et al.* [D0 Collaboration], "Observation of the top quark," Phys. Rev. Lett. **74** (1995) 2632 [hep-ex/9503003].

[67] G. Aad *et al.* [ATLAS Collaboration], "Observation of a new particle in the search for the Standard Model Higgs boson with the ATLAS detector at the LHC," Phys. Lett. B **716** (2012) 1 [arXiv:1207.7214 [hep-ex]].

[68] S. Chatrchyan *et al.* [CMS Collaboration], "Observation of a new boson at a mass of 125 GeV with the CMS experiment at the LHC," Phys. Lett. B **716** (2012) 30 [arXiv:1207.7235 [hep-ex]].

[69] R. P. Feynman, F. B. Morinigo, W. G. Wagner and B. Hatfield, "Feynman lectures on gravitation," pp. xxxvi-xxxviii, 211-212

[70] S. W. Allen, A. E. Evrard and A. B. Mantz, "Cosmological Parameters from Observations of Galaxy Clusters," Ann. Rev. Astron. Astrophys. **49** (2011) 409 [arXiv:1103.4829 [astro-ph.CO]].

[71] A. N. Taylor, S. Dye, T. J. Broadhurst, N. Benitez and E. van Kampen, "Gravitational lens magnification and the mass of abell 1689," Astrophys. J. **501** (1998) 539 [astro-ph/9801158].

[72] X. P. Wu, T. Chiueh, L. Z. Fang and Y. J. Xue, "A comparison of different cluster mass estimates: consistency or discrepancy ?," Mon. Not. Roy. Astron. Soc. **301** (1998) 861 [astro-ph/9808179].

[73] P. Natarajan *et al.*, "Mapping substructure in the HST Frontier Fields cluster lenses and in cosmological simulations," Mon. Not. Roy. Astron. Soc. **468** (2017) no.2, 1962 [arXiv:1702.04348 [astro-ph.GA]].

[74] A. Refregier, "Weak gravitational lensing by large scale structure," Ann. Rev. Astron. Astrophys. **41** (2003) 645 [astro-ph/0307212].

[75] G. Hinshaw *et al.* [WMAP Collaboration], "Five-Year Wilkinson Microwave Anisotropy Probe (WMAP) Observations: Data Processing, Sky Maps, and Basic Results," Astrophys. J. Suppl. **180** (2009) 225 [arXiv:0803.0732 [astro-ph]].

[76] C. Skordis, D. F. Mota, P. G. Ferreira and C. Boehm, "Large Scale Structure in Bekenstein's theory of relativistic Modified Newtonian Dynamics," Phys. Rev. Lett. **96** (2006) 011301 [astro-ph/0505519].

[77] D. Clowe, M. Bradac, A. H. Gonzalez, M. Markevitch, S. W. Randall, C. Jones and D. Zaritsky, "A direct empirical proof of the existence of dark matter," Astrophys. J. Lett. **648** (2006) L109 [astro-ph/0608407].

[78] V. Mukhanov, "Physical Foundations of Cosmology," pp. 276-279

[79] J. A. Peacock *et al.*, "A Measurement of the cosmological mass density from clustering in the 2dF Galaxy Redshift Survey," Nature **410** (2001) 169 [astro-ph/0103143].

[80] A. D. Sakharov, "Violation of CP Invariance, C asymmetry, and baryon asymmetry of the universe," Pisma Zh. Eksp. Teor. Fiz. **5** (1967) 32 [JETP Lett. **5** (1967) 24] [Sov. Phys. Usp. **34** (1991) no.5, 392] [Usp. Fiz. Nauk **161** (1991) no.5, 61].

[81] K. A. Olive *et al.* [Particle Data Group], "Review of Particle Physics," Chin. Phys. C **38** (2014) 090001.

[82] J. R. Batley *et al.* [NA48/2 Collaboration], "Measurements of Charged Kaon Semileptonic Decay Branching Fractions K+- —> pi0 mu+- nu and K+- —> pi0 e+- nu and Their Ratio," Eur. Phys. J. C **50** (2007) 329 Erratum: [Eur. Phys. J. C **52** (2007) 1021] [hep-ex/0702015].

[83] M. Antonelli *et al.*, "Flavor Physics in the Quark Sector," Phys. Rept. **494** (2010) 197 [arXiv:0907.5386 [hep-ph]].

[84] J. Ellis, M. Lewicki and J. M. No, "On the Maximal Strength of a First-Order Electroweak Phase Transition and its Gravitational Wave Signal," JCAP **1904** (2019) 003 [arXiv:1809.08242 [hep-ph]].

[85] http://universe-review.ca/F15-particle01.htm Figure 15-04a

[86] R. D. Peccei, "The Strong CP problem and axions," Lect. Notes Phys. **741** (2008), 3-17 [arXiv:hep-ph/0607268 [hep-ph]].

[87] C.T. Hill and E.H. Simmons, "Strong Dynamics and Electroweak Symmetry Breaking",(2003)

[88] K. Lane, "Two lectures on technicolour," hep-ph/0202255.

[89] C. Jarlskog, "A Basis Independent Formulation of the Connection Between Quark Mass Matrices, CP Violation and Experiment," Z. Phys. C **29** (1985) 491.

[90] J. M. Cline, "Baryogenesis," hep-ph/0609145.

[91] M. C. Chen, "TASI 2006 Lectures on Leptogenesis," hep-ph/0703087 [HEP-PH].

[92] N. Turok and J. Zadrozny, "Electroweak baryogenesis in the two doublet model," Nucl. Phys. B **358** (1991), 471-493

[93] K. Funakubo, A. Kakuto and K. Takenaga, "The Effective potential of electroweak theory with two massless Higgs doublets at finite temperature," Prog. Theor. Phys. **91** (1994), 341-352 [arXiv:hep-ph/9310267 [hep-ph]].

[94] M. Joyce, T. Prokopec and N. Turok, "Nonlocal electroweak baryogenesis. Part 2: The Classical regime," Phys. Rev. D **53** (1996), 2958-2980 [arXiv:hep-ph/9410282 [hep-ph]].

[95] M. Laine and K. Rummukainen, "Two Higgs doublet dynamics at the electroweak phase transition: A Nonperturbative study," Nucl. Phys. B **597** (2001), 23-69 [arXiv:hep-lat/0009025 [hep-lat]].

[96] L. Fromme, S. J. Huber and M. Seniuch, "Baryogenesis in the two-Higgs doublet model," JHEP **11** (2006), 038 [arXiv:hep-ph/0605242 [hep-ph]].

[97] R. D. Peccei and H. R. Quinn, "CP Conservation in the Presence of Instantons," Phys. Rev. Lett. **38** (1977), 1440-1443

[98] J. E. Kim, "Light Pseudoscalars, Particle Physics and Cosmology," Phys. Rept. **150** (1987), 1-177

[99] G. C. Branco, P. M. Ferreira, L. Lavoura, M. N. Rebelo, M. Sher and J. P. Silva, "Theory and phenomenology of two-Higgs-doublet models," Phys. Rept. **516** (2012), 1-102 [arXiv:1106.0034 [hep-ph]].

[100] S. L. Glashow and S. Weinberg, "Natural Conservation Laws for Neutral Currents," Phys. Rev. D **15** (1977), 1958

[101] E. A. Paschos, "Diagonal Neutral Currents," Phys. Rev. D **15** (1977), 1966

[102] V. Barger, P. Langacker, M. McCaskey, M. J. Ramsey-Musolf and G. Shaughnessy, "LHC Phenomenology of an Extended Standard Model with a Real Scalar Singlet," Phys. Rev. D **77** (2008), 035005 [arXiv:0706.4311 [hep-ph]].

[103] S. Profumo, M. J. Ramsey-Musolf and G. Shaughnessy, "Singlet Higgs phenomenology and the electroweak phase transition," JHEP **08** (2007), 010 [arXiv:0705.2425 [hep-ph]].

[104] D. N. Spergel *et al.* [WMAP], "Wilkinson Microwave Anisotropy Probe (WMAP) three year results: implications for cosmology," Astrophys. J. Suppl. **170** (2007), 377 [arXiv:astro-ph/0603449 [astro-ph]].

[105] J. A. Casas, D. G. Cerdeno, J. M. Moreno and J. Quilis, "Reopening the Higgs portal for single scalar dark matter," JHEP **05** (2017), 036 [arXiv:1701.08134 [hep-ph]].

[106] L. Feng, S. Profumo and L. Ubaldi, "Closing in on singlet scalar dark matter: LUX, invisible Higgs decays and gamma-ray lines," JHEP **03** (2015), 045 [arXiv:1412.1105 [hep-ph]].

[107] V. Barger, P. Langacker, M. McCaskey, M. Ramsey-Musolf and G. Shaughnessy, "Complex Singlet Extension of the Standard Model," Phys. Rev. D **79** (2009), 015018 [arXiv:0811.0393 [hep-ph]].

[108] K. Cheung, J. Song and Q. S. Yan, "Role of h —> eta eta in Intermediate-Mass Higgs Boson Searches at the Large Hadron Collider," Phys. Rev. Lett. **99** (2007), 031801 [arXiv:hep-ph/0703149 [hep-ph]].

[109] R. Dermisek and J. F. Gunion, "Consistency of LEP event excesses with an h —> aa decay scenario and low-fine-tuning NMSSM models," Phys. Rev. D **73** (2006), 111701 [arXiv:hep-ph/0510322 [hep-ph]].

[110] R. Dermisek, J. F. Gunion and B. McElrath, "Probing NMSSM Scenarios with Minimal Fine-Tuning by Searching for Decays of the Upsilon to a Light CP-Odd Higgs Boson," Phys. Rev. D **76** (2007), 051105 [arXiv:hep-ph/0612031 [hep-ph]].

[111] M. Carena, T. Han, G. Y. Huang and C. E. M. Wagner, "Higgs Signal for h $\to$ aa at Hadron Colliders," JHEP **04** (2008), 092 [arXiv:0712.2466 [hep-ph]].

[112] R. K. Ellis, Z. Kunszt, K. Melnikov and G. Zanderighi, "One-loop calculations in quantum field theory: from Feynman diagrams to unitarity cuts," Phys. Rept. **518** (2012) 141 [arXiv:1105.4319 [hep-ph]].

[113] A. Denner and S. Dittmaier, "Reduction schemes for one-loop tensor integrals," Nucl. Phys. B **734** (2006) 62 [hep-ph/0509141].

[114] W. Siegel, "Supersymmetric Dimensional Regularization via Dimensional Reduction," Phys. Lett. **84B** (1979) 193.

[115] P. Breitenlohner and D. Maison, "Dimensional Renormalization and the Action Principle," Commun. Math. Phys. **52** (1977) 11.

[116] G. Bonneau, "Preserving Canonical Ward Identities in Dimensional Regularization With a Nonanticommuting γ_5," Nucl. Phys. B **177** (1981) 523.

[117] A. J. Buras and P. H. Weisz, "QCD Nonleading Corrections to Weak Decays in Dimensional Regularization and 't Hooft-Veltman Schemes," Nucl. Phys. B **333** (1990) 66.

[118] G. 't Hooft and M. J. G. Veltman, "Regularization and Renormalization of Gauge Fields," Nucl. Phys. B **44** (1972) 189.

[119] D. A. Akyeampong and R. Delbourgo, "Dimensional regularization, abnormal amplitudes and anomalies," Nuovo Cim. A **17** (1973) 578.

[120] J. G. Korner, N. Nasrallah and K. Schilcher, "Evaluation of the Flavor Changing Vertex $b \to sH$ Using the Breitenlohner-maison-'t Hooft-Veltman $\gamma(5)$ Scheme," Phys. Rev. D **41** (1990) 888.

[121] T. Hahn, S. Passehr and C. Schappacher, "FormCalc 9 and Extensions," PoS **LL2016** (2016), 068 [arXiv:1604.04611 [hep-ph]].

[122] A. Pukhov, E. Boos, M. Dubinin, V. Edneral, V. Ilyin, D. Kovalenko, A. Kryukov, V. Savrin, S. Shichanin and A. Semenov, "CompHEP: A Package for evaluation of Feynman diagrams and integration over multiparticle phase space," [arXiv:hep-ph/9908288 [hep-ph]].

[123] G. Belanger, F. Boudjema, J. Fujimoto, T. Ishikawa, T. Kaneko, K. Kato and Y. Shimizu, "Automatic calculations in high energy physics and Grace at one-loop," Phys. Rept. **430** (2006) 117 [hep-ph/0308080].

[124] M. Wiebusch, "HEPMath 1.4: A mathematica package for semi-automatic computations in high energy physics," Comput. Phys. Commun. **195** (2015), 172-190 [arXiv:1412.6102 [hep-ph]].

[125] H. H. Patel, "Package-X: A Mathematica package for the analytic calculation of one-loop integrals," Comput. Phys. Commun. **197** (2015), 276-290 [arXiv:1503.01469 [hep-ph]].

[126] A. V. Smirnov, "FIRE5: a C++ implementation of Feynman Integral REduction," Comput. Phys. Commun. **189** (2015), 182-191 [arXiv:1408.2372 [hep-ph]].

[127] L. D. Landau, "On analytic properties of vertex parts in quantum field theory," Nucl. Phys. **13** (1960) no.1, 181 [Sov. Phys. JETP **10** (1959) no.1, 45] [Zh. Eksp. Teor. Fiz. **37** (1959) no.1, 62].

[128] M. Bohm, A. Denner and H. Joos, "Gauge theories of the strong and electroweak interaction," Stuttgart, Germany: Teubner (2001) pp. 287-288

[129] R. Aaij *et al.* [LHCb Collaboration], "Search for lepton-universality violation in $B^+ \to K^+\ell^+\ell^-$ decays," Phys. Rev. Lett. **122** (2019) no.19, 191801 [arXiv:1903.09252 [hep-ex]].

[130] T. Hahn, "Generating Feynman diagrams and amplitudes with FeynArts 3," Comput. Phys. Commun. **140** (2001) 418 [hep-ph/0012260].

[131] V. Shtabovenko, R. Mertig and F. Orellana, "New Developments in FeynCalc 9.0," Comput. Phys. Commun. **207** (2016) 432 [arXiv:1601.01167 [hep-ph]].

[132] R. Mertig, M. Bohm and A. Denner, "FEYN CALC: Computer algebraic calculation of Feynman amplitudes," Comput. Phys. Commun. **64** (1991) 345.

[133] V. Shtabovenko, "FeynHelpers: Connecting FeynCalc to FIRE and Package-X," Comput. Phys. Commun. **218** (2017) 48 [arXiv:1611.06793 [physics.comp-ph]].

[134] V. Shtabovenko, R. Mertig and F. Orellana, "FeynCalc 9.3: New features and improvements," arXiv:2001.04407 [hep-ph].

[135] S. Schael *et al.* [ALEPH, DELPHI, L3, OPAL, SLD, LEP Electroweak Working Group, SLD Electroweak Group and SLD Heavy Flavour Group], "Precision electroweak measurements on the Z resonance," Phys. Rept. **427** (2006), 257-454 [arXiv:hep-ex/0509008 [hep-ex]].

[136] M. Nowakowski and A. Pilaftsis, "On gauge invariance of Breit-Wigner propagators," Z. Phys. C **60** (1993), 121-126 [arXiv:hep-ph/9305321 [hep-ph]].

[137] D. de Florian *et al.* [LHC Higgs Cross Section Working Group], "Handbook of LHC Higgs Cross Sections: 4. Deciphering the Nature of the Higgs Sector," arXiv:1610.07922 [hep-ph].

[138] A. Denner and J. N. Lang, "The Complex-Mass Scheme and Unitarity in perturbative Quantum Field Theory," Eur. Phys. J. C **75** (2015) no.8, 377 [arXiv:1406.6280 [hep-ph]].

[139] A. Denner and S. Dittmaier, "The Complex-mass scheme for perturbative calculations with unstable particles," Nucl. Phys. B Proc. Suppl. **160** (2006), 22-26 [arXiv:hep-ph/0605312 [hep-ph]].

[140] D. A. Dicus and W. W. Repko, "Calculation of the decay $H \to e\bar{e}\gamma$," Phys. Rev. D **87** (2013) no.7, 077301 [arXiv:1302.2159 [hep-ph]].

[141] G. Passarino, "Higgs Boson Production and Decay: Dalitz Sector," Phys. Lett. B **727** (2013) 424 [arXiv:1308.0422 [hep-ph]].

[142] A. Abbasabadi, D. Bowser-Chao, D. A. Dicus and W. W. Repko, "Radiative Higgs boson decays H —> fermion anti-fermion gamma," Phys. Rev. D **55** (1997), 5647-5656 [arXiv:hep-ph/9611209 [hep-ph]].

[143] L. B. Chen, C. F. Qiao and R. L. Zhu, "Reconstructing the 125 GeV SM Higgs Boson Through $\ell\bar{\ell}\gamma$," Phys. Lett. B **726** (2013), 306-311 [arXiv:1211.6058 [hep-ph]].

[144] T. Han and X. Wang, "Radiative Decays of the Higgs Boson to a Pair of Fermions," JHEP **10** (2017), 036 [arXiv:1704.00790 [hep-ph]].

[145] S. Chatrchyan *et al.* [CMS], "Observation of a New Boson at a Mass of 125 GeV with the CMS Experiment at the LHC," Phys. Lett. B **716** (2012), 30-61 [arXiv:1207.7235 [hep-ex]].

[146] F. J. Botella and C. S. Lim, "Flavor Changing Yukawa Coupling in the Standard Model and Muon Polarization in $K_L \to \mu\bar{\mu}$," Phys. Rev. Lett. **56** (1986), 1651-1654

[147] B. Batell, M. Pospelov and A. Ritz, "Multi-lepton Signatures of a Hidden Sector in Rare B Decays," Phys. Rev. D **83** (2011), 054005 [arXiv:0911.4938 [hep-ph]].

[148] J. F. Kamenik and C. Smith, "FCNC portals to the dark sector," JHEP **03** (2012), 090 [arXiv:1111.6402 [hep-ph]].

[149] K. Schmidt-Hoberg, F. Staub and M. W. Winkler, "Constraints on light mediators: confronting dark matter searches with B physics," Phys. Lett. B **727** (2013), 506-510 [arXiv:1310.6752 [hep-ph]].

[150] J. D. Clarke, R. Foot and R. R. Volkas, "Phenomenology of a very light scalar (100 MeV $< m_h <$ 10 GeV) mixing with the SM Higgs," JHEP **02** (2014), 123 [arXiv:1310.8042 [hep-ph]].

[151] D. Aristizabal Sierra, F. Staub and A. Vicente, "Shedding light on the $b \to s$ anomalies with a dark sector," Phys. Rev. D **92** (2015) no.1, 015001 [arXiv:1503.06077 [hep-ph]].

[152] R. Aaij *et al.* [LHCb], "Search for long-lived scalar particles in $B^+ \to K^+\chi(\mu^+\mu^-)$ decays," Phys. Rev. D **95** (2017) no.7, 071101 [arXiv:1612.07818 [hep-ex]].

[153] V. V. Gligorov, S. Knapen, M. Papucci and D. J. Robinson, "Searching for Long-lived Particles: A Compact Detector for Exotics at LHCb," Phys. Rev. D **97** (2018) no.1, 015023 [arXiv:1708.09395 [hep-ph]].

[154] A. Ariga *et al.* [FASER], "FASER's physics reach for long-lived particles," Phys. Rev. D **99** (2019) no.9, 095011 [arXiv:1811.12522 [hep-ph]].

[155] J. A. Evans, "Detecting Hidden Particles with MATHUSLA," Phys. Rev. D **97** (2018) no.5, 055046 [arXiv:1708.08503 [hep-ph]].

[156] S. Alekhin, *et al.* [SHiP], "A facility to Search for Hidden Particles at the CERN SPS: the SHiP physics case," Rept. Prog. Phys. **79** (2016) no.12, 124201 [arXiv:1504.04855 [hep-ph]].

[157] J. A. Bailey *et al.* [MILC], "$B \to K l^+ l^-$ Decay Form Factors from Three-Flavor Lattice QCD," Phys. Rev. D **93** (2016) no.2, 025026 [arXiv:1509.06235 [hep-lat]].

[158] C. Bouchard *et al.* [HPQCD], "Rare decay $B \to K\ell^+\ell^-$ form factors from lattice QCD," Phys. Rev. D **88** (2013) no.5, 054509 [arXiv:1306.2384 [hep-lat]].

[159] Y. S. Amhis *et al.* [HFLAV], "Averages of b-hadron, c-hadron, and τ-lepton properties as of 2018," [arXiv:1909.12524 [hep-ex]].

[160] E. Kou *et al.* [Belle-II], "The Belle II Physics Book," PTEP **2019** (2019) no.12, 123C01 [arXiv:1808.10567 [hep-ex]].

[161] R. R. Horgan, Z. Liu, S. Meinel and M. Wingate, "Lattice QCD calculation of form factors describing the rare decays $B \to K^*\ell^+\ell^-$ and $B_s \to \phi\ell^+\ell^-$," Phys. Rev. D **89** (2014) no.9, 094501 [arXiv:1310.3722 [hep-lat]].

[162] A. Bharucha, D. M. Straub and R. Zwicky, "$B \to V\ell^+\ell^-$ in the Standard Model from light-cone sum rules," JHEP **08** (2016), 098 [arXiv:1503.05534 [hep-ph]].

[163] A. Kachanovich, U. Nierste and I. Nišandžić, "Higgs portal to dark matter and $B \to K^{(*)}$ decays," Eur. Phys. J. C **80** (2020) no.7, 669 [arXiv:2003.01788 [hep-ph]].